

**Bacterial Methane Formation and Distribution in Marine
Environments:**

Case Studies from Arkona Basin (Western Baltic Sea)
and Hotspots in the Central South Pacific

Dissertation

zur Erlangung des Doktorgrades
der Mathematisch-Naturwissenschaftlichen Fakultät
der Christian-Albrechts-Universität
zu Kiel

vorgelegt von

Olaf Thießen

Kiel 2005

Referent:	PD Dr. Mark Schmidt
Korreferent:	Prof. Dr. Klaus Wallmann
Tag der mündlichen Prüfung:	13. Dezember 2005
Zum Druck genehmigt: Kiel,	21. Dezember 2005

Der Dekan

Vorwort

Die Struktur dieser Dissertation folgt der Thematik ihrer Einzelbeiträge, die jedoch in Umfang und innerer Kohärenz auch einer monographischen Dissertation entsprechen. In Kapitel 1 sind einleitend die geochemischen Grundlagen zu Methanbildung und- Abbau zusammengefasst. Kapitel 2 beschreibt die Sedimentabfolge bzw. die sedimentphysikalischen Eigenschaften, die in den Kapiteln 3 und 4 bei den Untersuchungen zur Entstehung und Verteilung von Methan in organisch reichen Sedimenten des Arkona Beckens (westliche Ostsee) herangezogen werden. Die Verteilung und Dynamik von Methan in der Wassersäule bzw. in Fluidaustritten an submarinen Vulkanen im zentralen Süd-Pazifik wird in Kapitel 5 dargestellt. Den Kapiteln 3–5 ist jeweils eine Zusammenfassung, eine Einleitung und ein methodischer Teil vorangestellt. Diese Kapitel werden zur Veröffentlichung vorbereitet bzw. sind eingereicht oder schon publiziert.

Danken möchte ich besonders meinem Betreuer Dr. habil. Mark Schmidt auf dessen Anregung hin ich in dieses Projekt involviert wurde. Weiterhin möchte ich auch für seine gute Betreuung meinen herzlichsten Dank aussprechen, ebenso wie für die vielen Denkanstöße und ausgiebigen Diskussionen während der Entstehung dieser Arbeit. Ich danke Herrn Prof. Peter Stoffers, der es mir ermöglichte diese Arbeit hier am Kieler Institut neben meiner beruflichen Tätigkeit in Hannover durchzuführen. Herrn Dr. Friedrich Theilen danke ich für die Möglichkeit, dass ich im NATLAB Projekt promovieren konnte. Für ausgiebige Diskussionen und die Unterstützung hier an der Uni Kiel danke ich Reiner Botz. Manfred und Hiltrud Schmitt danke ich einmal dafür, dass ich die gesamte Gas- und Isotopenanalytik im GCA Labor in Lehrte „nebenbei“ erledigen konnte bzw. mir die Daten geliefert wurden und dafür, dass ich auch immer mal wieder sehr kurzfristig meinen Arbeitsplatz nach Kiel verlegen konnte.

Danke Inge Dold, für deine ständige Hilfsbereitschaft und die Durchführung der Bestimmung der „Physical Properties“ und der TOC Gehalte. Bei Bettina Dohmeyer und Dr. Eckhart Bedbur möchte ich mich für die Unterstützung bei den Porenwasser-Analysen bedanken. Klaus Ricklefs vom Forschungs- und Technologiezentrum Westküste danke ich für die Möglichkeit zur Durchführung von Korngrößenanalysen.

Besonders bedanken möchte ich mich bei den Nachbarn Christian Hensen, Anja Reitz und Sibylle Grandel für fachliche, praktische und kulinarische Betreuung in allen Phasen der Arbeit. Außerdem möchte ich all jenen danken, die mir, sei es direkt oder indirekt, geholfen haben, das Projekt zum Abschluss zu bringen, wobei der sportliche Charakter, ausgelöst durch die Utrechter wahl-„meisjes“ Gesa, Julia und schon wieder Anja, nicht unerwähnt bleiben soll.

Ein ganz dickes extra Danke für Beate, Heinke, Markus und „Mamse“, war bestimmt nicht immer ganz einfach mit mir in der letzten Zeit.

Die vorliegende Arbeit wurde vom Bundesministerium für Bildung und Forschung und der Deutschen Forschungsgemeinschaft (03 G 0564D) im Rahmen des Projektes GEOTECHNOLOGIEN und des Bundesministerium für Forschung und Technologien (03 G 0543A) gefördert.

Contents

Summary	1
Zusammenfassung	3
1 Introduction	5
1.1 Early Diagenesis	6
1.2 Methanogenesis	7
1.3 Thermogenesis	10
1.4 Methane in hydrothermal systems	11
1.5 Methanotrophy	13
1.6 Objectives	14
2 Sediment physical properties of fine grained sediments in the Arkona Basin, Baltic Sea	17
2.1 Introduction	17
2.2 Geological setting	18
2.3 Material and methods	21
2.4 Results and discussion	22
2.4.1 Lithostratigraphy	22
2.4.2 Grain size	25
2.4.3 Physical properties	27
2.4.4 Undrained shear strength	30
2.5 Summary	31
3 Methane formation and distribution of acoustic turbidity in organic-rich surface sediments in the Arkona Basin, Baltic Sea	33
3.1 Introduction	34
3.2 Material and methods	36
3.2.1 Study area	36
3.2.2 Seismic investigations	37
3.2.3 Coring and sediment sampling	38
3.2.4 Redox potential measurement	39
3.2.5 Bulk density, water content and porosity	39
3.2.6 Gas analysis	39
3.3 Results	40
3.3.1 Lithological description	40
3.3.2 Sediment redox conditions	42
3.3.3 Acoustic turbidity and sediment gases	42
3.4 Discussion	48
3.4.1 Lateral occurrence of acoustic turbidity	48
3.4.2 Gas accumulation	51
3.4.3 Origin of methane	54
3.5 Conclusions	57

4	Variable deposition of organic-rich sediments and related methane accumulation in the Arkona Basin, Baltic Sea	59
4.1	Introduction	60
4.2	Hydrography and geological setting in the study area	61
4.3	Material and methods	64
4.3.1	Coring and sediment sampling	64
4.3.2	Wet bulk density, water content and porosities	65
4.3.3	Sulphate and chloride concentrations	65
4.3.4	Total organic carbon	65
4.3.5	Gas analysis	66
4.3.6	Geochemical modelling	66
4.4	Results	71
4.4.1	Sediments and organic matter content	71
4.4.2	Pore-water geochemistry	71
4.5	Discussion	73
4.5.1	Geochemical characterisation of Arkona Basin sediments	73
4.5.2	Hypothetic TOC accumulation and gas formation	77
4.5.3	Methane C-isotope fractionation	81
4.6	Conclusions	83
5	Methane venting into the water column above the Pitcairn and the Society – Austral seamounts, South Pacific	85
5.1	Introduction	86
5.2	Geological setting	88
5.3	Methods	90
5.4	Results and discussion	92
5.4.1	Water column characteristics and methane distribution	92
5.4.1.1	CH ₄ concentration profiles	92
5.4.2	Origin of hydrothermal methane	100
5.5	Conclusions	103
	References	105
	List of figures	119
	List of tables	121
	Appendix	123

Summary

Within the framework of this thesis the investigation of methanogenesis and secondary degradation processes of methane in two distinctly different marine environments has been carried out. These two environments were (i) the gassy shallow-marine sediments of the Arkona Basin, western Baltic Sea and (ii) the hydrothermal submarine fluid/gas exhalations at hotspot volcanoes of the central South Pacific. Based on the results of geochemical, sedimentological and seismic investigations as well as geochemical modelling it was possible to reconstruct the occurrence, distribution, genesis and degradation processes of methane in these two environments. Particularly, the analyses of the molecular composition of the hydrocarbons extracted from the fluid/pore water in combination with the stable carbon and hydrogen isotopic signal enabled deductions regarding the methane formation processes in the respective working areas.

In the central Arkona Basin an area of about 1500 km² shows acoustic turbidity of the seismic signal in ~1.5 m depth in the surface sediments. This acoustic turbidity is an indication of free gas in post-glacial surface sediments which may reach about 12 m thickness in the basin centre. These sediments are characterised by a conspicuously high organic carbon content (ca. 5-8 %) and a clayey-silty structure. The degradation of organic matter produces anaerobic conditions in near surface sediments and in about 1 m sediment depth, below the sulphate reduction zone, it results in the accumulation of methane. The stable carbon and hydrogen isotopic results of all gas samples from the post-glacial sediment layer confirm bacterial methane production via CO₂ reduction. Solely, the d¹³C-CH₄ values of ~-40‰ of the upper few centimetres of the surface sediments indicate oxidised methane. The late- and post-glacial clay (reddish/brown and grey) that is located beneath the organic-rich sediments, however, shows rather low methane concentrations within the pore-water and the concentration profile as well as the d¹³C-CH₄ values point to diffusion of gas from the surface sediments in to the clay.

Overall, the measured methane concentrations in pore-water show distinct differences in methane concentration from trace concentrations at the northern rim of the basin to the point of methane saturation in the central basin. The increase in CH₄ concentration is generally accompanied by an increasing thickness of organic-rich surface sediments. Based on the concentrations of organic carbon, methane, and sulphate and the average sedimentation rate a numerical model was developed to characterise sulphate reduction, anaerobic oxidation of methane and methane production. The model results show that a sediment thickness of 3.5 m has to be achieved to obtain CH₄ production rates that enable the accumulation of methane in the sediments. Furthermore, it could be shown that a sufficient amount of methane required to cause oversaturation and gas bubble formation can not be generated until a sediment thickness of 5-6 m is reached. This minimum sediment thickness established by the geochemical model correlates nicely with the sediment thickness at which the seismic readings show acoustic turbidity.

During research cruises Sonne 65 (1989) and Polynaut (1999) methane analyses were conducted on water column and fluid samples above submarine volcanoes of the Pitcairn, Austral, and Society island chains, central South Pacific. Weak hydrothermal activity was determined at hotspot volcanoes Bounty and Teahitia in 1999. The 1999 results, in comparison with methane results from 1998, point to a rather calm exhalation activity of the hotspot volcanoes. The higher methane concentrations determined in the water column in 1998 could be attributed to the eruption of the Macdonald seamount that occurred at that time.

The importance of bacterial methane production by CO₂ reduction, also for hot exhalations of submarine volcanoes, could be described the first time by means of the ¹³C/¹²C and D/H isotope ratios of methane. At the Bounty seamount the stable isotopic values of methane from the fluids refer to an almost 100% bacterial production of methane at about 88°C. An amount of about 50% bacterially produced methane besides the abiogenic produced methane could be determined at Macdonald seamount.

Zusammenfassung

Im Rahmen dieser Arbeit wurde die Methangene und sekundäre Abbauprozesse des Methans in zwei sehr unterschiedlichen marinen Milieus untersucht. Zum einen wurden die gasreichen flachmarinen Sedimente der westlichen Ostsee im Arkona Becken untersucht. Zum anderen waren submarine hydrothermale Fluid/Gas-Ausströmungen an Hotspot Vulkanen des zentralen Südpazifiks Ziel der in dieser Dissertation zusammengefassten Arbeiten. Anhand der Ergebnisse aus geochemischen, sedimentologischen und seismischen Untersuchungen, sowie geochemischen Modellierungen konnten Vorkommen, Verteilung, Genese und Abbauprozesse von Methan in den zwei Beispielgebieten geklärt werden. Insbesondere aus der Analyse der molekularen Zusammensetzung der aus den Fluid- bzw. Porenwasserproben extrahierten Kohlenwasserstoffe, in Kombination mit der stabilen Kohlenstoff- und Wasserstoff-Isotopie des Methans, konnten Rückschlüsse auf die Methanbildungsprozesse in den jeweiligen Arbeitsgebieten gezogen werden.

Im zentralen Bereich des Arkona Beckens wurde durch seismische Messungen ein ca. 1500 km² großes Areal bestimmt, in dem die akustische Auslöschung der seismischen Signale in den Oberflächensedimenten bei ca. 1,5 m Sedimenttiefe auftritt. Dieses weist auf freies Gas in den post-glazialen, bis zu ca. 12 m mächtigen Oberflächensedimenten hin. Diese Sedimente werden durch einen sehr hohen (ca. 5-8 %) Anteil an organischem Kohlenstoff und eine tonig-siltige Struktur geprägt. Der Abbau der organischen Substanz führt bereits oberflächennah zu anaeroben Bedingungen und in ca. 1 m Sedimenttiefe wird unterhalb der Sulfatreduktionszone Methan gebildet und akkumuliert. Die stabilen Kohlenstoff- und Wasserstoff-Isotopenwerte aller im Bereich der post-glazialen Sedimentschicht gemessenen Gasproben bestätigen eine bakterielle Methanbildung über die Reduktion von CO₂. Lediglich in den oberen Zentimetern des Oberflächensediments weisen $\delta^{13}\text{C-CH}_4$ -Werte von $\sim -40\%$ PDB auf oxidiertes Methan hin. Die unterhalb der organischreichen Sedimente liegenden spät- und post-glazialen (rötlich-braune und graue) Tone zeigen eher geringe Methankonzentrationen im Porenwasser und der Konzentrationsverlauf sowie die $\delta^{13}\text{C-CH}_4$ -Werte deuten auf eine Diffusion des Gases aus den Oberflächensedimenten in die Tone hinein.

Insgesamt zeigen die gemessenen Methankonzentrationen der Porenwasserproben starke Unterschiede, von Spurenkonzentrationen am nördlichen Rand des Beckens bis hin zur Methansättigung im zentralen Becken. Diese Zunahme der CH_4 -Konzentration geht mit einer ansteigenden Mächtigkeit der organischreichen Oberflächensedimente einher. Basierend auf den gemessenen Gehalten an organischem Kohlenstoff, Methan- und Sulfatkonzentrationen, und den gemittelten Sedimentationsraten wurde ein numerisches Modell entwickelt, das die Sulfatreduktion, die anaerobe Oxidation von Methan und die Methanproduktion beschreibt. Die Ergebnisse zeigen, dass eine Sedimentmächtigkeit von 3,5 m erreicht werden muss, um CH_4 -Produktionsraten zu erreichen, die zur Akkumulation von Methan im Sediment führen. Weiterhin konnte mit dem Modell gezeigt werden, dass erst bei einer Sedimentmächtigkeit von 5-6 m die entsprechende Methanmenge generiert wird, die zur Übersättigung und Gasblasenbildung führt. Die durch das geochemische Modell ermittelte Mindestmächtigkeit korreliert hervorragend mit der Sedimentmächtigkeit, ab der in den seismischen Messungen die akustische Auslöschung auftritt.

Im zentralen Süd-Pazifik wurden während der Forschungsfahrten R.V. SONNE 65 (1989) und Polynaut (1999) Methanmessungen in der Wassersäule und in Fluiden über submarinen Vulkanen der Pitcairn-, Austral- und Society-Inselketten durchgeführt. Schwache hydrothermale Aktivität wurde 1999 an den Hotspot Vulkanen Bounty und Teahitia festgestellt. Verglichen mit Methandaten von 1989 deuten die neueren Werte auf eine eher ruhigere Exhalationsaktivität der Hotspot Vulkane hin. Die älteren hohen Methan-Wassersäulenkonzentration konnten insbesondere der damaligen Eruption des Macdonald Seamount zugeordnet werden.

Mittels der $^{13}\text{C}/^{12}\text{C}$ und D/H Isotopenverhältnisse am Methan konnte zum ersten Mal die Wichtigkeit der bakteriellen Methanproduktion durch CO_2 -Reduktion auch für heiße, submarine, vulkanische Exhalationen beschrieben werden. Am Bounty Seamount weisen die stabilen Isotopenwerte des Methans aus den Fluiden auf eine nahezu 100-prozentige bakterielle Produktion von Methan bei ca. 88°C hin. Am Macdonald Seamount konnte immer noch ein Anteil von ca. 50 % bakteriell erzeugtem Methan neben einem abiogen produzierten Methan bestimmt werden.

Chapter 1

Introduction

1 Introduction

Methane (C_1 ; CH_4) is the gaseous, highly reduced form of hydrocarbons (HC) which is found under specific conditions in the marine environment. In general, the formation of natural hydrocarbon gases, i.e. methane, is related to biogenic or abiogenic processes in the subsurface. Biogenic methane is produced by the anaerobic degradation of organic matter either by thermocatalytic processes in the deep subsurface at elevated temperatures $>50^\circ C$ (from hereon '*thermal*' or '*thermogenic*' methane or gases) or by bacterial alteration of organic matter during early diagenesis at shallow depth or in the deep subsurface (in the following referred to as '*bacterial*' methane or gases). Moreover, bacterial methane formation may also occur in hydrothermal systems at or near the sediment surface at low temperatures. Abiogenic methane is formed during inorganic synthesis in association to hydrothermalism or submarine volcanism and/or as a product of deep crust/mantle degassing. These abiogenic processes strictly exclude the involvement of organic matter degradation and bacterial processes (e.g. Claypool and Kaplan, 1974; Whiticar et al., 1986; Schoell, 1980; 1988; Galimov, 1988; Welhan, 1988; Whiticar, 1990).

The different generation pathways of CH_4 may be identified by i) the ratio of the molecular gas composition of its light hydrocarbons (C_1 – C_6 ; e.g. "gas wetness" $C_1/[C_2+C_3]$), and ii) the stable carbon ($^{13}C/^{12}C$ or $\delta^{13}C$) and hydrogen (D/H or δD) isotopic composition of methane (e.g. Bernard et al., 1976; Schoell, 1980; 1988; Whiticar et al., 1986; Wehlan, 1988). However, the oxidation of methane results in an enrichment of higher molecular-weight hydrocarbons and in stable carbon and hydrogen isotope

shifts of methane to more positive values, which may obscure the isotopic signal of the original formation pathway (e.g. Whiticar, 1999).

Carbon dioxide (CO₂) that is formed co-genetically plays an important role in the methane cycle. It can serve as the precursor carbon source for methane formation as well as it may be the oxidation product of methane degradation (e.g. Whiticar and Faber, 1986; Whiticar et al., 1986). Therefore the molecular and stable carbon isotopic composition of CO₂ provides additional information about the generation or degradation processes in the methane cycle (Whiticar and Faber, 1986).

Generally, CH₄ is dissolved in the pore-water at low concentrations as a product of methane formation in shallow organic-rich sediments or its accumulations within deep subsurface sedimentary units. However, it may exceed saturation levels with increasing concentrations and therefore form gas bubbles within the sediments pore-space. Consequently, the occurrence of free gas (e.g. gas bubbles) is common in shallow organic-rich, muddy sediments (Judd and Hovland, 1992), as well as in the deep subsurface in sedimentary basins. The distribution of these gas-charged sediments or accumulations is easily determined by seismo-acoustic profiling, since gas bubbles have a dramatic effect on compressional wave (P-wave) velocities. The related effects, termed bright spots, acoustic blanking or masking, acoustic wipeouts, velocity pull downs or even acoustic turbidity, are caused by acoustic energy adsorption and/or backscattering and do obscure deeper sedimentary layers (e.g. Anderson and Hampton, 1980a; Lyons et al., 1996). On account of its time saving and relatively inexpensive application, mapping of large seafloor regions during seismic surveys is nowadays the most frequently utilised evidence for gas bubble formation (e.g. methane oversaturation) and the distribution of gas-rich marine sediments (e.g. Fleischer et al., 2001).

This chapter gives a general introduction to the background of the major processes discussed in chapters 2-5.

1.1 Early diagenesis

Organic matter buried in marine environments is mostly produced by algae in the euphotic water column, but may also be of terrestrial origin in near coastal areas, delivered by river discharge or atmospheric input. However, degradation of organic matter in the sediment starts directly after deposition driven by a number of different available oxidants. The general depth sequence of oxidants used is

$O_2 \rightarrow NO_3^- \rightarrow Mn(IV) \rightarrow Fe(III) \rightarrow SO_4^{2-} \rightarrow CO_2$ (Tab. 1.1) in order of decreasing energy supply per mol of oxidised C_{org} (Claypool and Kaplan, 1974; Froehlich et al., 1979; Berner, 1980; and others). Quantitatively the most important oxidants are oxygen and sulphate, whereas 25-50% of the organic carbon may be mineralised anaerobically by sulphate reducing bacteria (Jørgensen, 1982; Jørgensen, 2000).

Table 1.1: Pathways of organic matter oxidation and hydrogen transformation in the seafloor and their standard energy yields, ΔG^0 , per mol of organic carbon, according to Jørgensen (2000, and references therein).

Pathway and stoichiometry of reaction	ΔG^0 (kJ mol ⁻¹)
Oxic respiration: $CH_2O + O_2 \rightarrow CO_2 + H_2O$	-479
Denitrification: $5CH_2O + 4NO_3^- \rightarrow 2N_2 + 4HCO_3^- + CO_2 + 3H_2O$	-453
Mn (IV) reduction: $CH_2O + 3CO_2 + H_2O + 2MnO_2 \rightarrow 2Mn^{2+} + 4HCO_3^-$	-349
Fe (III) reduction: $CH_2O + 7CO_2 + 4Fe(OH)_3 \rightarrow 4Fe^{2+} + 8HCO_3^- + 3H_2O$	-114
Sulphate reduction: $2CH_2O + SO_4^{2-} \rightarrow H_2S + 2HCO_3^-$	-77
$4H_2 + SO_4^{2-} + H^+ \rightarrow HS^- + 4H_2O$	-152
$CH_3COO^- + SO_4^{2-} + 2H^+ \rightarrow 2CO_2 + HS^- + 2H_2O$	-41
Methane production: $CO_2 + 4H_2 \rightarrow CH_4 + 2H_2O$	-136
$CH_3COO^- + H^+ \rightarrow CH_4 + CO_2$	-28

According to the above mentioned depth sequence of oxidants utilised and due to the fact that methane is generated by bacterial CO_2 reduction (see 1.2), methane production will become dominant in the methanogenic zone (Fig. 1.1) as a consequence of quantitative sulphate reduction in the sulphate reduction zone (SRR). The depth at which both components (methane and sulphate) are exhausted is termed the sulphate-methane-transition (SMT), which is an important marker during early diagenesis in anaerobe marine sediments (Fig. 1.1).

1.2 Methanogenesis

In principal two dominant formation pathways of bacterial methane formation (methanogenesis) can be distinguished: CO_2 reduction and acetate fermentation

(Claypool and Kaplan, 1974; Martens and Berner, 1974; Whiticar et al., 1986). Although both pathways may occur in marine as well as in freshwater sediments, CO₂ reduction is the dominant process in anaerobe sulphate depleted marine and brackish environments, such as salt marshes, estuaries, shelf and deep sea sediments. The process proceeds according to the following general reaction:



where the ambient water, e.g. pore-water, is the source for the hydrogen.

Acetate fermentation on the other hand is the major pathway in anaerobe freshwater sediments and can be expressed with the general reaction:



where the * indicates the intact transfer of the methyl group to the generated CH₄.

Methane is the dominant hydrocarbon formed during methanogenesis and higher molecular-weight hydrocarbons may be generated just in very low quantities (Oremland, et al., 1988). This results in molecular C₁/(C₂+C₃) ratios of >1000 (C₂₊ <0.05% with C₂₊ = ΣnC₂-nC₅; Schoell, 1984), which are identified to be typical for the bacterial formation pathway (e.g. Bernard et al., 1976).

During bacterial methane formation carbon isotope fractionation (α_C) occurs, resulting in ¹²C enrichment of the related methane in comparison to the precursor material. The isotopic shift is caused by a kinetic effect, whereas ¹²C-¹²C bonds are preferentially cleaved rather than ¹²C-¹³C bonds. As a consequence, methane produced by CO₂ reduction in marine sediments is enriched in ¹²C by about 50 to 100% (α_C = 1.05 to 1.1; Whiticar et al., 1986; Botz et al., 1996) in comparison to the precursor material and methane produced by acetate fermentation in freshwater sediments by α_C of 1.04 to 1.06 (Whiticar et al., 1986).

The hydrogen isotopic composition of methane formed via CO₂ reduction, however, is directly related to the formation water with an associated hydrogen fractionation of –180 ± 20‰ (Whiticar et al., 1986). The hydrogen isotopic fractionation during acetate fermentation is much larger, due to the intact transfer of the deuterium depleted methyl group of the precursor organic matter to the resulting methane. The left fourth hydrogen (Eq. 2) comes from the formation water, but is identified to be isotopically fractionated as well (Whiticar et al., 1986).

The different formation pathways, however, can be distinguished using the molecular composition of hydrocarbon gases and the carbon and hydrogen stable isotope

compositions of methane as a function of the co-existing carbon dioxide, the precursor organic material and the associated formation water (e.g. Claypool and Kaplan, 1974; Martens and Berner, 1974; Bernard, et al., 1976; Schoell, 1980; 1984; 1988; Whiticar et al., 1986).

In general, methane in marine and brackish sediments generated by CO₂ reduction can be isotopically defined by their $\delta^{13}\text{C}$ values of -110 to -60‰ and by their δD values of $>-250\text{‰}$ with typical values close to $-190\text{‰} \pm 20\text{‰}$. In contrast, methane from acetate fermentation in freshwater sediments ranges from $\delta^{13}\text{C}$ -65 to -50‰ with typical δD values between -355 and -290‰ (e.g. Schoell, 1980; 1984; 1988; Whiticar et al., 1986).

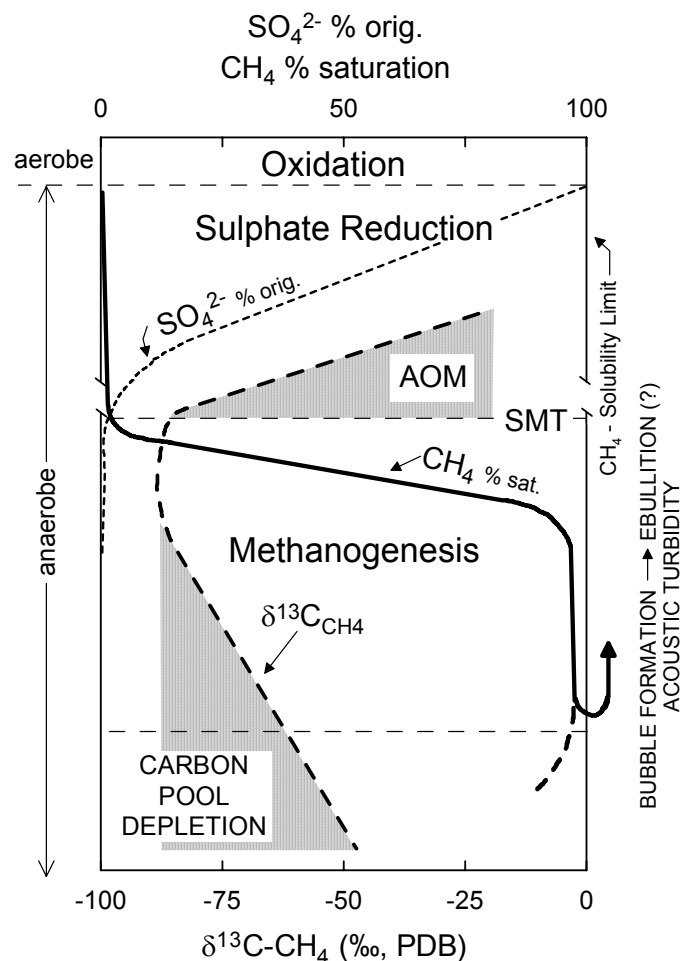


Fig. 1.1: Generalised diagenetic scheme for anaerobe marine environments after Whiticar and Faber (1986). The penetration depth of the sulphate reduction zone (SRZ) is the limiting factor at which sediment depth methanogenesis occurs. Methane production starts below the sulphate-methane-transition (SMT) with a typical $\delta^{13}\text{C}_{\text{CH}_4}$ depletion of $<-60\text{‰}$. In the SRZ methane is generally degraded to CO₂ by anaerobic methane oxidation (AOM), which lead to strong enrichment of ¹³C in the residual CH₄. Methane upward flux to the sulphate bearing zone, however, may take place by diffusive or advective fluid transport or even by ebullition, when the CH₄ saturation limit is arrived and gas bubble formation occurs. In seismo-acoustic investigations gas bubble occurrence is observed by acoustic turbidity, i.e. by the obscuring of deeper sediments.

The isotope ratios are given in the common δ -notation in parts per million (‰) relative to the isotopic composition of international standards:

$$\delta R(\text{‰}) = \left(\frac{R_{\text{Sample}} - R_{\text{Standard}}}{R_{\text{Standard}}} \right) \times 1000 \quad \text{with} \quad R = \frac{^{13}\text{C}}{^{12}\text{C}}; \frac{\text{D}}{\text{H}}$$

$\delta^{13}\text{C}$ relative to PDB

PDB = **Pee Dee Belemnite**

δD relative to SMOW

SMOW = **Standard Mean Ocean Water**

The fractionation factor α defines the distribution of a stable isotope between substances A and B:

$$\alpha_{\text{A-B}} = \frac{R_{\text{A}}}{R_{\text{B}}} \quad \text{or} \quad \alpha_{\text{A-B}} = \frac{1000 + \delta\text{A}}{1000 + \delta\text{B}}$$

1.3 Thermogenesis

As pointed out above gaseous thermogenic hydrocarbons are generated during burial of organic matter, i.e. by the degradation (cracking) of long-chain hydrocarbons at elevated temperatures during catagenesis and metagenesis (Tissot and Welte, 1984; Hunt, 1996). However, at temperatures $>50^{\circ}\text{C}$ light molecular-weight HC formation (e.g. methane, ethane, propane) is associated to oil generation from kerogen (Schoell, 1980; Tissot and Welte, 1984; Hunt, 1996) and released thermogenic gases may therefore contain $>10\%$ of C_2 and C_3 hydrocarbons (wet gases; $\text{C}_{2+} >5\%$). The process of thermogenic methane generation in sediments and its reflections in the composition of stable carbon isotopes and light molecular-weight hydrocarbon composition is schematically summarised in Fig. 1.2.

With increasing maturity (higher subsidence and therefore increasing temperatures) more and more short-chain HC are formed due to ongoing cracking processes and under overmature conditions only thermogenic methane is formed (dry gases; $\text{C}_{2+} <5\%$). Nevertheless, typical molecular $\text{C}_1/(\text{C}_2+\text{C}_3)$ ratios for thermogenic hydrocarbon gases are <100 (Bernard et al., 1976; Schoell, 1984).

During cracking of organic matter the same kinetic isotope fractionation effects occur as described for the bacterial methane formation process (see 1.2). This leads to an enrichment of ^{12}C in the related gases (methane and higher molecular-weight gaseous hydrocarbons) with respect to the precursor material (e.g. Clayton, 1991; Berner et al.,

1995). The organic source material is characterised by carbon isotope values of $\delta^{13}\text{C}$ -15 to -25‰ as marine-sapropelic and with values of $\delta^{13}\text{C}$ -24 to -34‰ as humic/terrestrial (e.g. Schoell, 1984; Tissot und Welte, 1984; Hunt, 1996). Moreover with increasing maturity and ongoing cracking the carbon pool becomes depleted in ^{12}C , which lead to a significant enrichment in ^{13}C of thermogenic methane (Fig. 1.2; Tissot and Welte, 1984; Hunt, 1996).

Typical thermogenic methane is characterised by stable carbon isotope ratios $>-55\text{‰}$ (Fig. 1.2). D/H- CH_4 ratios typically range between -375 and -100‰ and in general values become more positive with increasing maturity (e.g. Schoell, 1980; 1984; 1988).

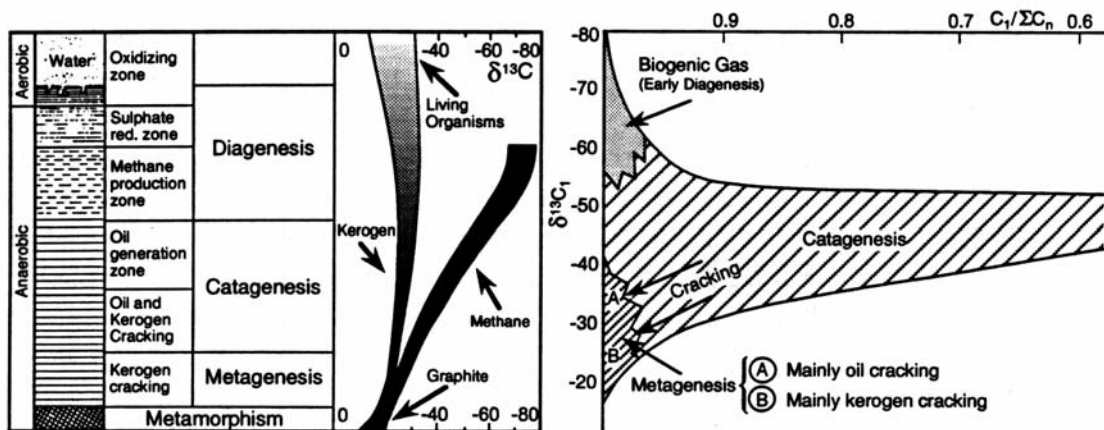


Fig. 1.2: Generalised scheme of diagenetic and thermogenic hydrocarbon gas generation and their reflections in the stable carbon isotopic composition of methane ($\delta^{13}\text{C}\text{-CH}_4$) and the relative abundance of molecular light-weight hydrocarbons ($\text{C}_1/\Sigma\text{C}_n$) after Tissot and Welte (1984) from Lammers (1994).

1.4 Methane in hydrothermal systems

According to Welhan (1988, and references therein.) four possibilities are generally considered for the origin of methane in hydrothermal systems: (a) bacterial production, predominantly at low temperatures; (b) thermal degradation of organic matter at temperatures above $\sim 100^\circ\text{C}$ ("thermogenic CH_4 "); (c) outgassing of primordial CH_4 from the mantle; and (d) formation during inorganic (abiogenic) synthesis, involving CO_2 , H_2 , or other C-H molecules at temperatures $>300^\circ\text{C}$ (Fischer-Tropsch-Type reactions).

(a) Bacterial methane formation in hydrothermal systems occurs in relatively shallow depth by hypothermophilic archaea at temperatures below 113°C (Burggraf et al., 1990;

Huber et al., 1990). Bacterial methane in hydrothermal fluids is characterised by $\delta^{13}\text{C}$ values of $<-60\text{‰}$ and by δD values of $<-150\text{‰}$ (Welhan, 1988).

(b) Methane (and higher molecular-weight HC) generation as a consequence of thermal degradation (cracking) of organic matter is also observed at elevated temperatures in hydrothermal systems (Simoneit, 1983; Welhan and Lupton, 1987; Welhan, 1988). The stable carbon and hydrogen isotopic composition of the generated HC is affected by the primary organic material (section 1.3). Typical $\delta^{13}\text{C}$ values for methane generated by organic matter degradation in hydrothermal systems are $> -50\text{‰}$ with δD values of -120 to -200‰ (e.g. Schoell, 1980; 1984; 1988; Welhan and Lupton, 1987).

(c) + (d) Abiogenic hydrocarbons are generally formed by the reduction of carbon dioxide (similar to Eq. 1), a process which is thought to occur at high temperatures during magma cooling (e.g. Kelly, 1996) and –more commonly– in hydrothermal systems during water-rock interactions, e.g. involving Fischer-Tropsch reactions and the serpentinisation of mafic and ultramafic rocks (e.g. Lancet and Anders, 1970; Apps, 1985; Welhan, 1988; Abrajano et al., 1990; Charlou and Donval, 1993; Sherwood Lollar et al., 1993; Berndt et al., 1996; Botz et al., 1996b; Charlou et al., 1996; 2002; Horita and Berndt, 1999; Kelley and Früh-Green, 1999).

Methane stable carbon isotope ratios of $\delta^{13}\text{C} >-20\text{‰}$ are characteristic of an abiogenic origin in hydrothermal fluids (Welhan, 1988; Charlou et al., 1996; Kelley and Früh-Green, 1999; Charlou et al., 2000; Charlou et al., 2002) and are correlated with the generation by Fischer-Tropsch synthesis from co-existing CO_2 , whereas $\delta^{13}\text{C}\text{-CH}_4$ values of about -7‰ are assumed to be typical for serpentinisation processes (Abrajano et al., 1988). Correlating $\delta\text{D}\text{-CH}_4$ ratios range between -250 and -100‰ (e.g. Welhan and Craig, 1983; Abrajano et al., 1988; ; Welhan, 1988; Kelley and Früh-Green, 1999) and co-existing magmatic CO_2 , has typical $\delta^{13}\text{C}$ values of about -8 to -5‰ (Welhan, 1988 etc.).

Overall stable carbon and hydrogen isotope values of abiogenic methane synthesised in hydrothermal systems are dependant on the temperature of gas formation in the $\text{CH}_4\text{-CO}_2$ and $\text{CH}_4\text{-H}_2\text{O}$ systems (e.g. Botz et al, 1996b; Kelley and Früh-Green, 1999; Charlou et al., 2002). In this context the isotope equilibrium ($^{13}\text{C}/^{12}\text{C}$ and D/H) is based on the Richet et al. (1977) equation and on the $\delta^{13}\text{C}$ and D/H value of the precursor CO_2

and H₂ (H₂O), respectively. It should further be mentioned that complex mixing of methane generated by the above discussed formation pathways (a)–(c), or dilution of hydrothermal fluids with ambient seawater and/or methane oxidation processes may occur and may therefore relate to highly variable stable carbon and hydrogen isotopic composition of emanating methane and carbon dioxide in hydrothermal systems.

1.5 Methanotrophy

Generally, two pathways of methane degradation (methanotrophy) could be distinguished in marine environments (Fig. 1.1): (a) the bacterial degradation of methane under oxic conditions and (b) the anaerobic bacterial oxidation of methane (AOM).

(a) As pointed out above methane formation occurs under anaerobic conditions in marine sediments or hydrothermal systems. When methane reaches aerobic sediments, the sediment-water interface, or is released to the water column by diffusion, advection, ebullition, seeping or even venting, methane is effectively bacterially degraded to carbon dioxide in the presence of oxygen by the net reaction:



(b) In anoxic marine sediments methanogenesis is restricted to the sulphate-free environment (1.1 and 1.2). If methane encounters the SMT by upward diffusion, advection or ebullition it is degraded by AOM to CO₂ (e.g. Alperin et al., 1988; Whiticar, 1999). AOM is a microbial process catalysed by a consortium of sulphate reducing bacteria and retrograde methanogenic bacteria (Hoehler et al., 1994; Hansen et al., 1998) according to the following equations:



which can be summarised by the net equation:



During methane oxidation, the degradation of CH₄ is favoured over that of higher molecular-weight hydrocarbons (ethane and propane), which may lead to a shift of the diagnostic molecular gas ratio of typical bacterial to a potential thermal signature. Moreover, kinetic isotope fractionation effects lead to more positive stable carbon and hydrogen isotope values in the residual methane. Thus, partly oxidised bacterial methane

may carry a stable carbon and hydrogen isotopic composition, which is typical for thermal hydrocarbons too.

1.6 Objectives

This thesis is focused on the methane distribution and methane formation and degradation processes associated with both, early diagenesis in shallow brackish-marine organic-rich surface sediments of Arkona Basin (Baltic Sea), and methane exhalations associated to hydrothermalism at the Pitcairn and the Society – Austral seamounts, Central South Pacific.

Typically, anaerobic bacterial methane generation during early diagenetic degradation of organic matter is observed to be the dominant CH₄ formation pathway in marine sediments (Claypool and Kaplan, 1974; Martens and Berner, 1974; Whiticar et al., 1986). Thus, it is assumed that bacterial methane generation is also the relevant process which lead to methane formation and accumulation in the Arkona Basin organic-rich sediments. In contrast, in hydrothermal systems associated to submarine volcanism abiogenic methane formation is the dominant formation pathway and bacterial methane generation is rather untypical (e.g. Apps, 1985; Welhan, 1988; Abrajano et al., 1990; Sherwood Lollar et al., 1993; Botz et al., 1996b; Charlou et al., 1996; 2002). However, Wehlan (1988) reported of bacterial methane in low temperature hydrothermal systems. Moreover, methanogens are found during a submarine volcanic eruption at low temperatures (<113°C; Huber et al., 1990), indicating that bacterial methane formation may also be present in hydrothermal systems.

The Baltic is a shallow intracontinental sea located in north-western Europe. The water body is brackish and is characterised by a more or less stable thermo-haline stratification due to a estuarine circulation (inflowing dense higher saline bottom water and outflowing specifically lighter less saline surface water). Moreover, several basins and swells restrict bottom water renewal, which therefore may lead to anoxic condition in the water body in the deep basins. Variable hydrodynamic conditions lead in addition to a dynamic sedimentation regime with coarse sediments (gravel and sand) at shallow water depth and with the accumulation of fine grained sediments (clay and silt) in the basins at water depth below the wave base.

In the central Arkona Basin these fine grained soft surface sediments with high organic loading are found. Due to a high oxygen demand during organic matter degradation anaerobic conditions prevail directly beneath the sediment surface. Thus, methane generation should be favoured in these sediments. However, seismo-acoustic surveys show variable gas concentrations in surface sediments, indicated by regions with resolvable seismic profiles and by regions with acoustic turbidity, obscuring deeper sedimentary layers. Therefore it is of interest to investigate which parameters do control the distribution of acoustic blanking, e.g. the gas distribution in Arkona Basin sediments. The main questions to be answered were: Do the accumulated gas affect sediment physical properties or rather do variable physical properties have an effect on the gas distribution and therefore influence the distribution of acoustic turbidity? What in general is the lateral distribution of the acoustic turbid zone and is there any relation to the surface sediments? What is the vertical distribution of gases in different surface deposition sequences? Is bacterial generated methane from degradation of organic matter during early diagenesis the only source or do thermogenic hydrocarbons contribute as well to the gases found in the zone of acoustic turbidity, especially when the Arkona Basin was target during the Petro Baltic oil and gas exploration campaign and Upper Cretaceous limestones are found in about 40 m depth bsf?

The Pitcairn and the Society – Austral island chains are located in the south central Pacific Ocean. Their origin is related to submarine, and later on subaeric, hotspot volcanism. The seafloor between the islands is at about 4000-5000 m water depth but observed submarine volcanoes may reach 50 m water depth below the sea surface. The aims of the investigations focused on the Pitcairn and the Society – Austral regions were to investigate recent methane venting into the water column above active submarine volcanoes. Results from Polynaut cruise in 1999 should be compared with already observed methane emanations at the same seamounts investigated 10 years before during R.V. SONNE SO65 cruise in 1989. Moreover, the methane distribution in the water column above active submarine volcanoes, estimated from water samples taken with a rosette water sampler, should be correlated with methane concentrations of emanating fluids taken by precise sampling with the submersible *Nautilie*. In addition the molecular hydrocarbon gas composition and the stable carbon and hydrogen isotope ratios of extracted CH₄ should give evidence for the methane formation pathway and/or influences

due to methane oxidation. Finally, investigations should be focused on indications in hydrothermal emanations for bacterial methane production at the investigated seamounts, when methanogens were found in the crater and sea-water plume during 1989 Macdonald eruption.

Chapter 2

Sediment physical properties of fine grained sediments in the Arkona Basin, Baltic Sea

2.1 Introduction

In the Arkona Basin (western Baltic Sea) the surface sediments are fine-grained, very soft, of high porosity, with high organic loading, and contain varying amounts of methane gas. Methane is generated and accumulated in the uppermost sedimentary unit and may exceed saturation levels and then form gas bubbles (Chapter 4). The distribution of methane oversaturation, i.e. gas bubble formation, is characterised by a broad zone of acoustic turbidity conducted in seismo-acoustic surveys in the centre of the basin (Thießen et al., *subm.*).

The aim of this chapter is to characterise the surface sediments by the physical properties including the vertical and areal variability within the transition zone from acoustic transparent to acoustic turbid sediments in terms of properties and parameters that can be related to sediment fabric and geoacoustic behaviour. Moreover, processing of cores also included grain size distribution. The focus of this chapter is on the uppermost organic-rich deposits containing variable gas content, but additional data is presented from underlying sediments (to 11.2 m depth) with respect to the lithological correlation of visually differentiated macroscopic sedimentary units to the depositional history of the Arkona Basin.

2.2 Geologic setting

The Baltic Sea is an adjacent sea located at the western European continent and is characterised from West to East by a sequence of basins and swells (Duphorn et al., 1995; Reinheimer, 1995). The study area is situated in the Arkona Basin, south-western Baltic Sea (Fig. 1).

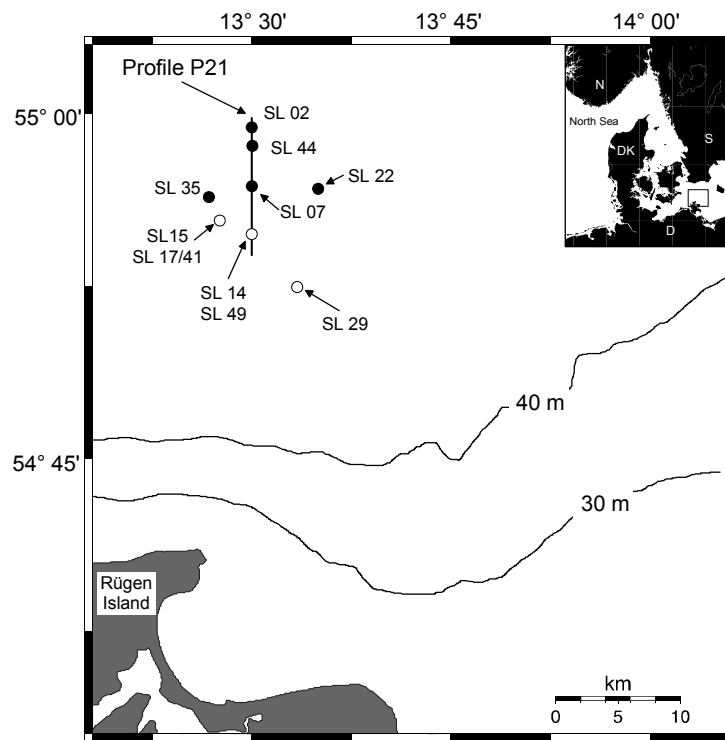


Fig. 2.1: Map of the study area Arkona Basin with locations of coring sites and of seismo-acoustic profile P21. Cores taken in zones with acoustically transparent sediments are indicated by black dots and by open dots in the zone with acoustic turbidity indicating free gas (gas bubble formation) in the sediments.

Depositional history began with the retreat of the Pleistocene glaciers and the formation of a melt water lake, the Baltic Ice Lake (BIL; e.g. Björck, 1995; Lemke, 1998; Emeis et al., 2002). Under late glacial conditions typical deposits from the BIL are reddish/brown clays, almost barren of fossils and with very low organic carbon concentrations (e.g. Neumann, 1981; Jensen, 1992; Jensen et al., 1997). The BIL stage is characterised by two drainage events which occurred at Mt. Billingen in southern Sweden at about 12800 cal. yr BP and 11300 cal. yr BP, respectively (Björck, 1995; Jensen et al., 1997; Moros et al., 2002). The latter regression event lead in the Arkona Basin to the formation of a prominent sandy layer which marks the transition to sediments of the Yoldia and Ancylus Lake stages (Björck, 1995; Moros et al., 2002). The Yoldia stage is the period after the final drainage of the Baltic Ice Lake. However, a first

salt water inflow lead to the Yoldia Sea but the connection to the ocean was restricted again. Gradual freshening of the water body followed and the Yoldia Lake was formed (Mörner, 1995; Emeis et al., 2002). The sediments deposited at this stage are also reddish/brown homogenous clays, quite similar to those deposited under BIL conditions (Lemke, 1998; Emeis et al., 2002; Moros et al., 2002). Finally another regression event at 10600 cal. yr BP lead again to the formation of a characteristic sandy layer in the Arkona Basin which marks the transition from the Yoldia Lake to the Ancylus Lake stage (Moros et al., 2002). In combination with this transition a colour shift from reddish/brown to greyish fine grained deposits is observed (Neumann, 1981; Björck, 1995; Jensen et al., 1997; Lemke, 1998). Characteristic for the topmost Ancylus Lake deposits are black spots or bands caused by iron sulphides. The postglacial global rising of the sea level lead to marine-brackish conditions of the Littorina stage in the western Baltic Sea between 8300 and 8000 not corrected ^{14}C yr (Björck, 1995; Jensen et al., 1997; Emeis et al., 2002). Similar to the actual Baltic Sea, the water column was strongly stratified and locally near seafloor anoxic conditions may have existed (Emeis et al., 2002; 2003). Moreover, homogenous fine grained organic-rich sediments are deposited under low energy hydrographic conditions in the basins of the Baltic Sea since the early Littorina transgression (e.g. Emeis et al., 2002; 2003).

Table 2.1: Stations, sampling locations, water depths and recoveries from sediment cores taken during Poseidon 266, Alkor 201 and Alkor 214 cruises in the Arkona Basin, Baltic Sea.

Station	Position		Water Depth m	Recovery Gravity Corer m	Recovery Rumohr Corer m
	N	E			
<i>Poseidon 266</i>					
SL 07	54°57.00'	013°30.17'	51.0	11.20	---
SL 15	54°55.50'	013°27.10'	45.0	6.98	---
SL 22	54°57.01'	013°38.38'	48.0	6.93	---
SL 29	54°52.25'	013°34.41'	45.0	9.23	---
<i>Alkor 201</i>					
SL 17/41	54°55.50'	013°27.70'	47.6	7.84	0.65
SL 35	54°56.29'	013°26.96'	46.0	5.30	0.66
SL 44	54°58.48'	013°30.07'	46.0	6.80	0.62
SL 49	54°54.80'	013°30.00'	47.8	3.52	0.65
<i>Alkor 214</i>					
SL 02	54°59.29'	013°30.14'	47.0	5.56	0.80
SL 14	54°54.81'	013°30.01'	47.8	5.75	---

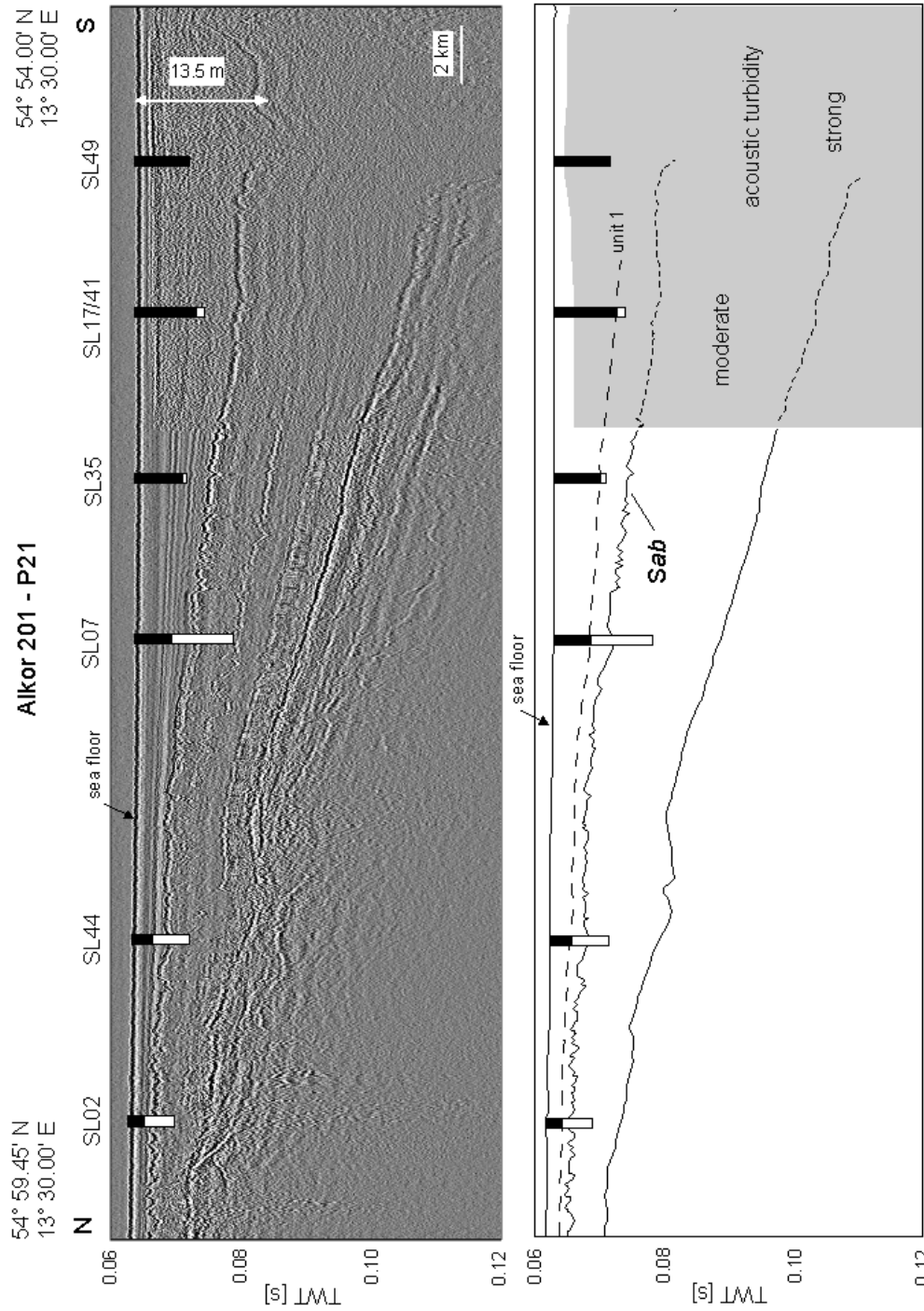


Fig. 2.2: N-S Boomer profile P21 with interpretative sketch (below) and with core locations SL02, SL44, SL07, SL35, SL17/41 and SL49 (SL14). The sediment thickness of unit 1 sediment is marked by black bars at all core locations and interpolated in between by the dotted line. The shaded area marks the occurrence of acoustic turbidity. For better visibility of the subsurface morphology two main reflectors are pointed out. A high resolution correlation of the reflectors to sedimentary units is given by Mathys et al. (2005). Sab = Reflector marking the final regression of the Baltic Ice Lake (Moros et al., 2005). TWT = two way travel time.

2.3 Material and methods

The shallow marine Arkona Basin was the target of the “Natural Laboratory Baltic Sea” (NATLAB) during three cruises with R.V. ALKOR and R.V. POSEIDON. Mushy surface sediments were cored with a 1.0 m long acrylic glass corer (Rumohr corer) with an inner diameter (ID) of 74 mm. Sub-sampling was carried out by pushing the sediments from the bottom to the top of the liner via a piston. In addition, a standard gravity corer (PVC liner 125 mm ID) was used that gained a maximum core length of up to 11.50 m. Directly after retrieval the cores were cut into 1 m sections and closed with caps. For further sub-sampling on board the sections were cut into halves (one working and one archive half).

For standard determination of physical properties as water content, wet bulk density, porosity and grain size analysis sub-samples of 5 ml bulk sediment were taken with cut-off syringes, and transferred and stored in pre-weighed glass bottles until post cruise analyses. Immediately after the cruise wet bulk density was calculated via sediment weight and the water content was determined by weight difference of wet and dried sediment after drying the bulk sediment sample at 105°C for 24 hours. Porosity was calculated with a mean grain density of Arkona Basin bottom sediments of 2.6 g cm⁻³ (Endler, 1989). Results are given in g cm⁻³, percent by weight (wt%), and percent (%) for bulk density, water content, and porosity, respectively. Analytical errors were estimated to be about 5%, respectively.

Grain size analyses were performed at the Forschungs- und Technologiezentrum Westküste, of University of Kiel, Germany using a laser optical Galai CIS-1 (Computerised Inspection System) particle size analyser (Tsai and Rau, 1992). Prior to analyses bulk sediment samples were treated with hydrogen peroxide to remove organic matter, diluted with water and placed in an ultrasonic bath. To analyse silt to clay size sediments from the Arkona Basin a particle size range of 0.5 to 150 µm was chosen. Grain size measurements were done in intervals of 0.5 µm and the summarised particle size is given in % by weight. Percentages of fractions 0.15-0.06, 0.06-0.02, 0.02-0.006, 0.006-0.002, and <0.002 mm are determined from summarised particle size data files. Statistical parameters such as the median grain size (MD) and sorting (SO) are calculated by the program from the cumulative grain size curve according to Trask (1930).

Undrained shear strength (S_u) determination was carried out on-board using a Wille Geotechnik (Göttingen, Germany) FL 1420 hand held shear vane. The used vane blade had a diameter of 47 mm and the blades a height of 5 mm and a length of 17 mm. Results of shear strength determination are given in kg cm^{-2} . The summarised estimated error for shear strength measurements is about 10%.

2.4 Results and discussion

The data presented here are based on analyses from 10 cores taken south of 55° N in the Arkona Basin (Figs. 2.1, 2.2; Tab. 2.1).

2.4.1 Lithostratigraphy

The sediment sequence in the Arkona Basin is dominated by fine grained deposits (silt and clay size), with intervals of silt to fine sand layers. Recovered sediments were divided into three lithostratigraphic units based on the visual description of sedimentary structure, grain size and sediment colour.

Lithostratigraphic unit 1: This unit typically consists of fine clastic (silt and clay sized, $<63 \mu\text{m}$) deposits of greenish black (5GY 2/1) colour near the sediment surface, which changes at about 100 cm depth to olive green - greenish grey (5Y 3/2; 5G 4/1; 5GY 4/1). A persistent smell of H_2S and in the deeper greenish part the occurrence of pyrite is characteristic for this unit. Macroscopic biogenic components as mussel shells or shell debris are rare in this unit. However, in general, these sediments have a high organic loading (2-8 wt% TOC; Chapter 4; Moros et al., 2002) which is derived from primary production in the water column and from terrestrial input due to river discharge (Miltner et al., 2005). Degradation of this organic matter is believed to produce high gas concentrations (i.e. Chapter 4) that can be correlated to acoustic turbidity occurrence (Fig. 2.2). Thus, fractures and voids observed during onboard sediment sampling in cores taken in the zone of acoustic turbidity are likely the result of gas expansion upon core recovery. In this study this sediment type is defined as “mud”. The range of sediment thickness in the investigated area is between about 150 cm at the northern rim of the basin (SL02) and more than 750 cm found at site SL29, but may reach more than 12 m in the centre of the basin (Lemke, 1998).

Unit 1 generally forms the sediment surface in the central Arkona Basin below about 25 m water depth and is typically found in quiescent deeper waters in the basins of the

Baltic Sea (e.g. Borg, 1985; Emelyanov et al., 1995; Huckriede et al., 1996; Repečka, 2001). This unit corresponds clearly to the sediments deposited under brackish-marine conditions since the onset of the Littorina transgression some 8000 yr ago (Björck, 1995; Jensen et al., 1997; Lemke et al., 1998; Emeis et al., 2002).

Lithostratigraphic **unit 2**: This unit is composed of medium to dark grey, bluish grey or greenish grey (N4; N5; 5B 5/1; 5G 6/1) silty clay. In single spots or layers black iron sulphide minerals are common. Silt to fine sand layers of up to 2 cm thickness may be found in the lower part of this sequence. Visually no fossils are observed. The thickness of this unit range from about 50 cm to more than 1.5 m. This variability in sequence thickness is on the one hand caused by the wedge out of the greyish deposits at the northern subsurface rim of the basin (Mathys et al., 2005), which is obvious from Fig. 2.2. On the other hand, Moros et al. (2002) pointed out that the greyish colour is caused by an diagenetic colour shift and not by changing depositional conditions. Thus, Moros et al. (2002) correlated the distinguished Baltic Sea stages (Yoldia Lake and Ancylus Lake) in this unit (and in the following unit) by sandy/silty layers formed as a result of well-known regression events during the Baltic Sea's history under low-stand conditions. However, the sampling resolution of grain size analyses (see below) was not high enough to distinguish the different stages in this deposition sequence, but the greyish sediments directly below the unit 1 deposits most likely correspond to deposits of the Ancylus Lake stage (Moros et al., 2002).

Lithostratigraphic **unit 3**: The distinction between lithostratigraphic unit 2 and 3 is based primarily by the colour shift from grey to reddish/brown (olive grey, 5Y 4/1) silty clay. The clayey deposits are very homogenous at sites SL02 and SL44, but show abundant occurrence of very fine sand layers in 1 to 1.5 m thick intervals at sites SL07 and SL22. Macroscopically this unit is barren of fossils and organic material.

As discussed for unit 2 deposits, a clear correlation with a Baltic Sea stage is not possible by the lithologic description alone, even when reddish/brown deposits may correlate with both, the Yoldia and the Baltic Ice Lake stage. However, Moros et al. (2002) correlated the most prominent shallow acoustic reflector (*Sab*; Fig. 2.2) with a sandy layer resulted by the final drainage of the Baltic Ice Lake (BIL) at mount Billingen at 11600 yr BP. Hence we estimated the depth of reflector *Sab* from seismic profile P21

(Fig. 2.2) based on a seismic velocity of 1350 m/s for the overlying muddy sediments (Mathys et al., 2005). The calculated sediment depth of reflector *Sab* at the northern rim of the Arkona Basin is about 2.5 m, 4 m, and 6 m at sites SL02, SL44 and SL07, respectively. Thus, at these sites the deposits below this calculated depth most likely correlate with deposits of the BIL stage and are older than 11600 yr BP (Moros et al., 2002).

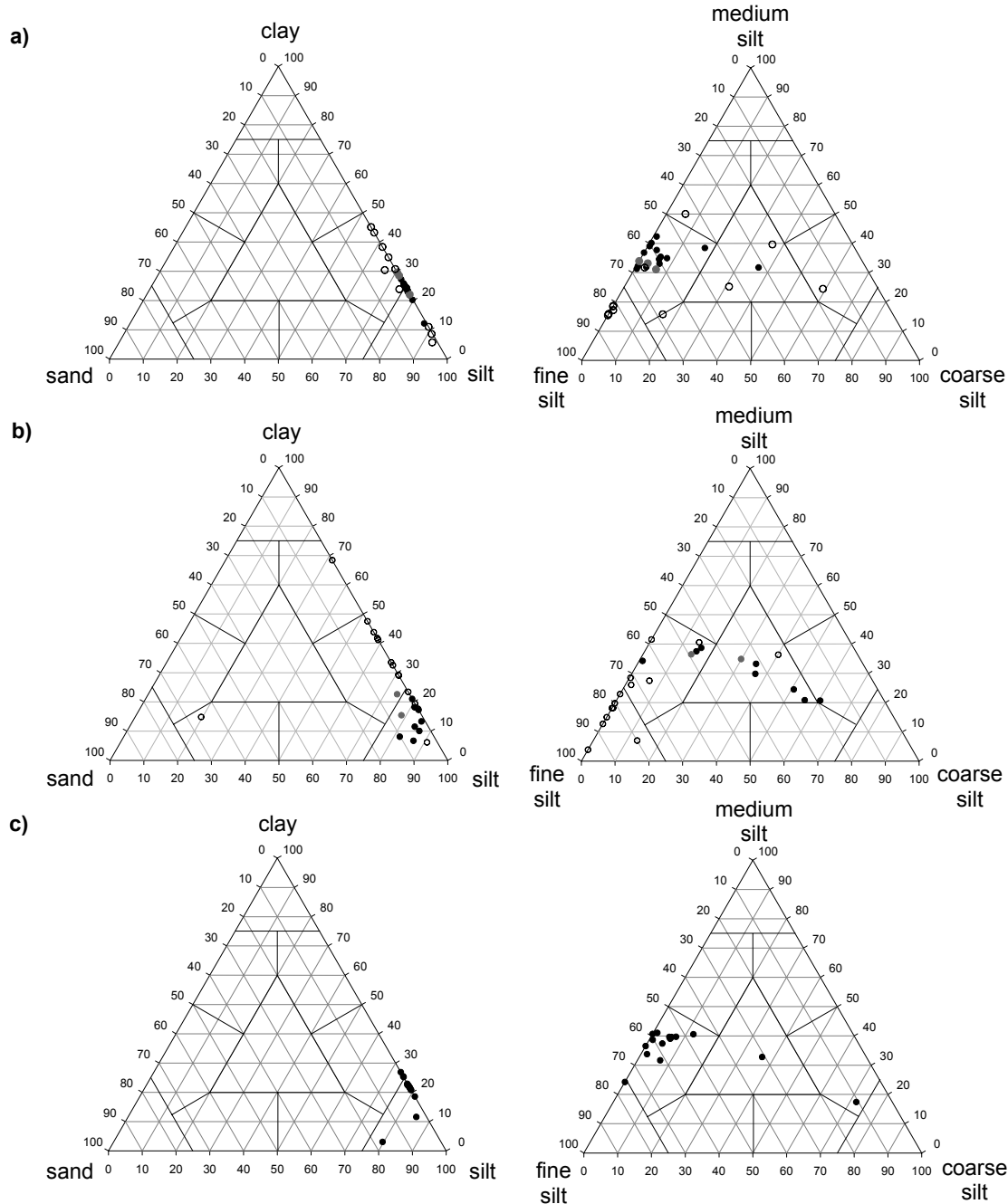


Fig. 2.3: Ternary diagrams (Shepard, 1954) showing the grain-size distribution in the sand-silt-clay and the coarse silt-medium silt-fine silt systems for sediment samples of cores SL44 (a), SL07 (b), and SL49 (c), respectively from the northern rim of the Arkona Basin. The different colours indicate the three macroscopic sedimentary units: black dots = unit 1 olive grey mud; dark grey dots = unit 2 grey silty clay; open dots = unit 3 reddish/brown silty clay.

2.4.2 Grain size

Grain size analyses were performed on 66 sediment samples selected from cores SL07, SL44, and SL49 and are summarised in Tab. 2.2 and listed up in detail in Tab. 2.3 (Appendix).

The bottom sediments of the Arkona Basin are fine grained with particles >0.06 mm having a mean amount of 1.8% and particles <0.06 mm having a mean amount of about 98% of all analysed samples (Tab. 2.2). Accordingly, sediments of the Arkona Basin could generally be characterised as aleuritic (0.1-0.01 mm) to pelitic (<0.02 mm) mud. Using the ternary sand - silt - clay diagram for clastic sediments of Shepard (1954), sediments plot in a low grain size range and could be classified as silt, clayey silt, and silty clay, respectively (Fig. 2.3). The more detailed fine silt - medium silt - coarse silt ternary diagram shows slight variations in the grain size composition of unit 1 sediments (Fig. 2.3).

More detailed, the silt fraction (0.06-0.002 mm) of the olive green mud of unit 1 has a mean value of 78.6% (72.2-87.1%) and the clay fraction (<0.002 mm) has a mean amount of 20.5% (6.7-27.3%). The grey coloured unit 2 sediments are characterised by mean amounts of 77.2% (70.4-91.1%) and 21.1% (8.6-29.6%) for the silt and clay fractions, respectively. Distinct differences in particle size are observed in unit 3 reddish/brown sediments that display a mean silt fraction of 66.2% (19.6-92.7%) and a mean clay fraction of 30.7 % (5.7-68.4%). Furthermore, fine grained sedimentation is documented by a average median (MD) of 0.007 mm (0.001-0.089 mm) in generally poorly to very poorly sorted ($SO = 1.48-3.06$, mean 1.95) deposits (Trask, 1932; Tab. 2.3).

Since a mean amount of 98% of the total grain size is <0.06 mm (fine fraction) this fraction is separately displayed versus depth (Fig. 2.4). Accordingly, two typical features become obvious:

i) Unit 1 muddy sediments at site SL07 are of coarser composition in comparison to sites SL44 and SL49. However, we cannot explain this difference logically, even though all cores are located quite close to each other at the northern rim of the basin. Moreover, no distinct change in the basin morphology is observed. Thus, the only explanation might be, that this variability is caused by slightly variations of lateral bottom water current strength.

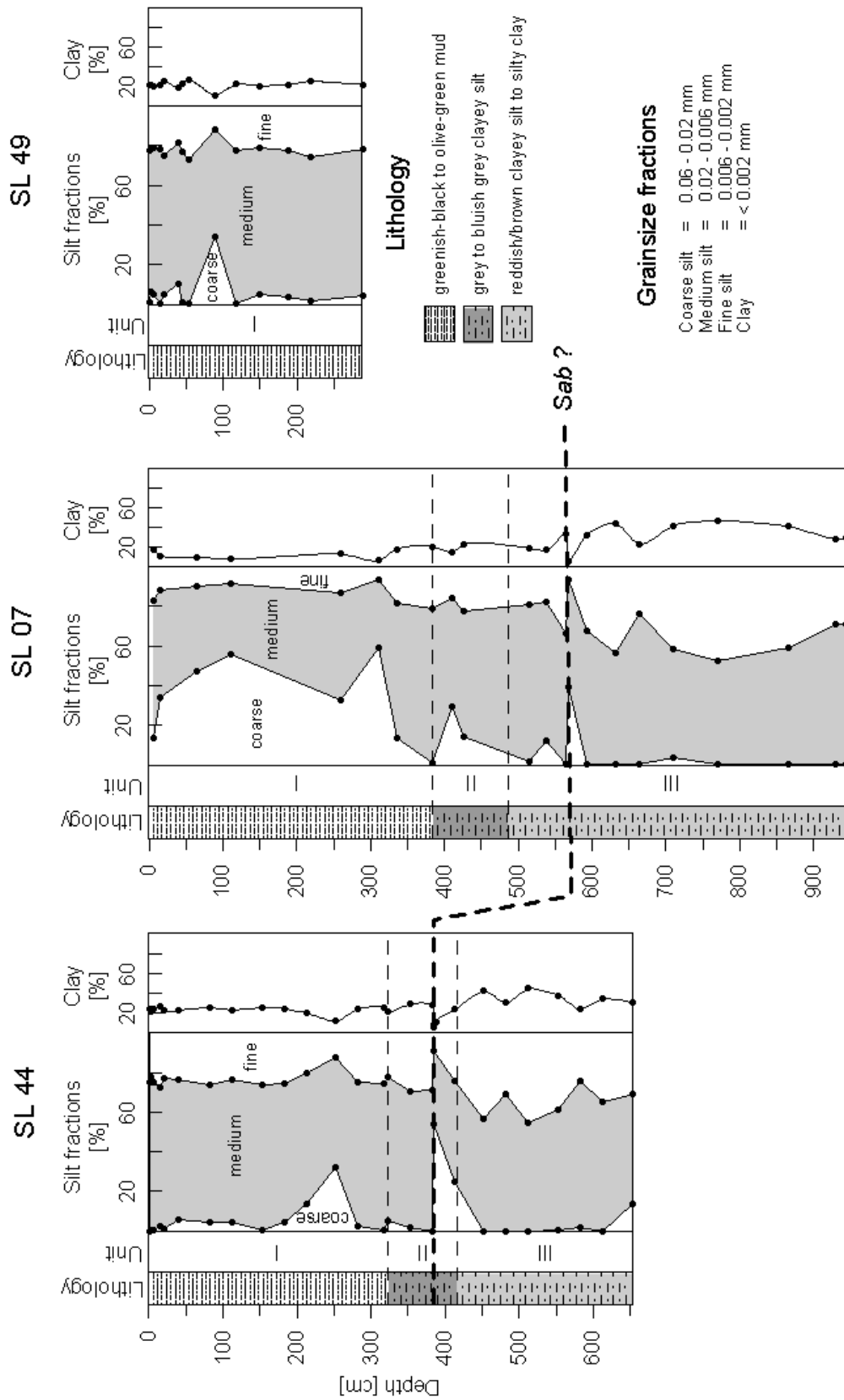


Fig. 2.4: Lithostratigraphy and proportions of coarse silt, medium silt, fine silt and clay for sites SL44, SL07, and SL49, respectively. The sandy layer Sab (Moros et al., 2002) is indicated by the bold dotted line.

ii) The second feature is that the sediments becoming finer with depth. This is indicated by an increasing fraction of clay sized material from about 20% in unit 1 and unit 2 deposits to values of 30-70% in reddish/brown unit 3 (Fig. 2.4). This change is found starting below a coarse grained layer at 384 cm and 569 cm at sites SL44 and SL07, respectively. However, as estimated above (see 3.1) these two sandy layers may correlate with the *Sab* reflector. Consequently, these layers represent the upper lithostratigraphic boundary of the Baltic Ice Lake deposits. In addition this sandy layer is found at core SL44 the in grey unit 2 and in reddish/brown unit 3 at site SL07, which is in good agreement with Moros et al. (2002) who postulated that the colour change may occur above or below *Sab* and hence do not represent a stratigraphic boundary.

Table 2.2: Summarised data of grain size analyses. The different macroscopic sedimentary units 1 to 3 are marked by different colours: white = unit 1 olive grey organic-rich mud; dark grey = unit 2 grey clayey silt; light grey = unit 3 reddish/brown clayey silt.

Sediment unit	n	>0.06 mm		0.06-0.002 mm		<0.002 mm	
		Range	Mean	Range	Mean	Range	Mean
all sediments	66	0-65,6	1,8	19,6-92,7	74,0	5,7-68,4	24,3
unit 1 (all)	36	0-10,2	0,9	72,2-87,1	78,6	6,7-27,3	20,5
unit 1 (SL44)	14	0-0,7	0,1	72,7-87,1	76,5	12,2-27,3	23,4
unit 1 (SL07)	8	0-10,2	3,3	79,0-86,5	83,4	6,7-21,0	13,3
unit 1 (SL49)	14	0-3,1	0,2	73,1-85,3	78,0	11,6-26,9	21,7
unit 2 (all)	6	0-6,0	1,7	70,4-91,1	77,2	8,6-29,6	21,1
unit 2 (SL44)	4	0-0,3	0,1	70,4-91,1	77,7	8,6-29,6	22,2
unit 2 (SL07)	2	3,7-6,0	4,9	73,7-78,6	76,1	15,4-22,6	19,0
unit 3 (all)	24	0-65,6	3,2	19,6-92,7	66,2	5,7-68,4	30,7
unit 3 (SL44)	10	0-3,3	0,7	54,9-92,7	72,4	5,7-45,1	26,9
unit 3 (SL07)	14	0-65,6	4,6	19,6-90,8	63,1	6,2-68,4	32,0

2.4.3 Physical properties

Results of wet bulk density, water content, and porosity determination are summarised in Table 2.4 and are listed up in detail in Table 2.5 (see Appendix).

Wet bulk densities range in general between 1.1 g cm^{-3} in the uppermost surface sediments and 2.01 g cm^{-3} in deeper layers (Fig. 2.5; Tabs. 2.4). In the olive green unit 1 mud wet bulk densities vary from 1.03 g cm^{-3} in uppermost surface sediments to 1.41 g cm^{-3} at the basis of this lithologic section. The grey clayey sediments (unit 2) are characterised by values of 1.32 to 1.64 g cm^{-3} with a maximum value of 1.89 g cm^{-3} in the sandy layer at the basis. Reddish/brown unit 3 bulk density varies between 1.10 and

2.01 g cm⁻³ caused by the typical intervals of sandy, silty, and clayey layers (Tab. 2.5, Appendix). The water content (Fig. 2.5) decreases with increasing depth from maximum values of 620 wt% at the top-most sediment surface in the olive green mud (unit 1) to about 70 wt% at depth in reddish/brown clayey sediments. However, values down to 22 wt% are found in silty and sandy layers of the grey and reddish/brown units. The porosity decreases from 93% at the water sediment interface in the greenish-black unit 1 deposits to about 60% at maximum sediment depth in the reddish/brown clays. Minimum values of up to 31% are correlated with silty/sandy layers of units 2 and 3, respectively (Fig. 2.5A).

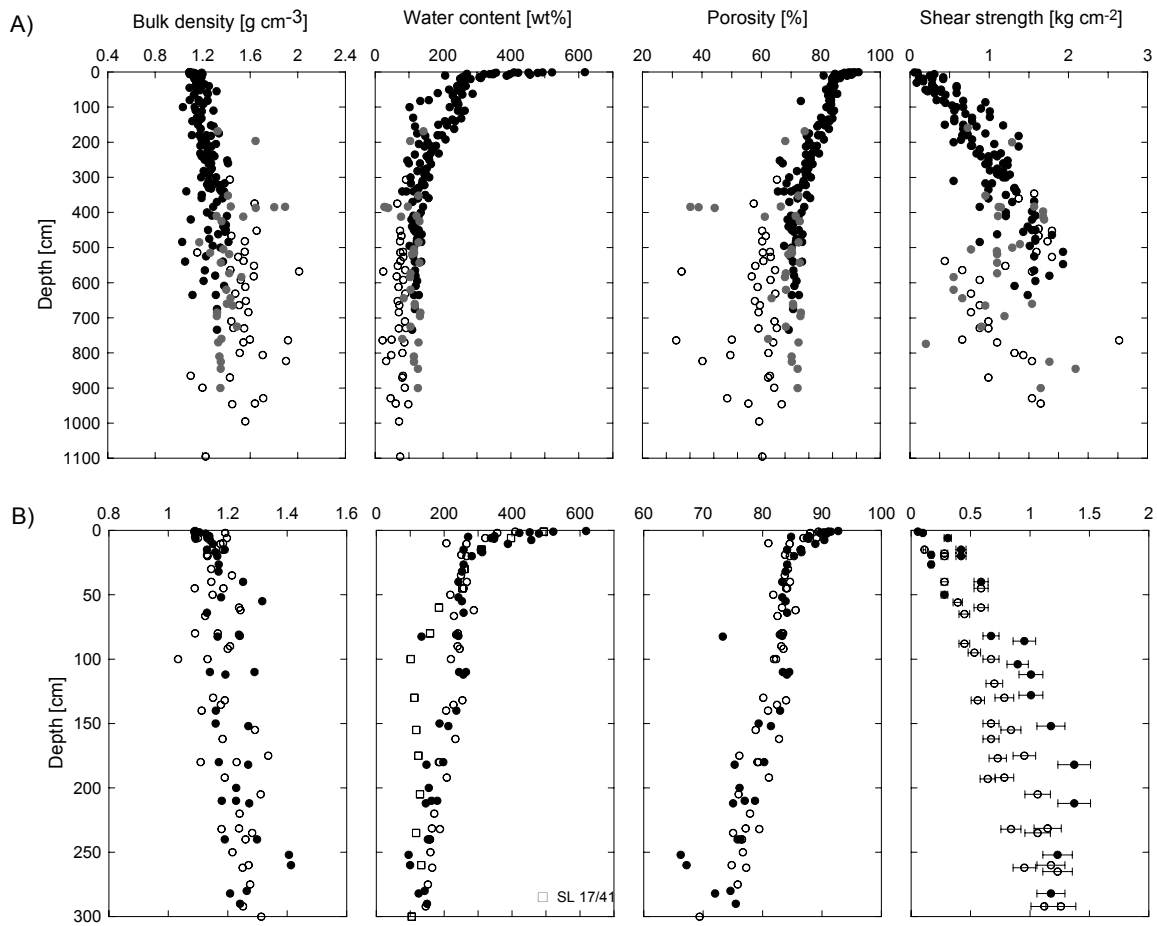


Fig. 2.5: **A)** Depth profiles of bulk density, water content, porosity and undrained shear strength of all cores taken at the northern rim of the Arkona Basin (for location see Fig. 1). The different colours give indication to the macroscopic sediment units: black dots = unit 1 olive grey organic-rich mud; dark grey dots = unit 2 grey clayey silt; open dots = unit 3 reddish/brown clayey silt. **B)** Depth profiles of the uppermost 300 cm sediment depth of bulk density, water content, porosity and undrained shear strength of cores taken in zones with acoustically transparent sediments (black dots) and in the zone with acoustic turbidity (open dots/symbols), indicating gas rich sediments. The estimated uncertainty for shear strength determinations of about 10% is indicated by error bars.

Sediment physical properties

Table 2.4: Summarised and averaged amounts of physical properties as water content, wet bulk density, porosity and shear strength from Arkona Basin sediments determined from cores SL02, SL44, SL22, SL07, SL35, SL15, SL17/41, SL14, SL49, and SL29 (from North to South). The different macroscopic sedimentary units 1 to 3 are marked by different colours: white = unit 1 olive grey organic-rich mud; dark grey = unit 2 grey clayey silt; light grey = unit 3 reddish/brown clayey silt.

Interval		Water Content		Wet Bulk Density		Porosity		Shear Strength	
cm	n	Range wt%	Mean wt%	Range g cm ⁻³	Mean g cm ⁻³	Range %	Mean %	Range kg cm ⁻²	Mean kg cm ⁻²
Aik 214 SL02									
0-100	7	133.2-617.9	347.6	1.09-1.18	1.13	73.3-92.7	85.9	0.168-0.952	0.392
153-206	2	103.4-142.3	122.9	1.33-1.64	1.48	68.1-74.6	71.3	0.728-1.288	1.008
206-556	5	65.5-91.1	76.9	1.43-1.64	1.52	57.5-65.2	61.1	1.372-1.792	1.593
Aik 201 SL44									
0-100	7	241.9-521.1	336.1	1.09-1.25	1.17	83.3-91.5	86.7	0.056-0.672	0.366
100-344	8	95.1-256.2	158.2	1.19-1.41	1.28	66.2-84.1	75.4	0.896-1.372	1.148
344-406	5	27.4-127.7	64.2	1.41-1.89	1.64	36.1-72.5	51.7	0.952-1.680	1.294
406-680	8	63.7-82.4	71.5	1.54-1.65	1.59	56.8-62.9	59.5	1.204-1.792	1.617
Po 266 SL22									
101-459	7	118.9-162.3	137.6	1.23-1.40	1.31	71.0-77.0	73.8	0.770-1.430	1.116
459-680	7	102.9-137.1	117.1	1.33-1.53	1.41	68.0-73.9	70.6	0.550-1.100	0.943
680-893	10	22.1-104.4	64.7	1.20-1.92	1.57	31.3-68.3	54.8	0.550-2.640	1.137
Po 266 SL07									
0-100	3	257.1-270.5	261.5	1.09-1.13	1.12	84.1-84.8	84.3	---	---
100-387	7	99.4-264.4	158.1	1.14-1.41	1.26	67.2-84.5	75.3	0.440-0.990	0.733
387-490	2	121.9-130.8	126.3	1.32-1.36	1.34	71.5-72.9	72.2	1.11	1.11
490-1120	17	24.1-97.9	75.4	1.10-2.01	1.49	33.2-66.9	59.8	0.440-1.650	1.054
Aik 201 SL35									
0-100	8	235.1-478.9	327.0	1.13-1.32	1.18	82.9-90.8	86.3	0.084-0.420	0.246
100-494	12	92.4-243.8	150.7	1.16-1.38	1.27	65.6-83.4	74.2	0.560-1.583	1.070
494-520	2	114.9-128.2	121.5	1.17-1.26	1.22	70.3-72.5	71.4	1.096-1.583	1.340
Po 266 SL15									
0-100	5	239.4-257.1	247.4	1.13-1.21	1.18	83.2-84.1	83.6	0.280-0.336	0.301
100-696	13	107.0-185.8	133.9	1.06-1.40	1.28	68.8-79.3	73.0	0.880-1.540	1.289
Aik 201 SL17/41									
0-100	8	101.4-493.2	269.7	1.09-1.24	1.13	82.3-91.0	85.5	0.588-0.672	0.616
100-635	13	101.4-132.2	118.3	1.11-1.38	1.26	67.6-80.1	73.1	0.700-1.583	1.201
636-775	4	80.1-132.2	108.4	1.32-1.49	1.40	62.3-73.2	68.6	0.201-1.193	0.811
Aik 214 SL14									
0-100	2	228.8-265.5	247.1	1.12-1.18	1.15	82.5-84.6	83.5	0.392-0.448	0.420
100-575	5	116.2-227.4	152.9	1.18-1.40	1.28	70.6-82.4	75.0	0.644-1.932	1.313
Aik 201 SL49									
0-100	8	245.5-409.2	307.6	1.09-1.24	1.17	83.5-89.4	86.1	0.112-0.532	0.280
100-332	7	127.9-253.6	188.5	1.18-1.27	1.22	72.5-83.9	78.9	0.560-1.316	0.892
Po 266 SL-29E									
0-100	3	206.5-219.8	214.7	1.03-1.18	1.12	81.0-81.9	81.6	0.252-0.588	0.411
100-735	14	109.1-205.6	143.5	1.03-1.32	1.20	69.2-80.9	74.3	0.660-1.760	1.176
735-901	5	114.2-128.0	121.8	1.33-1.35	1.34	70.2-72.5	71.5	1.650-2.090	1.833

Strong variations in the described physical properties versus depth are observed near the sediment surface (Fig. 2.5). Water contents and porosities are extremely high at the top-most 20 cm of sediments and in contradiction wet bulk densities are unusual low. However, similar values for density, water content and porosity are reported from western Baltic Eckernförde Bay muddy deposits by Brandes et al. (1996) and Silva et al. (1996). Keller (1982) also found unusual high water contents and low densities in continental slope deposits and suggested that these values are related to the high organic loading above 4%. Below about 20 cm sediment depth the values show a typical almost linear trend with depth in unit 1 and unit 2 sediments and this trend is most likely a function of depth (Silva et al., 1996). The above discussed increased fraction of coarse silt at site SL07 of unit 1 deposits could not be confirmed by wet bulk density investigations. However, distinctly diverging values are found in the reddish/brown unit 3 deposits (Fig. 2.5A), which may be the result of the observed increase of clay sized components. Moreover, high density values in combination with low porosities correlate with coarser clastic material in sandy/silty layers (Figs. 2.4, 2.5).

Focusing on unit 1 deposits (Fig. 2.5B) no general differences are observed in the lateral distribution of physical properties between samples from gas-rich sediments (indicated by acoustic turbidity) and non gassy sediments (cores taken in acoustically transparent sediments). This is in agreement with results presented from Eckernförde Bay containing similar fine grained, organic-rich, gassy sediments (Silva et al., 1996). However, the variations observed in the bulk density might represent greater error range with respect to sampling and analyses as a result of the very soft nature and high compressibility of the sediment. In addition expansion of the sediment might have occurred during recovery and sub-sampling caused by degassing at surface temperature and pressure conditions, which may also alter the sediment fabrics (Silva et al., 1996).

2.4.4 *Undrained shear strength*

The undrained shear strength show mean values of about 0.90 (0.06-1.93) kg cm⁻², 1.16 (0.20-2.09) kg cm⁻², and 1.29 (0.44-2.64) kg cm⁻² in the olive-green (1), the grey (2), and the reddish/brown (3) units, respectively (Tabs. 2.4, 2.5).

Silva et al. (1996) determined in Eckernförde Bay sediments a non-linear increasing shear strength with depth in the uppermost 50 cm of gas-rich mud. They further observed that the depth profile may become a linear character with greater depth. A linear shear

strength character is also obvious in the Arkona Basin organic-rich deposits of unit 1 and partly of unit 2 up to a depth of about 600 cm. Keller (1982) indicated on the one hand that the presence of organic carbon influences the physical properties, moreover that the shear strength show correlations with organic carbon concentrations of more than 4-5%. On the other hand he indicated that sediments containing less than 4-5% organic carbon do not show a distinct interrelationship between organic carbon and shear strength and that in these sediments other factors such as grain size and mineralogy have more pronounced influences on the strength properties of the sediment. At greater depth the shear strength decreases and fluctuate without any clear indication in unit 3 deposits. Hence, this might be a result of decreasing organic carbon content and increasing clay fraction, which may modify the sediment structure (Keller, 1982).

Shear strength variability is also observed by focusing on the organic-rich surface sediments and by comparing SU values determined at cores taken in acoustically transparent sediments with cores taken in the zone of acoustic turbidity (Fig. 2.5B). The latter ones show reduced values in a range of about 10-50%. According to Silva et al. (1996) a similar range of reduced values (15-40%) was found in the same core determined at “*in-situ*” pressure in an pressure chamber experiment and after decompression under 1 atm. Hence, the resulting SU reduction is caused by gas bubble formation under surface conditions and related in expansion of the sediment. Accordingly, Silva et al. (1996) implies for Eckernförde sediments, that shipboard shear strength values of these gassy sediments will tend to underestimate the true in situ strength, particularly in the gassy layer. Thus, the SU reduction found in gas-rich Arkona Basin sediments may also be related to sediment fabric modification due to the expansion under surface condition and could therefore not be related to in-situ sediment conditions.

2.5 Summary

This chapter presents a summary of macroscopic sediment description, grain size data, physical properties and shear strength determinations in the transition zone from acoustically transparent to acoustic turbid sediments of the Arkona Basin.

In general, the surface sediments of the Arkona Basin consist of silt, clayey silt, and silty clay, even though the deposits are from different geologic stages of the development of the Baltic Sea. Sedimentary unit 1 is characterised by organic-rich greenish mud and could be correlated with marine-brackish deposits accumulated since the Littorina

transgression some 8000 yr BP. Moreover, a sandy layer resulting from the final drainage event of the Baltic Ice Lake stage at 11300 yr BP could be identified by correlating grain size data and shallow seismo-acoustic profiles. A correlation of sub-sequences in the intermediate greyish sedimentary unit 2 to the Yoldia and Ancylus stages were not possible with the here presented data.

Physical properties as bulk density, water content and porosity were determined in the three macroscopic sedimentary units. No indications were found that the occurrence of acoustic turbidity is introduced by the alteration of physical properties. In addition it is shown, that slight variations in the undrained shear strength observed at cores taken in the acoustic turbid zone could not be correlated to in-situ gas bubble formation. Moreover, reduced shear strength values most likely result from the disruption of sediment fabric caused by depressurising during core retrieval and sub-sampling.

Chapter 3

Methane formation and distribution of acoustic turbidity in organic-rich surface sediments in the Arkona Basin, Baltic Sea

Olaf Thießen^{a,c}, Mark Schmidt^a, Friedrich Theilen^b, Manfred Schmitt^c, Gerald Klein^b

^a*Institut für Geowissenschaften der Universität Kiel, Abteilung Marine und Terrestrische Geochemie, Ludwig-Meyn-Str. 10, D-24118 Kiel, Germany*

^b*Institut für Geowissenschaften der Universität Kiel, Abteilung Geophysik, Otto-Hahn-Platz 1, D-24118 Kiel, Germany*

^c*Geochemische Analysen (GCA), Glückaufstr. 50, D-31319 Sehnde-Ilten, Germany*

Abstract

This study was performed to investigate gas formation and gas saturation conditions related to acoustic turbidity in shallow (~40 m deep) marine basins. The Arkona Basin, Baltic Sea, with its organic-rich fine-grained surface sediment provides an ideal “Natural Laboratory” for free gas determination with seismic, geoacoustic, and geochemical methods.

The area of acoustic turbidity covers the centre of the Arkona Basin by about 1500 km² and is related to a minimum thickness of 4-6 m of organic-rich surface sediment, covering the whole basin. Whereas seasonal lateral changes of the acoustic turbid area could not be observed, daily shifts of the solubility of methane mainly caused by atmospheric pressure drop may influence the upper boundary of acoustic turbidity in the sediment.

Highest concentrations of methane (7700 μmol L⁻¹ pore-water) exceeding the theoretical methane solubility at ambient temperature/salinity and pressure conditions were measured in the muddy surface sediment within the area of acoustic turbidity, whereas only 4 μmol L⁻¹ could be determined in muddy sediment outside the acoustic turbidity.

Stable carbon (about -80 to -90‰) and hydrogen (-143 to -185‰) isotope values of methane indicate that methane is exceptionally formed by bacterial CO₂ reduction in Arkona Basin surface sediments and rules out contributions from other sources. Moreover, stable isotope data and hydrocarbon ratios measured in gases derived from

muddy sediment and clay units (which underlay the organic-rich surface sediment), point to methane oxidation processes at the upper and lower boundary of the muddy sediment unit.

3.1 Introduction

The occurrence of hydrocarbon gas in shallow marine sediments is well known (e.g. Claypool and Kaplan, 1974; Bernard et al., 1978; Davis, 1992; Judd and Hovland, 1992). Beside carbon dioxide, hydrogen sulphide, traces of ethane and propane, methane is the only component found in considerable quantities in anoxic marine sediment (Claypool and Kaplan, 1974; Oremland et al., 1988). Methane accumulated in the sediment can be generated from different sources e.g. as thermogenic methane, which is derived from organic matter by thermal degradation (e.g. Bernard et al., 1976; Schoell, 1988), or as methane formed by bacterial processes during methanogenesis (e.g. Whiticar et al., 1986). Moreover, abiogenic methane derived from high temperature water/rock interaction is also found in venting fluids at the seafloor (e.g. Welhan, 1988; Botz et al., 1999). Methanogenesis occurs in sediments and soils when oxidants as O₂, NO₃, Fe, Mn and finally sulphate are depleted (e.g. Claypool and Kaplan, 1974; Martens and Berner, 1974; Whiticar, 1999). There are two major pathways of biogenic methane formation: bacterial carbonate reduction and acetate fermentation (Whiticar et al., 1986). Whereas carbonate reduction, with the general reaction:



is the dominant formation pathway in marine sediments, acetate fermentation is the dominant formation process in freshwater environments and can be expressed with the general reaction:



where the * indicates the intact transfer of the methyl group to the generated CH₄. However, it is assumed that trace amounts of methane could be generated by acetate fermentation in marine environments, when CH₄ formation by CO₂ reduction is inhibited by the occurrence of sulphate (Whiticar, 2002).

Methane concentration in interstitial waters of anoxic surface sediment is not only controlled by the actual production rate but also by its degradation, whereas the anaerobic microbial oxidation of methane (AOM) is the most effective degradation process of methane in marine surface sediments (e.g. Boetius et al., 2000). Moreover,

pressure, temperature, and salinity conditions control the maximum methane concentration which can be dissolved in pore-water (Abegg and Anderson, 1997; Wever et al., 1998). Oversaturation of methane e.g. induced by a drop in pressure or increasing temperature leads to bubble formation in the sediment.

Free gas is known to have a dramatic effect on physical properties of sediment and thus on sediment stability and geoacoustic properties (Anderson and Hampton, 1980a; Wilkens and Richardson, 1998). Acoustic turbidity, as recorded during seismo-acoustic surveys, is the most frequently cited evidence used to infer the presence of free gas in surface sediments (e.g. Fleischer et al., 2001).

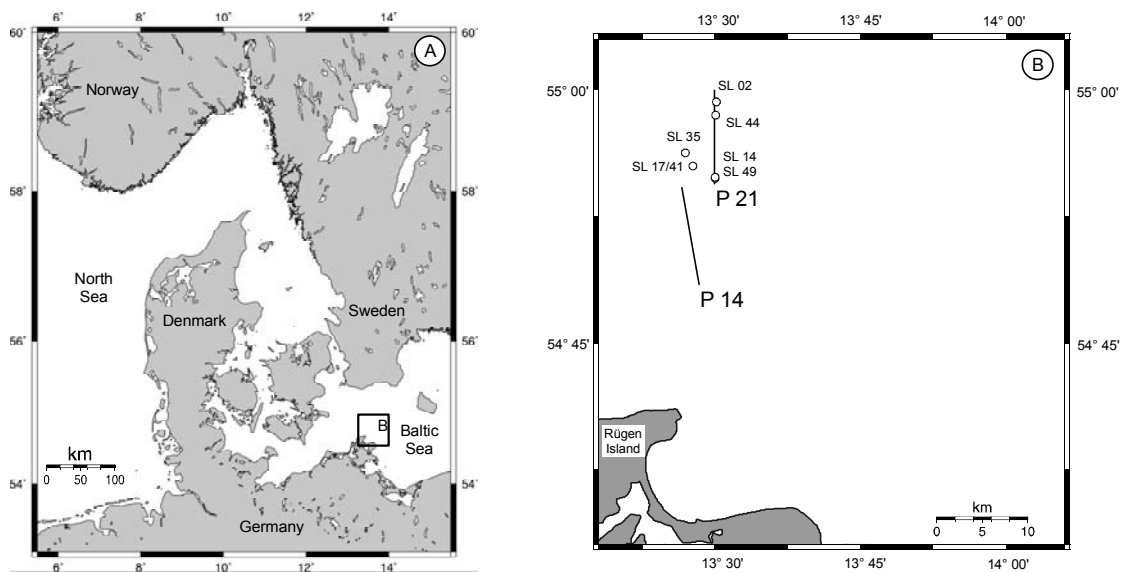


Fig. 3.1: **A** Overview of the western Baltic region with location of the study area Arkona Basin. **B** Arkona Basin with the locations of high-resolution seismic profile sections P 14 and P 21 (lines) and gravity cores SL02, SL14, SL17/41, SL35, SL44, and SL49 (open dots) taken during R.V. ALKOR cruises 201 and 214.

The Baltic Sea with its organic-rich surface sediment, high sea floor temperature variability, variability in salinity (from 20 PSU in the south-west up to 2 PSU in most northern part) and intermittent changing of oxic and anoxic conditions in the bottom water represents a “natural laboratory” to study sedimentary gas formation and its influence on surface sediment properties. Surface sediments in deep basins of the eastern Baltic Proper which lies under predominantly stagnant conditions were studied with respect to distribution of organic matter and diagenetic processes (e.g. Lein, 1983; Geodekyan et al., 1991; Piker et al., 1998; Schmaljohann et al., 1998). Based on early investigations of gassy sediments in the western Baltic Eckernförde Bay by Whiticar and Werner (1981) an intense investigation campaign with respect to acoustic properties,

methane concentration and oxidation was conducted in this narrow and shallow coastal bay during the Naval Research study Coastal Benthic Boundary Layer (CBBL) Program (Richardson, 1998). Acoustic turbidity, pockmarks and freshwater seepages were detected in the sampling area and could be related to methanogenesis (Wever and Fiedler, 1995; Wever et al., 1998; Martens et al., 1998; Whiticar, 2002).

Little is known about gas formation and gas accumulation processes in the Arkona Basin, which represents the connection between the shallow western bays and the deep eastern basins in the Baltic Sea (Lein, 1983; Geodekyan et al., 1991; Schmaljohann et al., 1998). Acoustic turbidity was detected in the Arkona Basin and in detail mapped during NATLAB (Natural Laboratory Baltic Sea) shallow seismic campaigns. A complex gas mixing situation in surface sediment was only postulated for this area because shallow gas could have been derived from deep Cambrian to Cretaceous source rocks (Rempel, 1992; Schlüter et al., 1997; Rempel and Schmidt-Thomé, 2004) and shallow bacterial methanogenesis (Geodekyan et al., 1991, Schmaljohann et al., 1998). Moreover, parameters, which control gas accumulation and free gas bubble formation in this area of the western Baltic Proper, where water depths of 40 m allow seasonal or even daily pressure/temperature/salinity variability are still unknown. Our study of physical and geochemical properties of surface sediment and the detailed molecular and stable isotope study on hydrocarbons aims to clarify the situation of gas sources and acoustic turbidity distribution in the Arkona Basin, Baltic Sea

3.2 Materials and methods

3.2.1 Study area

The area of investigation, the Arkona Basin, is situated on the western part of the Baltic Proper, in the transition zone from the shallow Belt Sea to the deep basins further east (Fig. 3.1). The investigations presented here are limited to the southern part of the Arkona Basin, located in the German territories south of 55°N. The survey area has a size of nearly 40 by 60 nautical miles with a maximum water depth of about 48 m. The hydrology of the brackish water body is dominated by estuarine circulation (Rheinheimer, 1995). However, intermittent inflowing of dense North Sea bottom water spilling over the shallow narrow Danish straits into the Arkona Basin led to a stratified water column and seasonal salinity variability of the bottom water between 10 and 20

PSU (Krauss and Brügge, 1991; Liljebladh and Stigebrand, 1996; Lass and Mohrholz, 2003).

The present morphology of the Arkona Basin was formed by Quaternary glacial processes, subsequent erosion, and limnic and marine Holocene sedimentation (Neumann, 1981; Lemke, 1998; Moros et al., 2002). In the central basin organic-rich muddy surface sediments with total organic carbon (TOC) concentrations of about 5-8 wt% (Moros et al., 2002; Chapter 4) are ubiquitous and anoxic conditions due to high biological oxygen demand are present in the uppermost centimetres below the sediment surface. The lithology of sediments change with increasing depth from marine - brackish silty mud to brackish and limnic silty clay with TOC concentrations decreasing to ~ 0.2 wt% within the limnic clay (Moros, et al., 2002; Chapter 4). The upper boundary of late glacial boulder clay, which characterises the subsurface morphology of Arkona Basin, is found at about -40 m sediment depth at the basin rim and at about -72 m in the centre of the basin (Lemke, 1998). However, at local highs, the uppermost till build up the sediment surface (Neumann, 1981; Lemke, 1998).

Table 3.1: Stations, sampling locations, water depth and recoveries from sediment cores taken during Alkor 201 and Alkor 214 cruises in the Arkona Basin, Baltic Sea.

Station	Position		Water Depth m	Recovery Gravity Corer m	Recovery Rumohr Corer m
	N	E			
Alkor 201					
SL 17/41	54°55.50'	013°27.70'	47.8	7.84	0.65
SL 35	54°56.29'	013°26.96'	46.0	5.30	0.66
SL 44	54°58.48'	013°30.07'	46.0	6.80	0.62
SL 49	54°54.80'	013°30.00'	47.8	3.52	0.65
Alkor 214					
SL 02	54°59.29'	013°30.14'	48.0	5.56	0.80
SL 14	54°54.81'	013°30.01'	48.0	5.75	---

3.2.2 Seismic investigations

Seismic data is compiled from some surveys with the German research vessels R.V. ALKOR and R.V. POSEIDON in the Arkona Basin. A Nautik UWAK 04 boomer source was used with source energy of 300 Joule. The frequency range was 500-6000 Hz (main frequency range of 600-2600 Hz) with a pulse length of 2-3 ms providing signal penetration depths of about 40 m and a theoretical resolution of 15-50 cm. The seismic reflections were recorded with a single hydrophone or a single channel mini-streamer. Differential GPS was used for navigation and positioning, providing an accuracy of

approximately 2-10 m. The acoustic turbidity zones are localised by relating shot numbers with GPS data. The interchange from acoustically transparent to acoustic turbid sediments is given with an accuracy of about 10-20 m (estimated by the shot frequency and ship's speed and positioning).

3.2.3 *Coring and sediment sampling*

Sediment cores were taken at six sites in the investigation area during Alkor 201 and Aklor 214 cruises (Fig. 3.1 and Tab. 3.1). Gravity cores (1 t) were taken with a 5.75 m stainless steel tube using inner PVC liners with an diameter (ID) of 125 mm. To obtain cores with a minimum disturbance of mushy surface sediments a small gravity corer, fitted with a 1 m long and 74 mm ID acryl glass liner and a weight of 30 kg (constructed by J. Rumohr, Kiel) was used additionally. The combination of cores taken at the same spot with different coring devices is done by water content analysis. Coring stations and total recovery of sediments are characterised in table 1.

Immediately after recovery of the gravity cores, the liners were cut into 1 m segments and sediment temperatures were measured at the base of each section. Bulk sediment samples (5-10 cm interval) of about 50-100 g for gas analysis were taken immediately after the sections were split into two halves and cooled down and stored in liquid nitrogen for post cruise gas analyses. Further sediment samples for gas analysis were collected by storing 5 cm³ of bulk sediment together with 10 ml of saturated sodium chloride solution in 21.5 cm³ headspace glass vials that were sealed with a butyl rubber septum and a crimped metal cap. The vials were stored dark at 4°C until post cruise gas analyses were performed. Simultaneous to sediment sampling for the gas analyses redox voltage measurements were done on the split cores.

Sampling of the uppermost surface sediments taken with the Rumohr corer, is done by keeping the liner upright and moving the sediment by a piston to the top of the liner, where sediment samples were taken as 1 cm thick slices or with 5 ml cut of syringes. Sediment temperature and redox potential measurements were performed at selected depths.

Samples for determination of water content, bulk density, porosity, total organic carbon and total nitrogen were taken at 30-50 cm intervals from homogenous sediments. Sampling resolution was higher near the sediment surface and where lithological changes could be indicated by colour and/or grain size changes. Sediment colour description was

done visually according to the Rock-Colour Chart (The Geological Society of America, 8th printing, 1995).

3.2.4 Redox potential measurement

Redox potential (E_H) was measured on board with Schott PT 5900A electrodes. Results are expressed in millivolt (mV). The electrodes were calibrated daily in a redox test solution (+470 mV platinum against Ag/AgCl). The error was within ± 10 mV. Readings of redox values were stable after 3 minutes.

3.2.5 Bulk density, water content and porosity determination

Bulk sediment density was determined by weighing a defined volume of bulk sediment and water content was calculated from weight loss after drying at 105°C for 24 hours. Porosities are calculated with density and water content data. The error of volume determination is estimated to be in the range between 1 and 5%. The volume error has to be considered in all calculations based on sediment or pore water volume determination.

3.2.6 Gas analysis

Gas was released from core samples by two different methods: (1) a modified vacuum extraction technique based on the method described by Faber and Stahl (1983), and (2) the commonly used headspace procedure (Albert et al., 1998). Gases were released under vacuum by defrosting, stirring (here without acid treatment) and salting out the gas from bulk deep-frozen sediment samples in method (1). However, in order to degas small sediment samples of about 20-50 g the method of Faber and Stahl (1983) was modified by using a “Mini-Blender” degassing apparatus (Schmitt and Thießen, 2003). In method (2) headspace vials were shaken for 24 h and equilibrated for 2 h prior gas chromatographic and mass spectrometric analyses.

Gas composition was analysed by using a Shimadzu GC 14A gas chromatograph equipped with a Poraplot Q capillary column and a flame ionisation detector (FID). Chromatographic responses are calibrated against pre-analysed standards, and based on daily replicate standard analyses; analytical precision is within $\pm 5\%$. The gas concentrations are reported in $\mu\text{mol L}^{-1}$ pore-water. During coring and sampling of muddy sediments gas loss was observed. Therefore measured methane concentrations has to be seen as minimum values. However, methane concentrations, variability and distribution still provide important information in Arkona Basin sediments. Saturation

limits of methane are calculated according to Yamamoto et al. (1976) by using measured sediment temperature, atmospheric pressure measured at the sampling day (987-1017 hPa), and a mean salinity in interstitial waters of the Arkona Basin of about 18 ppt (Chapter 4.). Gas wetness, expressed as methane to ethane + propane ratio (C_1/C_2+C_3), is calculated with volumetric concentrations determined by gas chromatography.

Stable carbon isotope values of methane were measured according to the method described by Faber et al. (1998) by using a continuous flow isotope ratio mass spectrometer (Europa 2020 – CF-IRMS). Hydrogen isotope composition of CH_4 was analysed according to Dumke et al. (1989). Carbon and hydrogen isotope data are reported in the common δ – notation and expressed in ‰ relative to the Pee Dee belemnite (V-PDB) and standard mean ocean water (V-SMOW), respectively. The analytical precision of analyses is $\pm 1\text{‰}$ for $\delta^{13}C$ and $\pm 4\text{‰}$ for δD .

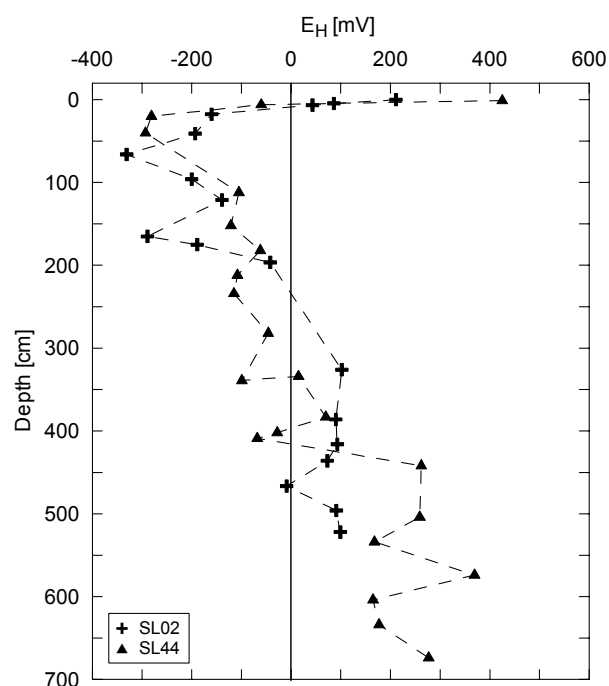


Fig. 3.2: Typical redox voltage (mV) profiles versus depth at core locations SL02 and SL44 where all three macroscopic sedimentary units were cored. Note the shift to positive redox values at about 330 cm depth in unit 2 and 3 silty-clays.

3.3 Results

3.3.1 Lithological description

The maximum sediment core recovery was of about 8 m and in general three different coloured sediment units are characteristic for all core stations (Tab. 3.1): (1) an uppermost greenish-black to olive-green homogenous silty mud unit with a characteristic smell of H_2S , (2) a lower grey to bluish-grey clayey silt to silty clay unit with typical

sandy layers of up to some cm thickness and black spots or zones coloured by iron sulphides, (3) a lowermost reddish/brown unit with mostly clayey sediments with typical sandy and/or silty layers of mm to cm thickness. Besides the uppermost mushy sediments a fluffy layer is present at the seafloor. The colour profile of the layer changes from brownish to dark olive grey within 1 cm merging into dark greenish black at about 4-6 cm below sea floor. H₂S smell was observed below 6 cm sediment depth which became very intense with increasing depth.

Table 3.2: Redox voltage (E_H) values and calculated redox gradients in Arkona Basin surface sediments. The different macroscopic sedimentary units 1 to 3 are marked by different colours: white = unit 1 olive grey organic-rich mud; dark grey = unit 2 grey clayey silt; light grey = unit 3 reddish/brown clayey silt. Cores taken in the zone with acoustic turbidity as indication for free gas in the sediments are pointed out with a "G".

Station Depth cm	E _H mV	Redox gradient mV cm ⁻¹	Station Depth cm	E _H mV	Redox gradient mV cm ⁻¹	Station Depth cm	E _H mV	Redox gradient mV cm ⁻¹	Station Depth cm	E _H mV	Redox gradient mV cm ⁻¹
Alkor 201 – SL44			Alkor 201 – SL35			Alkor 201 – SL17/41 "G"			Alkor 201 – SL49 "G"		
1	425	---	1	363	---	1	343	---	1	353 ¹⁾	---
6	-60	97.0	8	-265	96.6	6	-205	109.6	3	-229	388.0
20	-281	37.2	31	-237	20.3	15	-283	44.7	18	-301	38.5
40	-293	18.4	51	-259	12.6	45	-405	17.0	21	-270	31.9
112	-105	4.8	55	-316	12.6	60	-393	12.5	41	-247	15.2
152	-121	3.6	81	-343	8.8	130	-330	5.2	65	-283	9.9
182	-62	2.7	110	-273	5.8	155	-346	4.5	133	-209	4.3
212	-108	2.5	140	-340	5.1	175	-329	3.9	163	-210	3.5
234	-115	2.3	180	-309	3.8	235	-303	2.8	193	-247	3.1
282	-46	1.7	210	-263	3.0	260	-316	2.5	263	-124	1.8
339	-99	1.6	240	-259	2.6	300	-268	2.0	293	-142	1.7
334	15	1.2	280	-327	2.5	340	-151	1.5	---	---	---
383	70	0.9	317	-234	1.9	495	-131	1.0	---	---	---
402	-28	1.1	340	-201	1.7	525	-202	1.0	---	---	---
409	-68	1.2	370	-266	1.7	565	81	0.5	---	---	---
442	262	0.4	409	-184	1.3	595	53	0.5	---	---	---
504	259	0.3	440	-179	1.2	635	-31	0.6	---	---	---
534	168	0.5	475	-201	1.2	695	-173	0.7	---	---	---
574	369	0.1	515	-126	1.0	725	-550	1.2	---	---	---
604	165	0.4	---	---	---	---	---	---	---	---	---
634	177	0.4	---	---	---	---	---	---	---	---	---
674	277	0.2	---	---	---	---	---	---	---	---	---

¹⁾estimated mean value from SL 35 and SL 17/41 for redox gradient calculations

3.3.2 *Sediment redox conditions*

Redox voltage (E_H) values of about +340 mV to +425 mV at the sediment surface decreases to values of about less than -200 mV at 6 cm sediment depth (Tab. 3.2). A minimum value of about -400 mV was measured at 45 cm depth. The redox potential became more positive again at depth below about 100 cm and positive redox voltage between +20 and +370 mV could be measured within the grey/bluish-grey unit (2) and reddish/brown unit (3) at sediment depths below about 330 cm at stations Alk 201-SL44 and Alk 214-SL02, respectively (Fig. 3.2). Redox voltage gradients vary of about 100 mV/cm in uppermost 6-8 cm of surface sediments in cores taken outside and at the beginning of the acoustic turbid zone and up to about 390 mV/cm in uppermost 3 cm of surface sediments with intense acoustic turbidity (Tab. 3.2).

3.3.3 *Acoustic turbidity and sediment gases*

Acoustic turbidity in the Arkona Basin could be detected at SE-NW and N-S elongated seismic profiles P14 and P21, respectively (Figs. 3.3 and 3.4). Typically the onset of acoustic turbidity is indicated by deepening of the first strong seismic reflector (Fig. 3.4). A more or less coherent acoustic turbid area is defined in the centre of the Arkona Basin when seismic profiles recorded on Alkor 160, Alkor 201 and Poseidon 266 cruises are also considered (Fig. 3.5). However, small spots ($\sim 400 \text{ m}^2$) without acoustic turbidity were detected inside the central acoustic turbidity area when the upper strong subsurface reflector (boulder clay; Mathys et al., 2005) is approaching the sediment surface as seen in Figs. 3.3 and 3.4). On the other hand patches of acoustic turbidity occur outside of the central acoustic area in the outer rim of the Arkona Basin where generally acoustic transparent sediments occur. The patches are characterised by local depressions in the subsurface morphology (Fig. 3.3). Local subsurface depressions with acoustic turbidity could be determined mainly northeast and south of the central acoustic turbid area (Fig. 3.5).

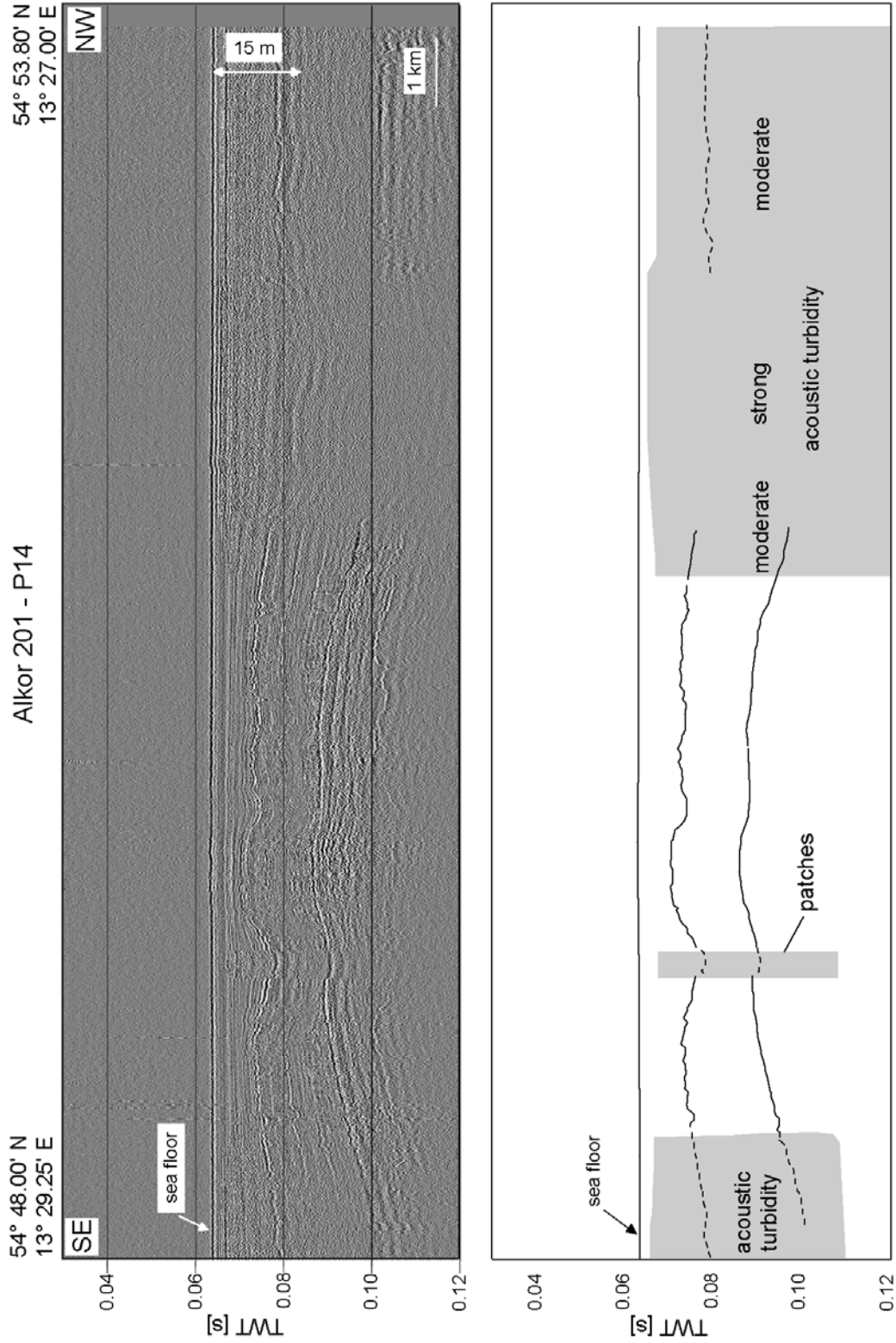


Fig. 3.3: SE-NW Boomer profile P14 with interpretative sketch (below). Note the local shallow depression in the subsurface morphology accompanied by acoustic turbidity (shaded area). For better visibility of the subsurface morphology two main reflectors are pointed out. A high resolution correlation of the reflectors to sedimentary units is given by Mathys et al. (in press.). TWT = two way travel time.

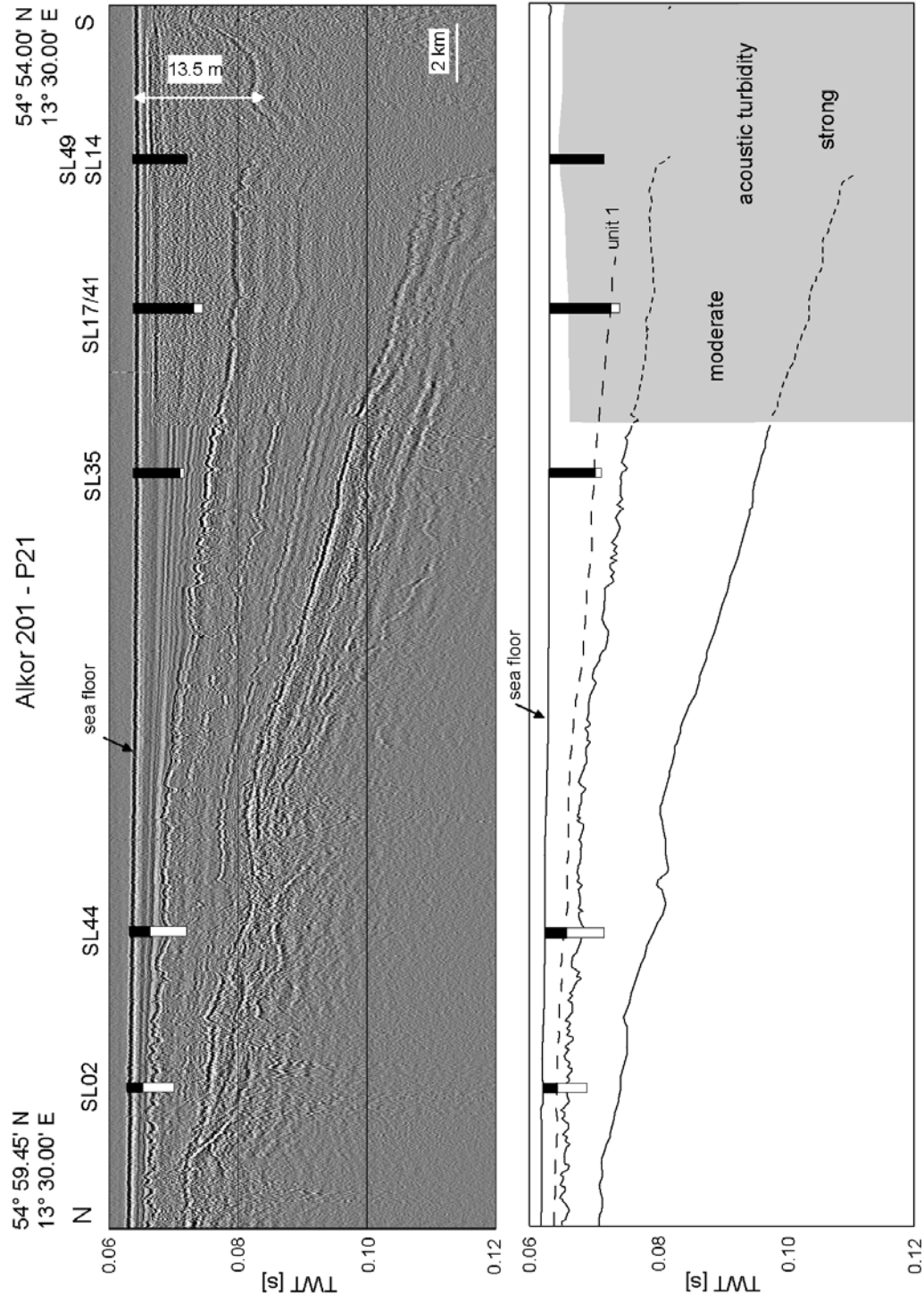


Fig. 3.4: N-S Boomer profile P21 with interpretative sketch (below) and with core locations SL02, SL44, SL35, SL17/41 and SL49 (SL14). The sediment thickness of unit 1 sediment is marked by black bars at all core locations and interpolated in between by the dotted line. The shaded area marks the occurrence of acoustic turbidity. For better visibility of the subsurface morphology two main reflectors are pointed out. A high resolution correlation of the reflectors to sedimentary units is given by Mathys et al. (in press.). TWT = two way travel time.

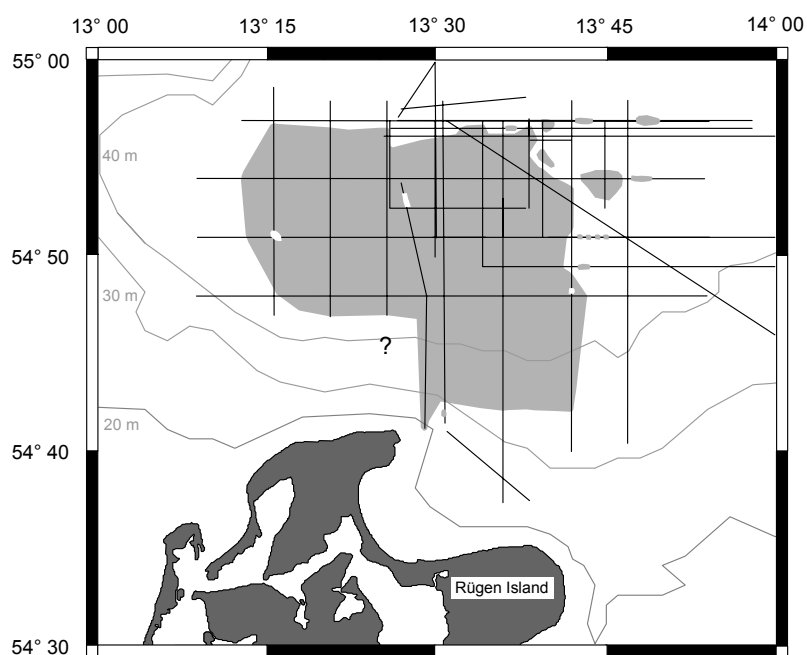


Fig. 3.5: Estimated acoustic turbidity zone (ATZ; light grey shaded area) as interpreted from seismic profiles acquired in the Arkona Basin. The recent morphology of the basin is indicated by the 30 m and 40 m isobaths.

Methane concentrations measured in cores along the seismic profiles P21 (Fig. 3.1) represent gas data in a transition from acoustic transparent to acoustically turbid sediments (Fig. 3.4). Pore water methane concentrations are presented in table 3 and reflect high variability in surface sediments of the Arkona Basin (Fig. 3.6). Two different regimes could be characterised: 1) overall low CH_4 concentrations near the detection limit between 0.5 and $5 \mu\text{mol L}^{-1}$ within the whole sampled sediment column at stations SL02 and SL44 and 2) increasing CH_4 concentrations from less than $10 \mu\text{mol L}^{-1}$ at the sediment surface up to a peak concentration of about $7600 \mu\text{mol L}^{-1}$ at about 100 cm depth at stations SL35, SL17/41, SL49 and SL14 (Fig. 6). The concentrations vary with depth below the highest concentration peak between 2000 and $6000 \mu\text{mol L}^{-1}$. $\text{C}_1/(\text{C}_2+\text{C}_3)$ gas ratios vary between 10 and 1000 in sediments with very low methane concentrations, both near the sediment surface and in deeper sediment depth, and between 1000 and about 90000 in sediments with a high CH_4 yield (Tab. 3.3, Fig. 3.7). Stable isotope values of methane range in general between -92 and about -70‰ for $\delta^{13}\text{C}$ and between -185 and -124‰ for δD , respectively (Tab. 3.4). However, in the uppermost surface sediments of cores SL35 and SL17/41 a methane carbon isotope shift to more positive values of -62 and -43‰ , respectively, was determined (Fig. 3.7).

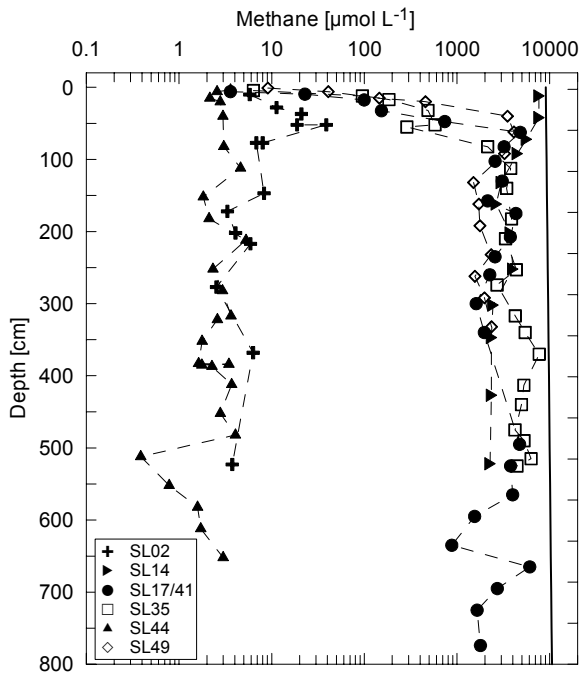


Fig. 3.6: Methane concentrations versus depth at core locations SL02, SL14, SL17/41, SL35, SL44, and SL49. The solid line indicates calculated mean methane solubility limit at 48 m water depth under normal pressure and temperature conditions during Mai sampling campaign Alk201. Note the two regimes: **a** low methane concentrations $<10 \mu\text{mol L}^{-1}$ pore-water in the entire sediment column; **b** strong increasing methane concentrations with depth to values $>1000 \mu\text{mol L}^{-1}$ pore-water.

Fig. 3.7: Molecular $C_1/(C_2+C_3)$ gas ratios (filled symbols) and $\delta^{13}\text{C-CH}_4$ values (open symbols) versus depth of stations SL17/41 (dots) and SL35 (squares) from the transition zone from acoustically transparent to acoustically turbid sediments.

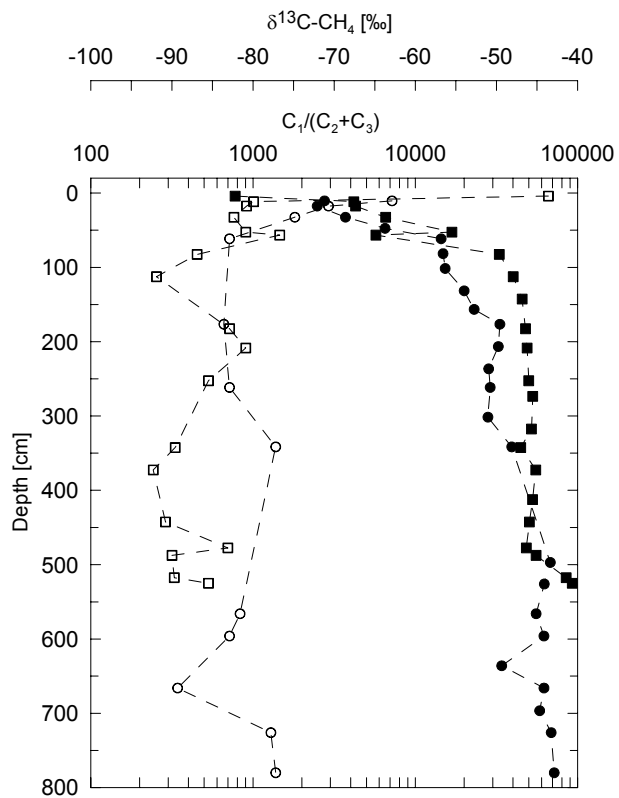


Table 3.3: Methane concentrations and “Bernard” ratios at stations SL02, SL44, SL35, SL17/41, SL49 and SL14 from Arkona Basin sediments. The different macroscopic sedimentary units 1 to 3 are marked by different colours: white = unit 1 olive grey organic-rich mud; dark grey = unit 2 grey clayey silt; light grey = unit 3 reddish/brown clayey silt. Cores taken in the zone with acoustic turbidity as indication for free gas in the sediments are marked with “G”.

Station Depth cm	Methane $\frac{C_1}{C_2+C_3}$ $\mu\text{mol L}^{-1}$	Station Depth cm	Methane $\frac{C_1}{C_2+C_3}$ $\mu\text{mol L}^{-1}$	Station Depth cm	Methane $\frac{C_1}{C_2+C_3}$ $\mu\text{mol L}^{-1}$	Station Depth cm	Methane $\frac{C_1}{C_2+C_3}$ $\mu\text{mol L}^{-1}$	Station Depth cm	Methane $\frac{C_1}{C_2+C_3}$ $\mu\text{mol L}^{-1}$
10	6 248	4	4 8	4	6 776	3	4 1125	1	9 185
28	11 805	7	3 33	12	95 4179	11	23 2759	6	41 374
37	21 1086	16	2 31	18	184 4286	18	100 2485	15	145 452
52	39 737	21	3 28	33	485 6563	33	153 3710	20	456 1289
77	8 169	41	3 32	53	579 16799	48	737 6511	40	3496 8748
147	8 171	82	3 29	57	288 5707	62	4804 14420	62	4096 8356
172	3 65	112	5 34	83	2140 32908	82	3216 14824	92	3253 7504
202	4 146	152	2 32	113	3788 40092	102	2576 15282	132	1503 8150
217	6 113	182	2 33	143	3431 45514	132	3072 19988	162	1717 8043
277	3 128	212	5 38	183	3872 47761	157	2136 23054	192	1763 12539
368	6 107	252	2 29	209	3334 48870	177	4317 33205	232	2335 12412
523	4 99	282	3 26	253	4355 50023	207	3754 32464	262	1560 7739
---	---	317	4 36	274	2697 52902	237	2569 28317	292	1973 10272
---	---	322	3 38	318	4244 52014	262	2252 28955	332	2351 6737
---	---	352	2 63	343	5433 44692	302	1607 28023	---	---
---	---	383	2 52	373	7701 55362	342	1965 39265	---	---
---	---	384	3 67	413	5254 52778	497	4732 67912	---	---
---	---	385	2 97	443	4957 50488	526	3780 62392	---	---
---	---	387	2 96	478	4219 48300	566	3979 55529	---	---
---	---	412	4 87	488	5277 55487	596	1549 62044	---	---
---	---	452	3 92	518	6291 85007	636	876 34080	---	---
---	---	482	4 112	525	4440 92841	666	6084 62121	---	---
---	---	512	0.4 73	---	---	697	2716 58417	---	---
---	---	552	1 61	---	---	726	1643 68780	---	---
---	---	582	2 85	---	---	780	1787 71799	---	---
---	---	612	2 68	---	---	---	---	---	---
---	---	652	3 54	---	---	---	---	---	---

3.4 Discussion

3.4.1 Lateral occurrence of acoustic turbidity

The macroscopic easily distinguished sediment units 1, 2 and 3 in Arkona Basin are consistent with the lithostratigraphic subdivision of Neumann (1981) and are reflecting different stages of the late- to post-glacial evolution of the Baltic Sea (i.e. Jensen, 1992; Björck, 1995; Lemke, 1998; Jensen et al., 1999; Emeis et al., 2002). According to the previous mentioned authors unit 1 olive-green silty muds (Fig. 3.4) corresponds with Littorina stage, post Littorina and recent sedimentation and represent deposits of marine – brackish conditions during the last 8000-8300 yr BP. Unit 2 grey to bluish grey silty clays, however, covers sediments from limnic and brackish Ancylus Lake, Yoldia Sea and the Baltic Ice Lake stages and the latter limnic sediments are found in unit 3 reddish/brown silty clays as well. However, unit 2 and unit 3 deposition sequences range from about 13000 cal. yr BP to the onset of the Littorina transgression at about 8000-8300 yr BP (Emeis et al., 2002).

More recent high resolution stratigraphical studies by Moros (1999) and Moros et al. (2002) presented a new subdivision for the sedimentation period from about 13000 cal. yr BP to 6500 cal. yr BP with the Ancylus Lake, Yoldia Sea, Yoldia Lake and Baltic Ice Lake I and II stages. Subdivisions, especially in the grey/bluish grey and reddish/brown silty clays, are separated by typical sandy or silty layers, which reflect erosional events in the Baltic Ice Lake, Yoldia Lake, Yoldia Sea and Ancylus Lake stages. Moreover the authors estimate that the colour change from unit 2 to unit 3 sediments, from grey to reddish/brown, is due to diagenetic processes and therefore does not represent a lithostratigraphic boundary caused by changing sedimentation. However, the typical sandy layers are characteristic in the deepest part of the Arkona Basin, but may be absent at the rim or at local highs probably caused by hiatuses. This is clearly seen in Figs. 3 and 4, when shallow reflectors wedge out at subsurface highs. Moreover, at coring sites sediments are not analysed with this high resolution, that all units or subunits could be distinguished. Therefore we use in the following the macroscopically distinguished units 1 to 3. In general, the sediments cored western Baltic Sea Arkona Basin reflect about 11000 years of late- and post-glacial sedimentation.

Recent morphology of the southern part of the Arkona Basin (south of 55° N, German territories) is smooth and the basin is more or less characterised by the 40 m isobath by a maximum water depth of about 50 m. However, after Neumann (1981) and

Lemke (1998) this is a result of late- and post-glacial sedimentation, which filled up subsurface glacial morphology. Highest smoothing effects are govern by unit 1 sediments, which result in sediment thickness variability of about 0-2 m at the basin rim or at local highs of the lying till and of more than 12 m thickness in the centre of the southern part of the basin (Lemke, 1998). This is confirmed regarding seismic profiles P14 and P21 (Figs. 3.3 and 3.4), when subsurface morphology is smoothed by younger deposits. Following unit 1 sediments on profile P21 (Fig. 3.4), the deposit thickens from about 150 cm (SL02), over 494 cm (SL35) to 648 cm (SL17/41) from North to South. At southernmost station SL14 about 577 cm of silty unit 1 muds are recovered (Fig. 3.4).

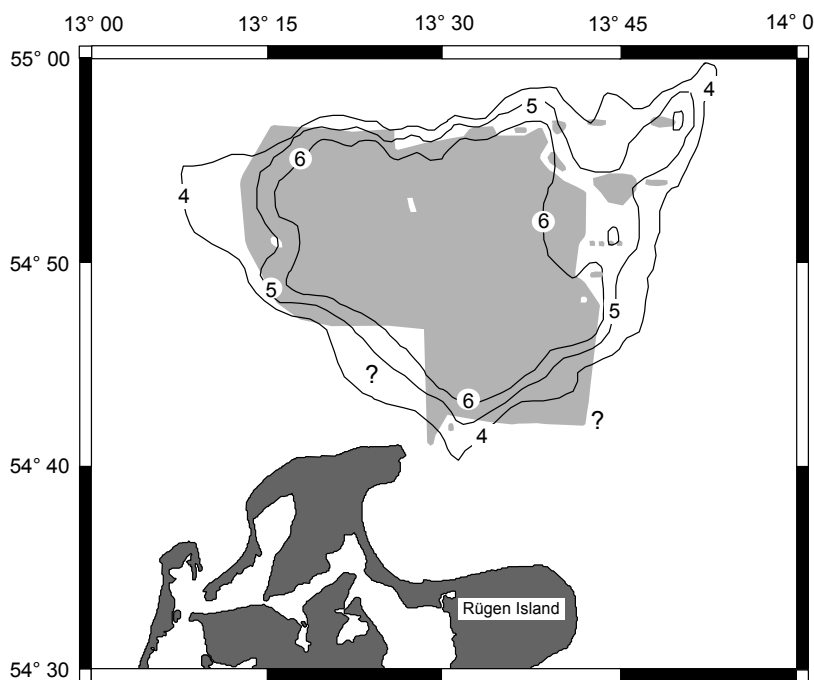


Fig. 3.8: Comparison of the acoustic turbidity area (light grey shaded area) with the sediment thickness of unit 1 (brackish to marine muddy sediment). Contour lines of 4, 5 and 6 m of unit 1 sediment thickness are plotted according to E5 unit defined by Lemke (1998).

Next important features on profiles P14 and P21 (Figs. 3.3 and 3.4) are the zones with acoustic turbidity. As indicated above, acoustic turbidity built up a more or less coherent zone in Arkona Basin sediments between 54° 41' N and 54° 57' N and between 013° 13' E and 013° 43' E. Some very small local exceptions of acoustically transparent sediments within this region are investigated in the centre and at the western rim and are indicated in figure 3.5 as white spots. Typical for these locations are updoming deeper reflectors combined with thinned near surface late-glacial and post-glacial sediments (Fig. 3.3). This is comparable with gently inclining deeper reflectors at the Northern rim of the investigation area, when sediments with acoustic turbidity change into acoustically transparent sediments (Fig. 3.4). Conversely, however, some spots with limited acoustic

turbidity are found in general transparent sediments, mainly in the NE and S region of the investigation area (Fig. 3.5). Here local spots with turbidity are combined with shallow depressions in subsurface morphology. Such an acoustic turbidity spot in combination with a shallow depression is seen as well in profile P14 (Fig. 3.3). In general, the onset of acoustic turbidity seems to be coupled to sediment thickness of post-glacial muddy deposits (unit 1).

Knowing that post-glacial sediments thicken from the rim of the sub-basin towards the centre (Neumann, 1981; Lemke, 1998) the area of acoustic turbidity is compared with the recent morphology of the Arkona Basin, indicated by the 40 m isobaths (Fig. 3.5). It is obvious from figure 3.5 that the area of acoustic turbidity does not fit the recent morphology. However, organic rich unit 1 sediment thickness isolines of 4, 5 and 6 m (Lemke, 1998), fits reasonably well with the acoustic turbid area (Fig. 3.8). The coherency from 4-6 m sediment thickness of unit 1 sediments (E5 in Lemke, 1998) and the occurrence of acoustic turbidity is confirmed by lithological data, when the lateral onset of acoustic turbidity lies between about 4.9 and 6.5 m sediment thickness of unit 1 deposits determined from cores SL35 and SL17/41, respectively. Therefore it is obvious, that acoustic turbidity is coupled to the thickness of organic-rich muddy unit 1 sediment (Tab. 3.2). This finding is in agreement with results reported by Whiticar (2002) from Western Baltic Sea Eckernförde Bay. Even when the water depth in Eckernförde Bay does not exceed 25 m, the acoustic turbidity is restricted to the central bay (> 10 m water depth) fine grained organic-rich (4-5 wt%) muds, similar to the unit 1 sediments described above from Arkona Basin. Whiticar (2002) points out that acoustic turbidity occurs in Eckernförde Bay when sediment thickness of organic rich muds reach about 800 cm and that the vertical onset of turbidity is found at around 2-4 m below the sediment surface. In Arkona Basin sediments acoustic turbidity occurs vertically at about 1.2-1.7 m (Fig. 3.4) sediment depth (Mathys, 2003) and when sediment thickness reach about 400-600 cm (Fig. 3.8). Hence, a shallower onset of acoustic turbidity, a minor minimum thickness of the organic-rich mud sequence, and a greater water depth and therefore higher gas solubility possibly indicate a higher methane production rate in Arkona Basin sediments compared to the Eckernförde Bay.

There is also some preliminary information on the occurrence of acoustic turbidity in the Gotland Basin, eastern Baltic Proper (Geodekyan et al., 1991; Endler, 1998). Acoustic turbidity could not be detected in the muddy sediments of the 240 m deep

central basin, but local features of acoustic turbidity occurred in Littorina age to recent muddy deposits at the NE-slope and in a local basin on the NE-shoulder in 60-80 m water depth (Endler, 1998). Moreover, acoustic turbidity was detected at some places in the deeper part of the Gotland Basin in combination with pockmarks or down-cuts (Geodekyan et al., 1991; Endler, 1998). The vertically onset of acoustic turbidity is generally at about 1-3 m below sediment surface (Endler, 1998), which is comparable with the onset depth determined from seismic profiles in the Arkona Basin (Mathys, 2003). The higher pressure in the Gotland Deep sediments, however, probably prevents formation of a large area of free gas bubbles in the surface sediments like it is observed in the Arkona Basin. However, places of focussed gas venting (pock marks), or free gas accumulation in 60-80 m shallow sub-basins indicate even higher gas formation rates than they are assumed for the Arkona Basin surface sediment.

3.4.2 *Gas accumulation*

In the central Arkona Basin organic-rich muddy sediments (5-8 wt% TOC; Moros et al., 2002), suboxic to anoxic conditions ($E_H < 0$) are common within the uppermost cm below the seafloor (Tab. 3.2; Figs. 3.2 and 3.9). Anoxic conditions are also indicated by the colour shift from brownish to greenish black sediments directly beneath the sediment surface. In anaerobe sediments strong increasing concentrations of pore-water methane with sediment depth indicate that sulphate is depleted and that methanogenesis occurs (Whiticar et al., 1986). This is obvious regarding the methane concentration profiles from stations SL35, SL17/41 and SL49 (Fig. 3.9; Tab. 3.3). Moreover, the sediment depth at which methanogenesis occurs and the methane concentration exceeds $1000 \mu\text{mol L}^{-1}$ decrease from 82 cm over 62 cm to about 40 cm at stations SL35, SL17/41 and SL49, respectively. The decreasing depth of the zone of methanogenesis correlates with the transition from acoustically transparent sediments, over moderate acoustic turbidity near the sharp demarcation from non turbid to turbid sediments to zones with intense acoustic turbidity (Fig. 3.4) and probably rather indicates higher methane production to the centre of the acoustic turbidity area than less intense oxidation of methane in the sulphate zone. In addition, at stations SL17/41 and SL49 the depths at which maximum methane concentration was found (62 and 40 cm, respectively) was compared with the onset depth of acoustic turbidity below the sediment surface (160 and 120 cm, respectively; Mathys, 2003). A difference of about 100 cm (80 cm) between methane peak concentration (i.e.

methane oversaturation) and the vertical onset of the acoustic turbidity was also determined in muddy sediments of Eckernförde Bay by Abegg and Anderson (1997). The authors assume that in this area, between theoretical gas bubble formation and the onset of acoustic turbidity, only a few small bubbles are formed and these do not affect the acoustic properties of the sediment significantly that acoustic blanking occurs.

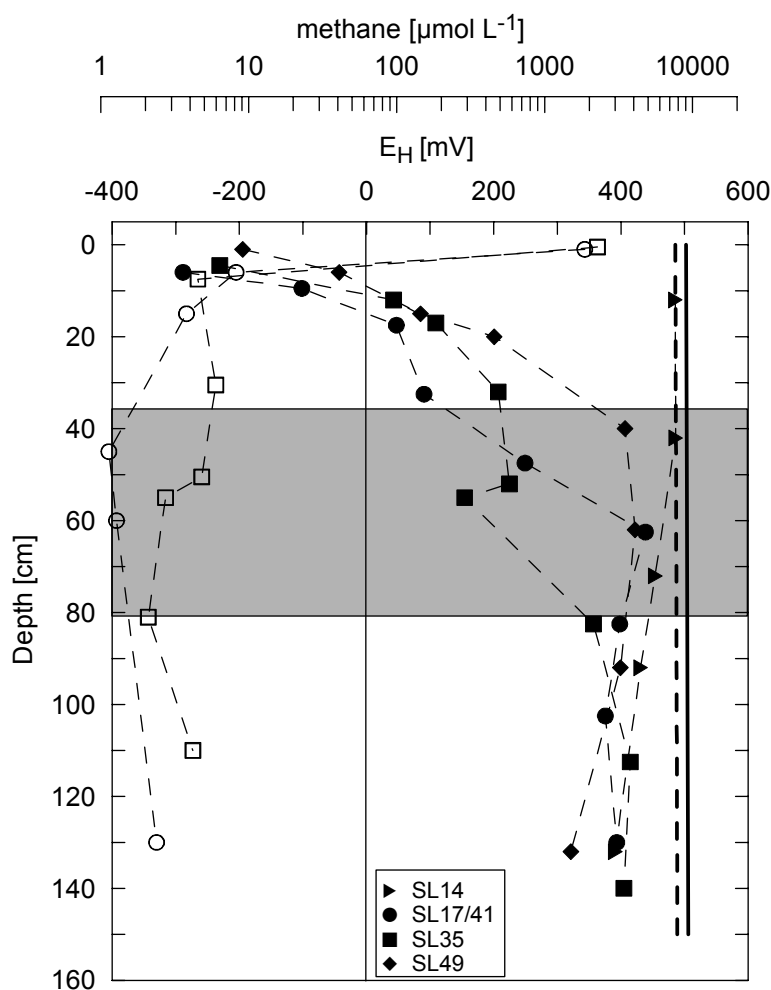


Fig. 3.9: Detailed 160 cm depth section of muddy surface sediments showing methane concentrations (filled symbols) and redox voltage (E_H) values (open symbols) versus depth in Arkona Basin for cores SL14, SL17/41, SL35, and SL49, respectively. The shaded area marks the decreasing depth interval at which methane concentration exceeds $1000 \mu\text{mol L}^{-1}$ pore-water in the transition zone from non turbid to acoustically turbid sediments for stations SL17/41, SL35, and SL49, respectively. The bold black line indicates calculated methane solubility limit under normal temperature, depth and pressure conditions (May R.V. ALKOR 201 cruise). The dotted line represents the methane solubility shift caused by short term atmospheric and seasonal temperature and salinity variations (October R.V ALKOR 214 cruise).

In our study methane concentrations of the acoustic turbidity zone of Arkona Basin reach values of up to about $7700 \mu\text{mol L}^{-1}$ (Tab. 3.3), which is comparable to one published concentration value of about $8900 \mu\text{mol L}^{-1}$ in 1 m sediment depth in the acoustic turbid region of Arkona Basin (Geodekyan et al., 1991). The highest measured methane concentrations of stations SL35, SL17/41 and SL49 plot near but are less than the theoretical calculated methane saturation limits (Fig. 3.9). The only site where measured methane concentrations exceed the theoretical solubility is core SL14 taken at

the same location as SL49 (Fig. 3.4). However, gas bubble formation is indicated by acoustic turbidity for sites SL17/41, SL49, and SL14 (Fig. 3.4). Although gas sampling procedures were optimized we have to account gas loss during core retrieval and sediment sampling, which was quantified to be in the range of 30% for gas saturated sediments of Eckernförde Bay (Wever et al., 1998; Abegg, 1999).

Table 3.4: Isotopic composition of free gases extracted from Arkona Basin sediments and lithologic short description. The grey shaded area marks values in the intermediate unit 2 grey clayey-silt.

Core sample depth cm	$\delta^{13}\text{C-CH}_4$ ‰ PDB	$\delta\text{D-CH}_4$ ‰ SMOW	Lithology
SL35			
4	-43.6	---	silty mud, greenish-black, unit 1
12	-79.9	---	silty mud, greenish-black, unit 1
18	-80.8	---	silty mud, greenish-black, unit 1
33	-82.4	---	silty mud, greenish-black, unit 1
53	-80.9	-173	silty mud, greenish-black, unit 1
57	-76.7	---	silty mud, greenish-black, unit 1
83	-86.9	---	silty mud, greenish-black, unit 1
113	-91.9	---	silty mud, greenish-black, unit 1
183	-82.9	-143	silty mud, greenish-black, unit 1
209	-80.9	---	silty mud, greenish-black, unit 1
253	-85.5	---	silty mud, greenish-black, unit 1
343	-89.6	---	silty mud, greenish-black, unit 1
373	-92.3	---	silty mud, greenish-black, unit 1
443	-90.8	---	silty mud, greenish-black, unit 1
478	-83.1	-124	silty mud, greenish-black, unit 1
488	-90.0	---	silty mud, greenish-black, unit 1
518	-89.7	-138	silty clay, grey, unit 2
525	-85.5	---	silty clay, grey, unit 2
SL17/41			
11	-62.9	---	silty mud, greenish-black, unit 1
18	-70.7	---	silty mud, greenish-black, unit 1
33	-74.9	---	silty mud, greenish-black, unit 1
62	-82.9	---	silty mud, greenish-black, unit 1
177	-83.6	---	silty mud, greenish-black, unit 1
262	-82.9	---	silty mud, greenish-black, unit 1
342	-77.2	---	silty mud, greenish-black, unit 1
566	-81.6	---	silty mud, greenish-black, unit 1
596	-82.9	-185	silty mud, greenish-black, unit 1
666	-89.3	-140	silty clay, grey, unit 2
726	-77.8	-144	silty clay, grey, unit 2
780	-77.2	-128	silty clay, grey, unit 2

Methane solubility is also dependent on annual salinity and temperature variations of bottom water and daily pressure variations. Short term pressure variations are induced by both, air pressure drops and combined extreme water depth variations due to wind driven water low and high stands (e.g. most extreme values for Kiel Bight -2.29 m and $+2.97$ m

concerning the mean water level; Rheinheimer, 1995). Water level differences of about 1 m are common once or twice a year in the western Baltic (Milkert, 1994 and references cited therein). Comparing Alkor 201 (May) and Alkor 214 (October) sampling campaigns seasonal temperature variations combined with an air pressure drop, from normal mean 1013 to about 987 mbar at sampling day, caused a shift in calculated methane solubility of about -1.7 mmol L^{-1} in 1 m sediment depth. At the same time a water level drop of 0.5 m is observed at Landsort gauge in southern Sweden (Lehmann et al., 2004), which can be estimated as well as minimum value for the central Arkona Basin. The resulting additional solubility shift is of about 0.08 mmol L^{-1} in 1 m sediment depth, which leads to a combined saturation level shift of about $-1.78 \text{ mmol L}^{-1}$ due to seasonal temperature and short term atmospheric and water depth variations. In summary, highest methane concentrations measured in core SL14 exceed the calculated methane solubility limit mainly caused by atmospheric introduced pressure drop (Fig. 3.9). Moreover, high methane concentrations of about $7700 \text{ } \mu\text{mol L}^{-1}$ were measured in 12 cm sediment depth at site SL14 indicating a strong shift of the free gas front to shallower sediment depth or even gas bubbling into the water column of Arkona Basin. These observations are in agreement with Mattson and Likens (1990) and Jackson et al. (1998), who showed that gas bubble ebullition occurs from muddy limnic and brackish sediments caused by methane solubility variations coupled to short term pressure drops.

3.4.3. *Origin of methane.*

The origin of methane (and higher hydrocarbons) in the gas-rich muddy sediment of the Arkona Basin can be deduced by plotting the $C_1/(C_2+C_3)$ ratio of low molecular-weight hydrocarbon gas composition versus the $\delta^{13}\text{C}$ values of methane in a modified Bernard plot (Fig. 3.10). The main hydrocarbon gas component is methane, which is evident by general high molecular $C_1/(C_2+C_3)$ ratios of 10^3 to 10^5 (Fig. 3.7; Tab. 3.3). Nearly all hydrocarbon ratios and $\delta^{13}\text{C}\text{-CH}_4$ isotope values (-96 to -70‰ ; Tab. 3.4) plot well in the domain known for methane derived from bacterial production (Fig. 3.10). In addition to $\delta^{13}\text{C}\text{-CH}_4$ isotope values $\delta\text{D}\text{-CH}_4$ values are used to distinguish between the methane formation pathway of thermogenic generation and the two major microbial formation pathways: acetate fermentation and CO_2 reduction (Schoell, 1980; Whiticar et al., 1986). In figure 3.11 D/H isotope ratios of methane are plotted vs. $\delta^{13}\text{C}\text{-CH}_4$ in the diagnostic plot after Schoell (1980) and Whiticar et al. (1986). Methane $\delta^{13}\text{C}$ values of

about -80‰ and δD values of around -170‰ , respectively, indicate that bacterial CO_2 reduction is the main methane formation pathway in Arkona Basin surface sediments (Fig. 3.10). However, methane is detected in considerable quantities in unit 2 and 3 deposits (Tab. 3.3), and it is possible that methane may be accumulated there by downward diffusion from marine muddy gas-rich surface sediments or by in situ methane formation. The slightly more positive $\delta^{13}\text{C}\text{-CH}_4$ values in the unit 2 grey clays combined with slightly increasing methane concentrations and rising $\text{C}_1/(\text{C}_2+\text{C}_3)$ ratios could indicate methane formation in unit 2 (Figs. 3.6, 3.7 and 3.11).

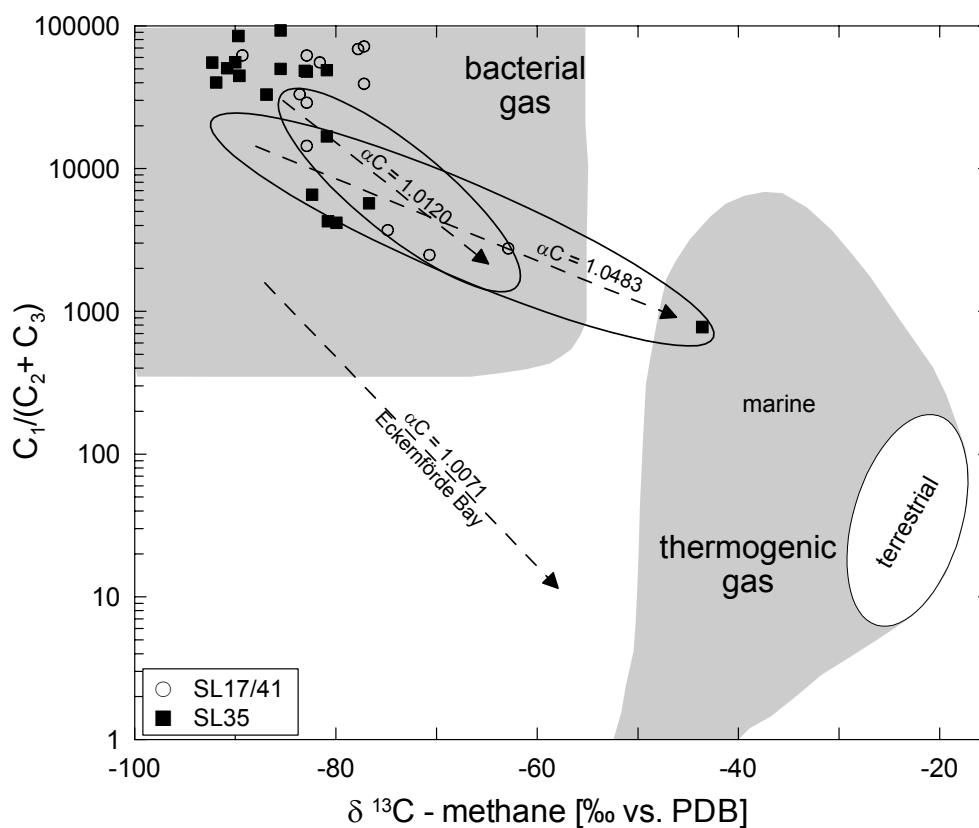
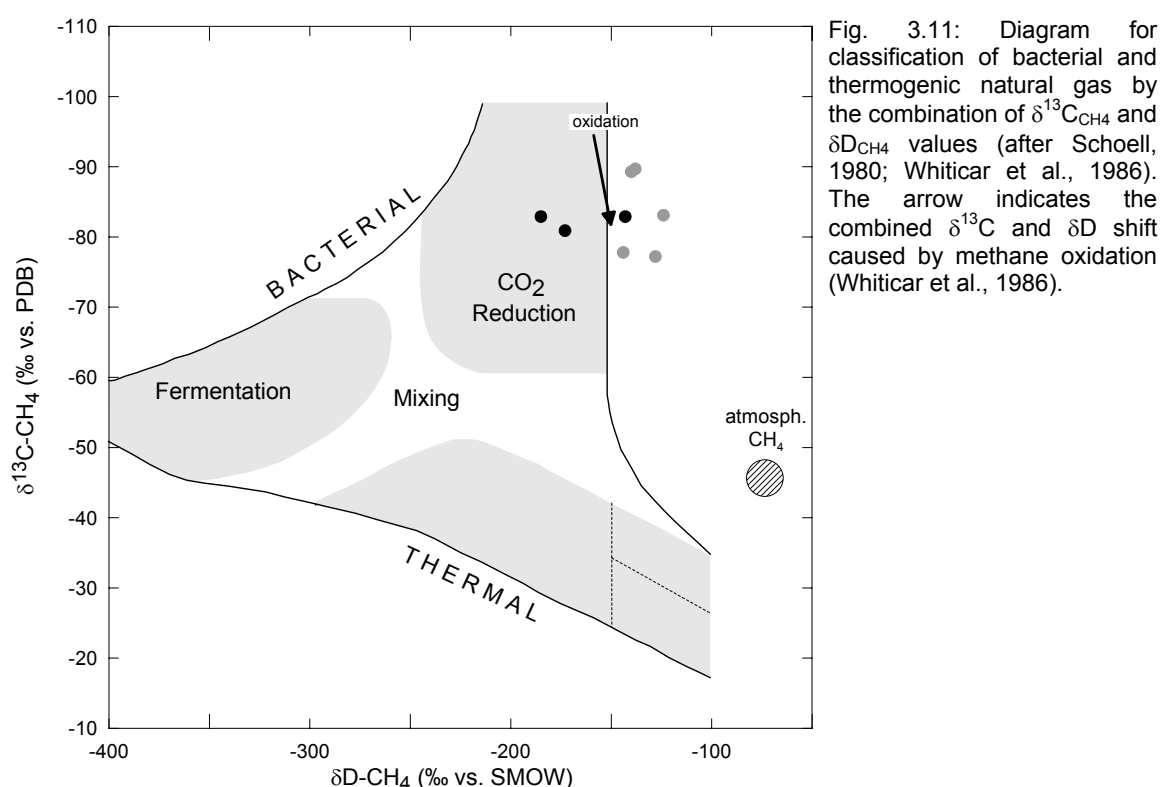


Fig. 3.10: Modified 'Bernard diagram', after Bernard et al. (1976), for classification of bacterial and thermogenic natural gas by the combination of molecular $[\text{C}_1/(\text{C}_2+\text{C}_3)]$ and methane carbon isotope ($\delta^{13}\text{C}_{\text{CH}_4}$) ratios. Dotted arrows showing the combined shifts in molecular and methane carbon isotope ratios due to bacterial methane oxidation. Carbon fractionation factors (αC) of 1.012 and 1.0483 from the Arkona Basin are compared to 1.0071 and 1.0079 from Eckernförde Bay (Whiticar, 1999).

However, no indications for methane formation are given for clay units at low-gas sites SL02 and SL44 (Fig. 3.4). Moreover, methane extracted from grey clays show δD values between -144 and -124‰ (Fig. 3.11, Tab. 3.4), which is more positive than the typical isotope range of methane generated by bacterial CO_2 reduction (e.g. Whiticar et al., 1986; Martens et al., 1999; Whiticar, 2002). In the case of methane production, a

Deuterium enriched pore-water, which could be derived from interstitial clay waters that has to be assumed to lead to the observed δD values (Yeh, 1980; Barrer, 1986). A more likely scenario, however, is downward diffusion of methane from the gas-rich overlying organic-rich mud. Methane could partly be oxidised in the transition zone from anoxic greenish grey muds to suboxic grey to reddish/brown clays. The resulting $\delta^{13}C$ and D/H isotope shift caused by methane oxidation is indicated in figure 3.11 (Whiticar et al., 1986).



However, no indications for methane formation are given for clay units at low-gas sites SL02 and SL44 (Fig. 3.4). Moreover, methane extracted from grey clays show δD values between -144 and -124 ‰ (Fig. 3.11, Tab. 3.4), which is more positive than the typical isotope range of methane generated by bacterial CO_2 reduction (e.g. Whiticar et al., 1986; Martens et al., 1999; Whiticar, 2002). In the case of methane production, a Deuterium enriched pore-water, which could be derived from interstitial clay waters that has to be assumed to lead to the observed δD values (Yeh, 1980; Barrer, 1986). A more likely scenario, however, is downward diffusion of methane from the gas-rich overlying organic-rich mud. Methane could partly be oxidised in the transition zone from anoxic

greenish grey muds to suboxic grey to reddish/brown clays. The resulting $\delta^{13}\text{C}$ and D/H isotope shift caused by methane oxidation is indicated in figure 3.11 (Whiticar et al., 1986).

A general trend to more positive $\delta^{13}\text{C}_{\text{CH}_4}$ values is also observed in the uppermost layer of the muddy surface sediments (Fig. 3.7), which probably indicates anaerobic oxidation in the sulphate reduction zone (Whiticar and Faber, 1986; Hoehler et al., 1994; Martens et al., 1999; Whiticar, 1999; Boetius et al., 2000). The $\delta^{13}\text{C}$ - CH_4 ratios of the shallow gas samples become more positive and $\text{C}_1/(\text{C}_2+\text{C}_3)$ ratios decrease with decreasing sediment depth indicating a Rayleigh-type fractionation during oxidation (Whiticar and Faber, 1986). Whiticar and Faber (1986) calculated the carbon isotopic fractionation factors (αC) for methane oxidation by the simultaneous shift in $\text{C}_1/(\text{C}_2+\text{C}_3)$ molecular gas composition and $\delta^{13}\text{C}$ methane for marine, marsh and brackish environments between 1.0018 and 1.0143. Moreover, Whiticar (1999) determined αC between 1.005 and 1.03 in culture experiments. The calculated αC values for methane oxidation in Arkona Basin sediments are between 1.012 at station SL35 (low gas), and 1.0207 at the gas-rich station SL17/41 (Fig. 3.10) and thus fit well into the range of published data for marine sediments (Whiticar and Faber, 1986; Whiticar, 1999; Whiticar, 2002 and references within). However, if the shallowest gas sample at core SL35 with a $\delta^{13}\text{C}$ - CH_4 value of -43.6‰ is considered in the fractionation calculation than αC would rise to 1.0483, which is the highest value found so far in Baltic Sea sediments, but still fit the range of data for marine sediments.

3.5 Conclusions

A broad ($\sim 1500 \text{ km}^2$) almost coherent area of acoustic turbidity is observed in the central Arkona Basin, Baltic Sea. The occurrence of acoustic turbidity is coupled to a minimum thickness of 4-6 m of organic-rich muddy sediment building up the uppermost Holocene sediment unit 1. The vertical onset of acoustic turbidity ranges from 160 cm to 120 cm sediment depth towards the centre of Arkona Basin. Lateral changes of acoustic turbidity due to seasonal sediment temperature changes could not be determined.

Methane concentrations range from less than $4 \mu\text{mol}$ per litre pore-water at the outer rim of the Arkona Basin (outside acoustic turbidity) to about $7700 \mu\text{mol L}^{-1}$ in the central Arkona Basin (acoustic turbidity zone). Highest methane concentrations exceeded the theoretical solubility of methane due to daily atmospheric pressure drops which may lead

to an upward shift of the vertical onset of acoustic turbidity and probably to gas emanations into the water column.

Stable carbon and hydrogen isotope investigations confirmed that methane is formed by bacterial CO₂ reduction and no indications for methane derived from thermal organic matter degradation was found in the area of investigation. The uppermost sediment layer is dominated by anaerobe methane oxidation and calculated carbon isotope fractionation values fit well in the range known for marine-brackish environments. Underlying silty clay units (2 and 3) show high methane contents probably indicating downward methane diffusion rather than methane production in “organic-free” clayey sediments. Moreover, stable hydrogen isotope values of clay-unit methane possibly indicates methane oxidation due to a yet unknown process.

Acknowledgement

We are grateful to the captains and crews of R.V. POSEIDON and R.V. ALKOR for their large efforts made during the sampling campaigns. For very helpful comments on an earlier draft we thank Anja Reitz and Christian Hensen. Investigations were made in the NATLAB-INGGAS project which was funded by the BMBF and DFG (contr. no. 03G0564D) in the framework of the GEOTECHNOLOGIEN research program.

Chapter 4

Variable deposition of organic-rich sediments and related methane accumulation in the Arkona Basin, Baltic Sea

Olaf Thießen^{a,c}, Christian Hensen^b and Mark Schmidt^a,

^a*Institut für Geowissenschaften der Universität Kiel, Abteilung Marine und Terrestrische Geochemie, Ludewig-Meyn-Str. 10, D-24118 Kiel, Germany*

^b*Leibniz-Institut für Meereswissenschaften, IFM-GEOMAR, Wischhofstr. 1-3, D-24148 Kiel, Germany*

^c*Geochemische Analysen (GCA), Glückaufstr. 50, D-31319 Sehnde-Ilten, Germany*

Abstract

In this study we present geochemical data from five gravity cores taken in the transition zone from acoustic transparent to -turbid sediments in Holocene organic-rich (5-8 wt% TOC) surface sediments of brackish-marine Arkona Basin, Baltic Sea. Acoustic turbidity is observed in seismo-acoustic profiling and is indicative for the occurrence of free gas bubbles, i.e. for high pore-water methane concentrations exceeding their solubility limit. Anaerobic conditions prevail directly beneath the sediment surface and pore-water SO_4 above gas-rich sediments is generally depleted within the first meter below the sediment surface. Calculated SO_4 fluxes increase from 241 $\text{mmol m}^{-2} \text{yr}^{-1}$ in acoustic transparent sediments to 675 $\text{mmol m}^{-2} \text{yr}^{-1}$ in sediments characterised by acoustic turbidity.

Pore-water methane concentrations range between 5-7700 $\mu\text{mol L}^{-1}$ and downward diffusion causes also variable methane concentrations in the underlying late glacial, TOC depleted (0.01-0.7 wt%) deposits. In combination with decreasing methane concentrations an atypical $\delta^{13}\text{C}_{\text{CH}_4}$ shift to more negative values (from -87 ‰ at the base of organic-rich deposits to -112 ‰) is observed in late glacial clayey sediments with increasing depth. This isotopic shift may be caused by various processes as diffusive fractionation, adsorption or geochromatography effects or may just reflect ^{12}C variations due to increasing methane generation in the overlying organic-rich surface sediments.

We present a numerical model study demonstrating that sediment accumulation is the dominant factor determining the onset of acoustic turbidity. Hence, we suggest that the accumulation of total organic carbon is the key parameter controlling gas production and accumulation in the homogenous muddy Holocene sediments of the Arkona Basin and, very likely explains this phenomenon in the whole Baltic Sea and similar environments.

4.1 Introduction

The Baltic Sea a shallow shelf sea, located within the north-western European continent (Fig. 4.1), is one of the major brackish water bodies of the world. Typically the Baltic Sea is divided by some basins and swells and Holocene organic-rich (>4 wt% TOC) fine grained sapropelic sediments (in the following termed as mud) are deposited in quiescent deeper waters in the basins (e.g. Huckriede et al., 1996; Nytoft and Larsen, 2001; Moros, et al., 2002; Miltner et al., 2005). The organic material is mainly derived from primary production in the marine-brackish environment ($\delta^{13}\text{C}_{\text{TOC}}$ values ranging from -30 to -20 ‰) but there is also input of freshwater algae and from other terrestrial sources due to river input (Miltner et al., 2005). In the organic-rich mud of the basins and bays anoxic conditions and intense sulphate reduction is observed directly beneath the sediment surface and methanogenesis occurs below the sulphate-methane-transition (e.g. Geodekyan et al., 1991; Abegg and Anderson, 1997; Schmaljohann et al., 1998; Martens et al., 1998; Wever et al., 1998; Whiticar, 2002). Methane accumulating in the shallow sediments may eventually exceed the solubility limit and form gas bubbles. Thus, broad zones of acoustic turbidity are observed in seismo-acoustic surveys, indicating gas-rich sediments (e.g. Wever and Fiedler, 1995; Whiticar, 2002).

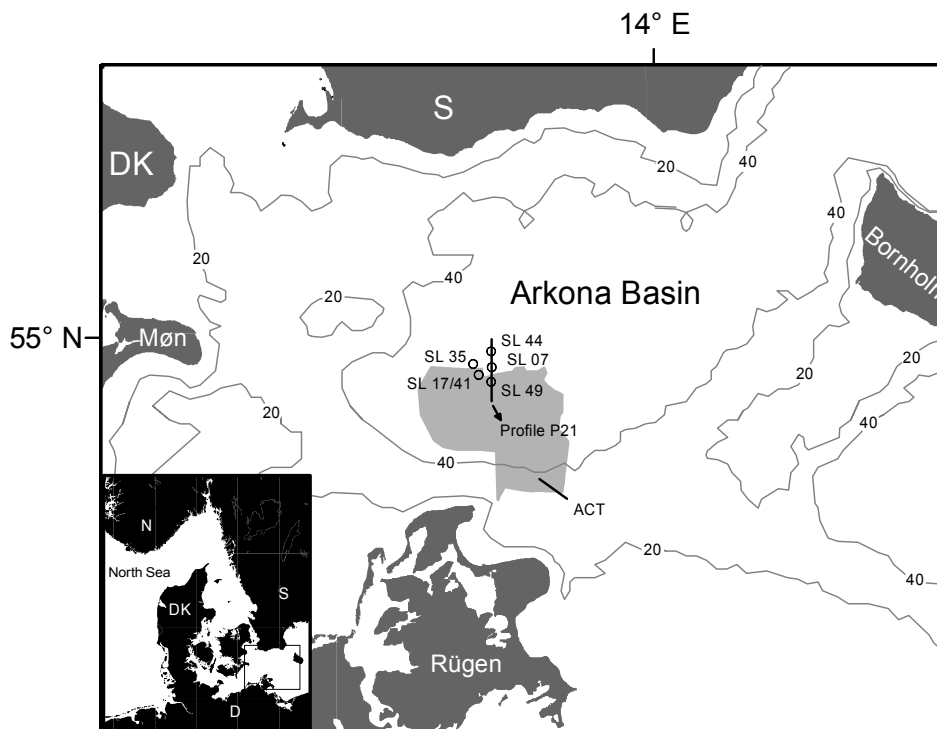


Fig. 4.1: Map of the Arkona Basin situated in the western Baltic proper with locations of the cores investigated. The light grey shaded area marks the zone of acoustic turbidity (ACT) determined from shallow seismic Boomer profiles (Thießen et al., sub.). The solid line indicates the North-South Boomer profile P21. Bathymetric contours are at 20 m intervals.

Intense studies concerning the diagenetic relationships of methane formation and distribution and the related occurrence of acoustic turbidity were performed in the muddy sediments of western Baltic Eckernförde Bay (e.g. Wever and Fiedler, 1995, Abegg and Anderson, 1997; Martens et al., 1998; Wever et al., 1998; Whiticar, 2002). However, acoustic turbidity occurs in Eckernförde Bay as sediment thickness of Holocene deposits exceed about 700-800 cm and the vertical onset of the acoustic turbid layer is observed between 100-200 cm sediment depth and at about 50 cm at a pockmark site (Orsi, et al., 1996; Abegg and Anderson, 1997; Whiticar, 2002). In contrast, in the Arkona Basin the acoustic turbid layer is observed at about 120-160 cm sediment depth (Mathys et al., in press) where the sediment thickness of Holocene organic-rich deposits reaches about 400-600 cm (Thießen et al., sub.).

While most of the former studies in gas-rich sediments of the Baltic Sea deal with the near surface sediments (<150 cm), we present detailed investigations on the sulphate and methane distribution in the entire sediment column (comprising organic-rich, brackish-marine Holocene surface sediments and underlying late glacial lacustrine deposits) within the transition zone from acoustic transparent to acoustic turbid sediments. Moreover, we present a geochemical model which consistently explores the interaction between TOC accumulation and methane production, controlling the distribution of acoustic turbidity in the Arkona Basin.

4.2 Hydrography and geological setting in the study area

The Arkona Sea is situated in the western Baltic Proper and bordered by the Danish islands Møn (in the West) and Bornholm (in the East), and in the North and South by the southern Swedish coast and northern Germany with the island of Rügen, respectively. The maximum water depth is about 50 m and the basin itself is shaped by the 40 m isobath (Fig. 4.1). In general, the water body in the Baltic Sea has a more or less stable thermo-haline stratification caused by estuarine circulation. In the Arkona Basin the seasonal temperature cycle typically refreshes the bottom water by advection and in combination with intermittently inflowing higher saline oxygenated water from the North Sea oxic bottom water conditions are stable (Rheinheimer, 1995 etc.). However, long warm summer periods may lead to oxygen depletion, but stagnant conditions, with long periods of hydrogen sulphide occurrence in the water column as they are observed in the deeper basins further east (e.g. Piker et al., 1998), are not observed in the Arkona Basin.

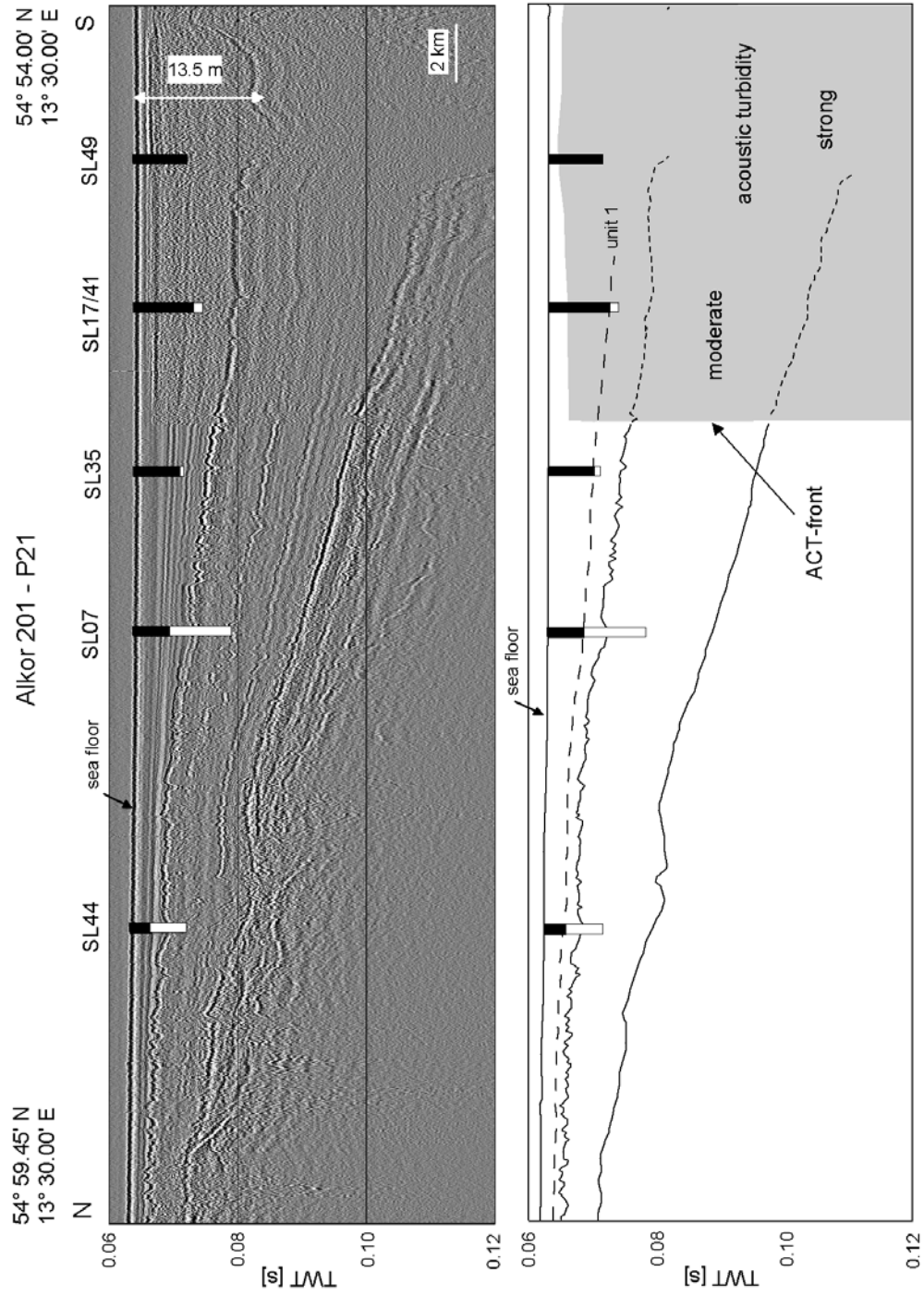


Fig. 4.2: Modified North-South shallow seismic Boomer profile P21 (Thießen et al., sub.) in the transition zone from acoustic transparent to acoustic turbid sediments with interpretation (for location of the profile see Fig. 4.1). Sediment thickness of the organic-rich muddy surface sediments of unit 1 is indicated in black at each core location. Please note: The cores SL35 and SL17/41 are taken slightly West of the profile P21 (Fig. 1) but shown here to point out their relative position to the zone with acoustic turbidity. TWT = two way travel time.

Near surface interstitial water in the Arkona Basin is affected by episodic changes in bottom water chemistry leading to non-steady-state conditions in the pore-water sediment system. Typical annual variations in salinity of the bottom water at 40 m depth are between 125 and 345 mmol L⁻¹. In addition, Lass and Mohrholz (2003) showed that inflowing bottom water is mixed with ambient water by crossing the Arkona Basin from west to east and arrived with a reduced salinity of about 5 mmol L⁻¹ at the more easterly Bornholm hydrographic station. Moreover, dense bottom water may be stored in more or less isolated pools (Krauss and Brüggel, 1991; Liljebladh and Stigebrand, 1996; Lass and Mohrholz, 2003). Hence, bottom water salinity below 30 m water depth could vary in the central Arkona Basin at the same time between about 155 and 313 mmol L⁻¹ (Lass and Mohrholz, 2003). Tides are almost absent in the Arkona Basin and water depth variations are mainly wind driven. Schlüter et al. (2000) assumed that wave or current induced fluid transport in similar fine grained impervious sediments in Kiel Bight is probably of minor importance. Thus, the Cl⁻ distribution in these sediments is mainly controlled by biologically mediated solute exchange and molecular diffusion.

Starting with glacial erosion and subsequent deposition of boulder clay and late glacial freshwater sediments from the Baltic Ice Lake, an undulating Pleistocene subsurface morphology is smoothed up to recent times by the Holocene limnic to brackish/marine sediment cover (Yoldia-, Ancyclus- and Littorina-stages to recent). This is evident by a generally flat recent morphology of the Arkona Basin and by a Holocene sediment cover variability from less than 1 m at the northern rim or at local subsurface highs to more than 20 m thickness in the centre of the investigation area (Lemke, 1998). In general, three main characteristics near surface deposition sequences can be differentiated:

1) Littorina stage to recent (from ~8000 not corrected ¹⁴C yr BP to recent, Emeis et al., 2002): greenish-black to olive-green, silt and clay size, organic-rich muddy sediments deposited under marine-brackish conditions. The topmost black section has a strong characteristic smell of H₂S. At about 1 m sediment depth the H₂S smell disappears and the colour changes from greenish-black to dark olive-green (Mathys et al., in press; Thießen et al., sub.). The permeability of the muddy surface sediment is estimated to be in the range of 10⁻¹³ to 10⁻¹⁵ m⁻² (similar to fine grained muddy sediments of Eckernförde Bay, western Baltic; Schlüter et al., 2004).

2) Baltic Ice Lake, Yoldia and Ancylus stages (>10300 to ~8000 not corrected ^{14}C yr BP, Emeis et al., 2002): grey to bluish-grey, clayey-silt to silty-clay, deposits of lacustrine-marine environments.

3) Baltic Ice Lake (>10300 not corrected ^{14}C yr BP, Emeis et al., 2002): reddish/brown, clayey-silt to silty-clay, sediments from the latter lacustrine stage as well.

A subsurface E-W striking up-doming shoulder of Pleistocene boulder clay divides the basin at around 55° N in a northern and southern sub-basin. However, our investigations are limited to the southern part of the Arkona Basin covering an area of about 40 x 60 nautical miles.

Table 4.1: Data from coring stations, positions, water depths, recoveries, unit 1 sediment thickness and calculated average sedimentation rates (since 8000 B.P.; Emeis et al., 2002) for unit 1 deposits of sediment cores taken in the Arkona Basin, Baltic Sea.

Station	Position		Water depth m	Recovery gravity corer m	Recovery "Rumohr" corer m	Unit 1 organic-rich deposits m	Calc. average sedimentation rate of unit 1 cm yr^{-1}
	N	E					
SL 44	54°58.48'	013°30.07'	46.0	6.80	0.62	3.22	0.040
SL07	54°57.00'	013°30.28'	51.0	11.20	---	3.90	0.049
SL 35	54°56.29'	013°26.96'	46.0	5.30	0.66	4.94	0.061
SL 17/41	54°55.50'	013°27.70'	47.8	7.84	0.65	6.48	0.081
SL 49	54°54.80'	013°30.00'	47.8	3.52	0.65	>3.52	---

4.3 Material and methods

4.3.1 Coring and sediment sampling

Results discussed here are from sediments sampled at 5 sites at the northern rim of the Arkona Basin (Figs. 4.1 and 4.2). Sediment cores of up to 66 cm length were taken by a small gravity corer equipped with an acrylic liner (1000 mm length, internal diameter 74 mm). In general, clear bottom water overlying the mushy surface sediment indicated the undisturbed sampling. Immediately after recovery of the core, the sediment was moved by a piston to the top of the liner and sediment samples were taken with cut off syringes or as sediment slices. A gravity corer with inner PVC liner (internal diameter 125 mm) was used additionally to obtain cores of up to 11.20 m length from muddy to clayey deposits for pore-water and sediment analyses. The cores were cut into 1 m sections immediately after recovery and split lengthwise for sediment sampling. In homogenous muddy sediments sampling distance was 30 to 50 cm. However, sampling

resolution was higher at the sediment surface and at lithological changes. Sediment samples were taken with cut-off syringes with a volume of 5 cm³ and transferred into pre-weighed glass vials. For pore-water analysis sediments were centrifuged and supernatant water was removed with a syringe and stored cooled until analyses. Bulk sediment samples (5-10 cm interval) of about 50-100 g for gas analysis were taken immediately after the sections were split into two halves and cooled down and stored in liquid nitrogen for post cruise gas analyses. Further sediment samples for gas analysis were collected by storing 5 cm³ of bulk sediment together with 10 ml of saturated sodium chloride solution in 21.5 cm³ headspace glass vials that were sealed with a butyl rubber septum and a crimped metal cap.

4.3.2 *Wet bulk density, water content and porosities*

Wet density and water content of the sediment were determined by weighing and from weight loss after drying (24 hours at 105°C) of a 5 cm³ volume of the bulk sediment. The precision of sediment density determination was within ± 0.08 g cm⁻³, resulting from a precision of $\pm 5\%$ of the sample volume determination. Porosities were calculated based on density and water content determinations.

4.3.3 *Sulphate and chloride concentrations*

Pore water subsamples for sulphate and chloride determinations were diluted 1:20 and filtrated (0.45 μ m cellulose acetate filter, Sartorius, Germany) prior to analysis. Measurements were done using ion chromatography with a Sykam S1100 solvent delivery system, Sykam S3110 conductivity detector, Spark Holland Basic+ Marathon autosampler (injection volume 50 μ L), and a LCA A 14 anion exchange column. The eluent, 7.5 mmol L⁻¹ Na₂CO₃ was applied at a flow rate of 1.75 mL min⁻¹. Concentrations are calibrated within each series against IAPSO seawater standard solutions and are reported in mmol L⁻¹.

4.3.4 *Total organic carbon*

Prior to total organic carbon (TOC) analyses, sediment samples were homogenised by gentle grinding in an agate mortar and sub-samples were treated with hypochloric acid, to remove carbonate carbon. TOC concentrations were determined by combustion/gas chromatography using a Carlo Erba EA 1108 CHN-O analyser. The chromatographic responses are calibrated against pre-analysed standards and the

elemental contents of sediments are reported in percent by weight (wt%). The error associated with the TOC is $\pm 3\%$ relative.

4.3.5 Gas analysis

Free volatile hydrocarbon gases were analysed using a modified vacuum extraction technique based on the method described by Faber and Stahl (1983). Free gases represent the unbound or only weakly bound gases dissolved in the pore-water or situated in the interstices of the sediment fabrics, which have mainly been formed by bacterial and early diagenetic processes. For free gas determination about 50 g of the deep frozen (-196°C) bulk sediment samples were degassed by a combination of stirring, heating and salting out the solved gases from sediment pore-water in a vacuum system (here without acid treatment). In general this gas fraction is comparable to the procedure commonly referred as “headspace” gases (Albert et al., 1998).

The hydrocarbon gas composition was determined with a SHIMADZU GC 14A gaschromatograph, equipped with a Poraplot Q capillary column and a flame ionisation detector. Chromatographic responses are calibrated against pre-analysed standards, and based on daily replicate standard analyses analytical precision is within $\pm 5\%$. Results are given in mmol L^{-1} pore-water. Stable carbon isotope values of methane were measured according to the method described by Faber et al. (1998) by using a continuous flow isotope ratio mass spectrometer (PDZ Europa 2020 CF-IRMS). Carbon isotope data are reported in the common δ – notation and expressed in ‰ relative to the Peedee belemnite (V-PDB) standard. The analytical precision of analyses is $\pm 1\text{‰}$ for $\delta^{13}\text{C}$.

4.3.6 Geochemical modelling

To quantify gas formation in the sediments of the Arkona Basin a simple Mathematica[®] -based, one dimensional, reactive-transport-model scheme has been formulated. The model set-up is similar to that described by Torres et al. (2004) and Hensen and Wallmann (2005) and enables the calculation of molecular diffusion, sediment accumulation, degradation of organic carbon by sulphate reduction and methanogenesis, anaerobic oxidation of methane and saturation of methane gas. A 1G-kinetics approach following that of Middelburg (1989) has been used to simulate the degradation of organic material. Rates of TOC degradation (R_{POC} in wt\% yr^{-1}) are calculated:

$$R_{TOC}(x, t) = kI_{TOC}(x) \cdot k_{TOC}(x) \cdot [TOC](x, t) \quad (1)$$

where $[TOC]$ is the concentration of total organic carbon in wt%. The rate constant k_{TOC} describes the degradation rate as a function of depth and sedimentation rate, thus considering the ageing of the material over time:

$$k_{TOC}(x) = k_1 \cdot \left(1 + \frac{x}{\omega(x)}\right)^{-k_2}, \quad (2)$$

$$kI_{TOC}(x, t) = \frac{kI_{meth}}{kI_{meth} + ([CH_4](x, t) + [CH_4]_g(x, t))}, \quad (3)$$

where ω is the sedimentation rate in cm yr^{-1} , k_1 and k_2 kI_{meth} is the inhibition constant limiting the rate of methanogenesis and $[CH_4]$, and $[CH_4]_g$ are the concentrations of dissolved (mmol dm^{-3}) and methane gas ($\text{cm}^3 \text{ gas cm}^{-3} \text{ pore volume}$), respectively. Equation (3) is related to that of Wallmann et al. (sub.) and assumes that the rates of methane formation are constantly reduced as the reaction product (methane) accumulates in the pore-water.

The distributions of dissolved species (CH_4 , SO_4), and methane gas are calculated using time-dependent partial differential equations. Molecular diffusion, burial and compaction-induced flow are considered as transport modes of dissolved species while solids are transported via burial modified by steady-state compaction (i.e. Luff and Wallmann, 2003; Torres et al., 2004). Burial of solids is expressed as steady-state compaction with:

$$\omega(x) = \frac{(1 - \phi_{bot}) \cdot \omega_{bot}}{(1 - \phi(x))}. \quad (4)$$

Accordingly, the porosity decrease over depth is approximated by:

$$\phi(x) = (\phi_{top} - \phi_{bot}) * e^{(-const \cdot x)} + \phi_{bot} \quad (5)$$

where ω_{bot} is the sedimentation rate at the lower boundary in cm yr^{-1} , ϕ_{top} and ϕ_{bot} are the porosity at the top and bottom of the model area, $const$ is the attenuation coefficient for the decrease of porosity, and top delineates the sediment surface.

Burial of gas follows the assumption that only available pore space is filled, thus neither affecting the fabric of the sediment nor the sedimentation rate. The advective component of pore-water flux is modified by compaction:

$$u(x) = \frac{\omega_{bot} \cdot \phi_{bot}}{\phi(x)}, \quad (6)$$

Temperature depending molecular diffusion coefficients of dissolved species were calculated after Boudreau (1997) and corrected for porosity decrease:

$$D_s(x) = \frac{D_0(x)}{1 - \ln(\phi(x))^2}, \quad (7)$$

where D_0 and D_s are the molecular diffusion coefficients in seawater and pore water, respectively.

The relevant processes of organic carbon degradation within the model area, sulphate reduction and methanogenesis, are implemented by rate laws using Monod-type kinetics:

$$R_{\text{TOC-SO}_4}(x, t) = R_{\text{TOC}}(x) \cdot \frac{[\text{SO}_4](x, t)}{k_{\text{SO}_4} + [\text{SO}_4](x, t)} \quad (8)$$

and

$$R_{\text{TOC-CH}_4}(x, t) = R_{\text{TOC}}(x) \cdot \frac{kI_{\text{SO}_4}}{kI_{\text{SO}_4} + [\text{SO}_4](x, t)}, \quad (9)$$

where $R_{\text{TOC-SO}_4}$ and $R_{\text{TOC-CH}_4}$ are the rates of sulphate reduction and methane production (in $\text{mmol dm}^{-3} \text{ yr}^{-1}$), k_{SO_4} is the Monod constant for sulphate reduction (in mmol dm^{-3}), kI_{SO_4} is the inhibition constant for initiation of methanogenesis (in mmol dm^{-3}), and t is time (in yr). Anaerobic oxidation of methane (AOM) follows the rate law:

$$R_{\text{AOM}}(x, t) = k_{\text{AOM}} \cdot [\text{SO}_4](x, t) \cdot [\text{CH}_4](x, t), \quad (10)$$

where k_{AOM} is the rate constant for AOM (in $\text{dm}^3 \text{ mmol}^{-1} \text{ yr}^{-1}$) and $[\text{SO}_4]$ and $[\text{CH}_4]$ are the corresponding concentrations (in mmol dm^{-3} of pore solution).

The solubility of pure methane gas has been calculated following the approach of Tishchenko et al. (2005), considering ambient pore-water conditions (temperature, pressure, salinity). Rates of gas formation and dissolution have been calculated according to the rate laws:

$$R_{\text{GF}}(x, t) = k_{\text{GF}} \cdot \left(\frac{[\text{CH}_4](x, t)}{[\text{CH}_4]_{\text{Sol}}(x, t)} - 1 \right); \text{ for } \left(\frac{[\text{CH}_4](x, t)}{[\text{CH}_4]_{\text{Sol}}(x, t)} - 1 \right) > 0 \quad (11)$$

and

$$R_{\text{GD}}(x, t) = -k_{\text{GD}} \cdot \left(\frac{[\text{CH}_4](x, t)}{[\text{CH}_4]_{\text{Sol}}(x, t)} - 1 \right) \cdot [\text{Gas}](x, t); \text{ for } \left(\frac{[\text{CH}_4](x, t)}{[\text{CH}_4]_{\text{Sol}}(x, t)} - 1 \right) \leq 0, \quad (12)$$

where k_{GF} ($\text{dm}^3 \cdot \text{dm}^{-3} \cdot \text{yr}^{-1}$) and k_{GD} (yr^{-1}) are rate constants for gas formation and dissolution, respectively, $[\text{CH}_4]_{\text{Sol}}$ is the solubility of methane in seawater at ambient conditions, and $[\text{Gas}]$ is the concentration of methane gas in $\text{dm}^3 \text{ dm}^{-3}$ (bulk sediment). Gas formation is solely determined by the degree of oversaturation. The reverse function is formulated as being additionally controlled by the amount of gas available for

dissolution. Both processes directly affect the concentration of dissolved methane. This can be expressed by the following rate law:

$$R_{CH_4}(x,t) = 10^6 \cdot \frac{d_{Gas}(x)}{M_{Gas}} \cdot \frac{R_{GF}(x,t)}{\phi(x)} - 10^6 \cdot \frac{d_{Gas}(x)}{M_{Gas}} \cdot \frac{R_{GD}(x,t)}{\phi(x)} \quad (13)$$

where R_{CH_4} are given in $\text{mmol dm}^{-3} \text{ yr}^{-1}$ of pore solution and M_{Gas} is the molecular weight of gas (g mol^{-1}). The density of gas d_{Gas} (in $\text{g}\cdot\text{cm}^{-3}$) has been calculated by:

$$d_{Gas}(x) = \frac{M_{Gas}}{vol(x)} \cdot 10^3 \quad (14)$$

where vol is the depth dependent molar volume of pure methane gas calculated after Duan (1992).

The set of partial differential equations defining the non-steady-state model (one for each species) is converted into a large number of ordinary differential equations (ODE) giving the temporal change of species concentrations at each depth interval. A centred finite difference scheme is used for dissolved species and an upward scheme is applied for the transport of solids. The resulting ODE-system is solved using the NDSolve object of MATHEMATICA (Vers. 5).

Table 4.3: Summary of sediment features which describe the distinguished zones in the transition from acoustic transparent to acoustic turbid sediments. Linear sulphate concentration gradients (SCG; $\Delta\text{SO}_4^{2-}/\Delta\text{depth}$ [$\text{mmol L}^{-1} \text{ cm}^{-1}$]) were calculated with a bottom water SO_4 concentration of 13.4 mmol L^{-1} . Estimated sulphate reduction rates (SRR_{CALC}) were calculated based on a sediment sulphate diffusion coefficient (D_S) of $148,98 \text{ mmol cm}^2 \text{ yr}^{-1}$ (Boudreau, 1997), an average porosity of 0.87 in the uppermost 50 cm sediment depth and the sulphate concentration gradients at cores SL44, SL35, SL17/41, and SL49, respectively. (n.d. = not determined).

	Type I	Type II		Type III	
Station	SL44	SL07	SL35	SL17/41	SL49
Methane accumulation	no	yes	yes	yes	yes
Acoustic turbidity	no	no	no	yes	yes
SCG _{MEAS} ($\text{mmol L}^{-1} \text{ cm}^{-1}$)	-0.186	n.d.	-0.210	-0.276	-0.521
SRR _{CALC} ($\text{mmol SO}_4^{2-} \text{ m}^{-2} \text{ yr}^{-1}$)	241	n.d.	272	357	675
SRR _{MODEL} ($\text{mmol SO}_4^{2-} \text{ m}^{-2} \text{ yr}^{-1}$)	258	n.d.	476	629	n.d.
AOM _{MODEL} ($\text{mmol SO}_4^{2-} \text{ m}^{-2} \text{ yr}^{-1}$)	2.8	n.d.	105	143	n.d.
$\Sigma \text{SSR}_{\text{MODEL}}$ ($\text{mmol SO}_4^{2-} \text{ m}^{-2} \text{ yr}^{-1}$)	261	n.d.	581	772	n.d.

Core SL44				Core SL07				Core SL35				Core SL17/41 "G"				Core SL49 "G"			
Depth	Cl ⁻	SO ₄	TOC	Depth	TOC	Depth	Cl ⁻	SO ₄	TOC	Depth	Cl ⁻	SO ₄	TOC	Depth	Cl ⁻	SO ₄	TOC		
cm	mmol L ⁻¹	mmol L ⁻¹	wt%	cm	wt%	cm	mmol L ⁻¹	mmol L ⁻¹	wt%	cm	mmol L ⁻¹	mmol L ⁻¹	wt%	cm	mmol L ⁻¹	mmol L ⁻¹	wt%		
BW	223.41	13.40	---	5	5.26	BW	246.08	12.21	---	1	---	---	6.21	0.5	224.91	13.06	---		
0.5	228.40	12.87	---	15	5.55	0.5	231.66	12.40	---	6	---	---	6.00	1	214.71	12.71	5.90		
1	229.17	13.24	5.25	64	7.39	1	223.86	12.36	---	9	266.26	10.41	---	2	230.44	11.15	5.84		
2	235.31	13.25	5.23	110	5.99	2	233.34	12.63	6.26	15	232.13	6.36	5.74	3	231.36	12.46	---		
3	221.79	11.29	---	150	5.33	4	248.05	12.50	---	30	278.10	1.97	5.46	6	257.00	11.67	5.93		
6	248.93	12.89	5.39	200	4.82	7	---	---	6.04	45	271.46	0.29	5.45	7	249.84	9.07	---		
10	234.25	10.49	---	260	3.13	10	251.34	11.94	6.09	55	271.42	0.99	---	15	282.58	7.44	5.79		
15	250.92	10.45	5.67	310	4.23	15	270.63	11.66	---	60	248.15	1.24	6.82	17	264.06	4.28	---		
17	257.62	9.66	---	335	3.67	17	---	---	5.88	80	291.91	1.63	7.77	20	---	---	5.62		
20	---	---	4.97	410	1.57	30	294.90	7.90	---	100	273.58	0.44	7.37	40	293.41	1.93	5.68		
22	264.70	8.14	---	425	2.85	32	272.11	5.95	5.01	130	282.46	1.66	6.08	42	273.35	0.97	---		
40	268.51	5.48	5.33	514	0.46	50	303.36	2.79	---	155	249.64	1.24	5.33	62	269.57	0.77	6.09		
82	268.65	5.56	5.58	538	0.42	52	---	---	5.60	175	284.21	0.69	4.48	92	266.94	0.35	6.02		
112	269.76	3.96	7.43	564	0.31	55	284.64	3.34	5.23	205	282.46	0.99	4.94	132	268.80	0.46	7.48		
152	268.70	3.30	6.15	568	0.11	81	260.67	0.99	5.93	235	269.34	1.14	4.80	162	271.65	0.45	7.02		
184	270.47	2.85	4.70	592	0.38	110	255.31	1.11	7.18	260	272.32	0.61	4.29	192	279.99	0.43	6.38		
212	270.26	2.59	4.51	631	0.41	140	236.19	0.40	6.91	300	264.03	0.89	3.55	219	272.13	1.46	---		
252	271.69	2.59	2.90	664	0.53	180	274.34	1.09	5.84	340	285.81	0.78	3.23	232	---	---	5.83		
282	266.72	2.66	3.68	729	0.54	210	275.16	0.90	5.56	495	262.05	2.56	3.39	262	277.01	1.50	5.69		
317	272.39	3.30	3.85	770	0.53	240	274.23	0.76	4.66	525	252.47	2.39	3.94	292	271.11	0.44	5.32		
322	---	---	3.77	800	0.65	272	281.19	1.58	---	565	---	---	3.85	332	276.73	0.71	4.82		
352	272.46	3.04	1.55	865	0.66	280	---	---	4.68	595	262.52	2.32	4.78	332	276.73	0.71	4.82		
383	274.18	3.27	1.26	929	0.33	317	288.03	1.55	3.27	635	279.06	1.91	4.60	---	---	---	---		
384	---	---	0.20	944	0.68	340	279.93	0.97	2.99	665	263.37	0.54	1.80	---	---	---	---		
385	---	---	0.23	946	0.82	370	283.62	0.97	3.48	695	234.19	0.25	4.31	---	---	---	---		
387	---	---	0.27	995	0.60	409	284.78	1.05	3.62	725	260.94	0.32	0.58	---	---	---	---		
412	281.60	3.74	0.41	1095	0.55	440	288.73	1.05	3.51	760	275.96	0.82	0.49	---	---	---	---		
452	---	---	0.65	---	---	475	271.92	0.64	4.25	---	---	---	---	---	---	---	---		
482	---	---	0.66	---	---	485	---	---	4.04	---	---	---	---	---	---	---	---		
512	---	---	0.60	---	---	492	284.40	0.96	---	---	---	---	---	---	---	---	---		
552	---	---	0.75	---	---	515	---	---	1.44	---	---	---	---	---	---	---	---		
582	---	---	0.71	---	---	522	279.03	1.73	---	---	---	---	---	---	---	---	---		
612	---	---	0.73	---	---	---	---	---	---	---	---	---	---	---	---	---	---		
652	---	---	0.67	---	---	---	---	---	---	---	---	---	---	---	---	---	---		

Table 4.2: Pore-water chloride (Cl⁻) and sulphate (SO₄) concentrations and total organic carbon (TOC) of Arkona Basin cores SL44, SL07, SL35, SL17/41 and SL49. Cores taken in gas-rich sediments, estimated by acoustic blanking, are marked with "G". The different macroscopic sedimentary units 1 to 3 are marked by different colours: white = unit 1 olive grey organic-rich mud; dark grey = unit 2 grey clayey silt; light grey = unit 3 reddish/brown clayey silt. BW = bottom water.

4.4 Results

4.4.1 Sediments and organic matter content

The total organic carbon contents of Arkona Basin sediments varies clearly in the differently coloured sequences of deposition (Figs. 4.3 and 4.4, Tab. 4.2). In uppermost greenish-black to olive-green mud of unit 1 the sediment thickness ranges from 3.2 m at station SL44 to 3.9 m, 4.9 m and 6.5 m at stations SL07, SL35, and SL17/41, respectively (Fig. 4.2). Nevertheless, similar organic carbon profiles are observed with depth. TOC concentrations of approximately 5-6 wt% near the sediment surface increase to a typical peak concentration of 7-8 wt% at about 100 cm sediment depth. With greater depth TOC generally decreases to levels around 3.5-4 wt% at the basis of olive-green muds. In the grey clayey-silts of unit 2 intermediate TOC values of 1-4 wt% are determined. The deepest cored reddish/brown clayey sediments, found at a depth below 336 cm at station SL44, and 489 cm at station SL07, respectively, are in general depleted in TOC (0.01-0.7 wt%; Figs. 4.3 and 4.4; Tab. 4.2).

4.4.2 Pore-water geochemistry

Results of pore-water chloride and sulphate concentrations are summarised in table 4.2 and Fig. 4.3. Chloride concentrations in bottom water during May 2002 sampling campaign vary between 223 mmol L⁻¹ at station SL44 and 246 mmol L⁻¹ at station SL35. Pore-water chloride concentrations increase slightly with depth to values between 270 and 290 mmol L⁻¹. Sulphate concentrations in bottom water during the sampling campaigns reach up to 13.7 mmol L⁻¹. At all stations pore-water sulphate concentrations show decreasing concentrations with depth (Fig. 4.3). However, two regimes could be distinguished: i) low concentration decrease with depth (5.5 mmol L⁻¹ in 85 cm) trending to values around 3 mmol L⁻¹ with greater depth at station SL44 and ii) a strong concentration decrease to values below 1 mmol L⁻¹ shallower than 50 cm sediment depth and with values around 0.2 to 2 mmol L⁻¹ with greater depth. It is remarkable, that sulphate is not consumed entirely at any station. In our opinion possible explanations for low level sulphate concentrations are on one hand seawater contaminations during coring/sampling and on the other hand either H₂S oxidation during storage/centrifugation of the sediments or in situ oxidation of downward diffusing H₂S in the transition zone to the sub-oxic to oxic grey-reddish/brown clay unit may cause sulphate relicts in the

sediments. The latter oxidation pathway might also be indicated by the sulphate profiles from cores SL44 and SL35, when slightly increasing sulphate concentrations are observed in the transition zone from grey to the reddish/brown clay (Fig. 4.3).

To simplify the comparability of the sulphate-depth-profiles, sulphate fluxes were calculated (SRR_{CLAC} ; Tab. 4.3) based on a sediment sulphate diffusion coefficient (D_s) of $148.98 \text{ cm}^2 \text{ yr}^{-1}$ (Boudreau, 1997), an average porosity of 0.87 and sulphate concentration gradients (SCG_{MEAS} ; $\Delta \text{ sulphate} / \Delta \text{ depth} [\text{mmol L}^{-1} \text{ cm}^{-1}]$) for sites SL44, SL35, SL17/41, and SL49, respectively. Gradients are calculated with an initial SO_4^{2-} concentration of 13.4 mmol L^{-1} in the bottom water during the sampling campaign, whereas non-steady-state bottom water conditions in the Arkona Basin due to intermittent inflowing of higher saline North Sea water lead to typical annual variability of bottom water sulphate between 7 and 19 mmol L^{-1} (calculated by the sulphate seawater relationship of $\text{SO}_4 = \text{Cl} \times 1.46$ and data reported by Elken et al., 1996). The calculated fluxes (SRR_{CALC}) range between $241 \text{ mmol SO}_4 \text{ m}^{-2} \text{ yr}^{-1}$ at core SL44 and $675 \text{ mmol SO}_4 \text{ m}^{-2} \text{ yr}^{-1}$ at site SL49 (Tab. 4.3).

Pore-water methane concentrations (Thießen et al., sub.) are summarised in Figs. 4.3 and 4.4 and Tab. 4.4. In general, two regimes could be observed: i) very low concentrations below $5 \text{ } \mu\text{mol L}^{-1}$ in the entire sediment column (SL44; Fig. 4.3) and ii) strong increasing methane concentrations with depth from values below $100 \text{ } \mu\text{mol L}^{-1}$ at the sediment surface to values between $2000 \text{ } \mu\text{mol L}^{-1}$ and about $8000 \text{ } \mu\text{mol L}^{-1}$ with greater depth. In the core with the highest recovery of about 1100 cm (SL07; Tab. 4.4) in contrast to all other cores slowly decreasing methane concentrations from about $7700 \text{ } \mu\text{mol L}^{-1}$ at about 500 cm to about $200 \text{ } \mu\text{mol L}^{-1}$ at 1100 cm depth are observed. The summarised sediment features which describe the distinguished zones (I, II, and III) in the transition from acoustic transparent to acoustic turbid sediments are given in Tab. 4.3.

Concerning the stable carbon isotope values of pore-water methane, core SL07 could be divided in three depth intervals: a) 0-60 cm, showing a shift to more positive $\delta^{13}\text{C}$ values from $-89 \text{ } \text{‰}$ at about 60 cm to $-81 \text{ } \text{‰}$ at 20 cm in combination with decreasing methane concentrations b) 60-510 cm, almost similar $\delta^{13}\text{C}$ values between -87 and $-90 \text{ } \text{‰}$ in the whole depth zone and c) an isotopic shift from -90 to $-112 \text{ } \text{‰}$ in the depth interval from about 510 to 1100 cm depth (Fig. 4.4; Tab. 4.4).

Depth cm	Pore-water methane $\mu\text{mol L}^{-1}$	$\delta^{13}\text{C-CH}_4$ PDB ‰
8	231	---
18	298	-80,8
63	3638	-88,9
428	5407	-87,7
513	7770	-90,0
868	1102	-95,8
1098	190	-112,5

Table 4.4: Pore-water methane and stable carbon isotope composition of methane at station SL07. The different macroscopic sedimentary units 1 to 3 are marked by different colours: white = unit 1 olive grey organic-rich mud; dark grey = unit 2 grey clayey silt; light grey = unit 3 reddish/brown clayey silt.

4.5 Discussion

4.5.1 Geochemical characterisation of Arkona Basin sediments

The increasing sediment thickness of unit 1 towards the centre of the Arkona Basin is a typical feature. The anoxic conditions directly beneath the sediment surface favour organic matter preservation. This is reflected by TOC values of about 4-8 wt% in the topmost layers (Tab. 4.2, Figs. 4.3 and 4.4). Organic matter content shows little variation in the transition zone from acoustically transparent (basin rim) to acoustically turbid (basin centre) sediments (Figs. 4.3 and 4.4). The organic-rich near surface sediments of unit 1 favour methane production in contrast to the underlying sedimentary units 2 and 3, which are characterised by low C_{org} -content and suboxic to oxic redox values (Thießen et al., sub.).

The TOC peak observed at about 1 m sediment depth (Figs. 4.3, 4.4) is characteristic for unit 1 sediments and is found in different Baltic Sea basins (i.e. Andrén et al., 2000; Voss et al., 2001; Dippner and Voss, 2004). Andrén et al. (2000) and Dippner and Voss (2004) correlate this TOC peak in Gotland Basin post Littorina sediments with the Medieval Warm Period, of around ~1150 to ~1190 AD.

Estimating that the deposition of greenish organic-rich muddy early Littorina and post-Littorina sediments (unit 1) occurred since about 8000 yr BP (uncorrected average ^{14}C years for initial Littorina phase, Emeis et al., 2002), mean sedimentation rates for the whole unit 1 depositions are between 0.040 cm yr^{-1} and 0.081 cm yr^{-1} at cores SL44, SL35, and SL17/41, respectively (Tab. 4.1). Moreover, the mean sedimentation rate rises in the centre of the Arkona Basin to about 0.15 cm yr^{-1} , when muddy unit 1 deposits may reach about 12 m thickness (Lemke, 1998).

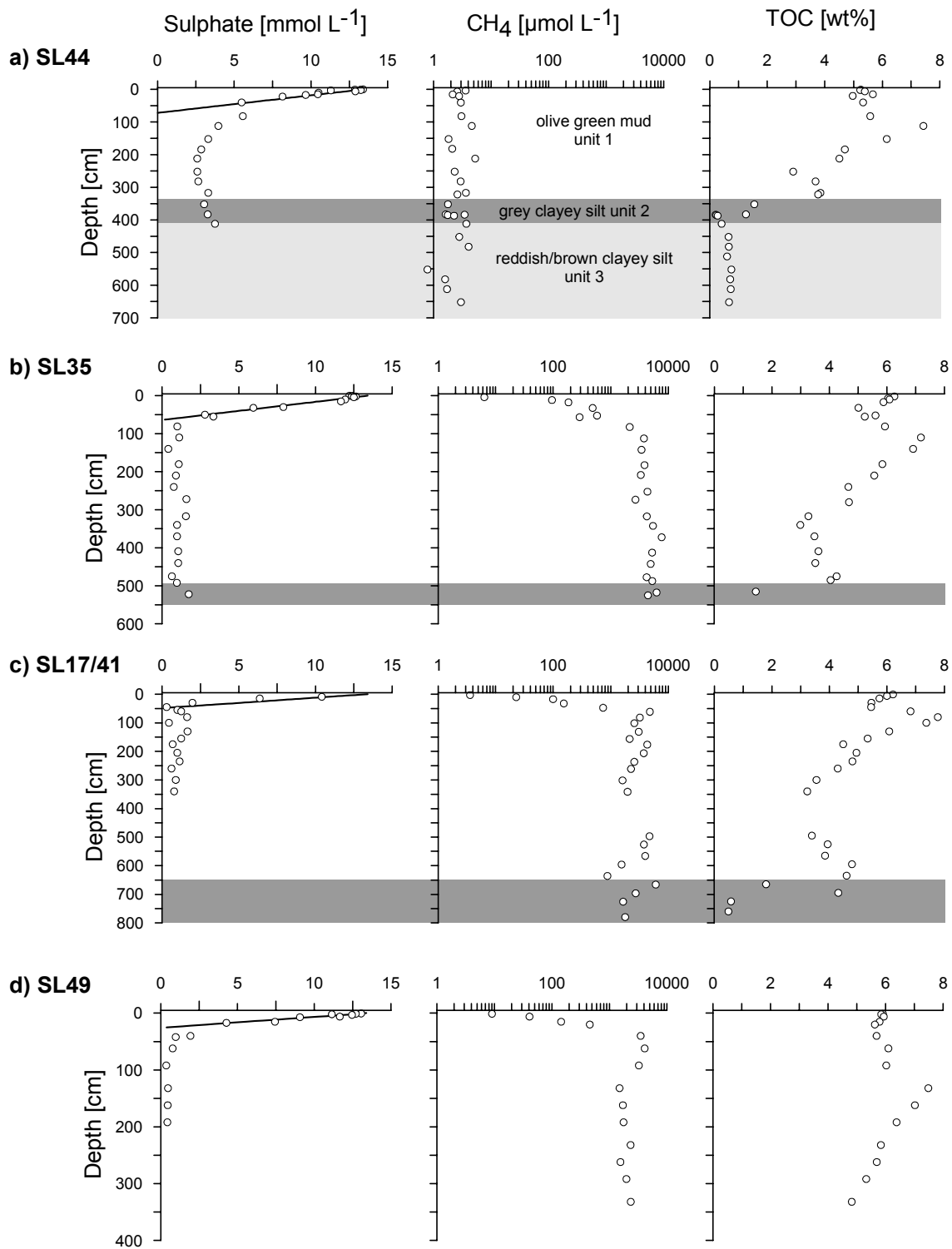


Fig. 4.3: Pore-water concentration profiles of SO_4 and CH_4 and profiles of TOC of gravity cores SL44 (a), SL35 (b) SL17/41 (c) and SL49 (d). The bold lines indicate the SO_4 concentration gradient (SCG; $\text{mmol L}^{-1} \text{cm}^{-1}$) calculated from SO_4 bottom water concentration of 13.4 mmol L^{-1} . The different macroscopic sedimentary units 1 to 3 are marked by different colours: white = unit 1 olive grey organic-rich muds; dark grey = unit 2 grey clayey silt; light grey = unit 3 reddish/brown clayey silt.

The strong sulphate reduction indicated by pore-water sulphate depletion (Fig. 4.3; Tab. 4.2) is common for anaerobic marine sediments and is in agreement with other locations in the Baltic Sea (e.g. Hansen et al., 1998; Martens et al., 1998; Piker et al., 1998; Martens et al., 1999; Whiticar, 2002). In general sulphate utilisation by sulphate reducing bacteria (SRB) is characterised by concave-down depth profiles of dissolved sulphate in the pore-water and linear sulphate pore-water profiles are characteristic, when methane flux from below is active and anaerobic oxidation of methane (AOM) controls sulphate depletion (Claypool and Kaplan, 1974; Martens and Berner, 1974; Kasten and Jørgensen, 2000; Hensen et al., 2003). A typical concave-down depth profile of pore-water sulphate is observed at station SL44 (acoustic transparent sediments), indicating that sulphate reduction is mainly controlled by C_{org} -decomposition and methane oxidation is not important. Overall, the sulphate profiles become steeper and almost linear when going from acoustically transparent sediments at core locations SL44 and SL35 to cores SL17/41 and SL49 taken within the zone of acoustic turbidity (Figs. 4.2, 4.3).

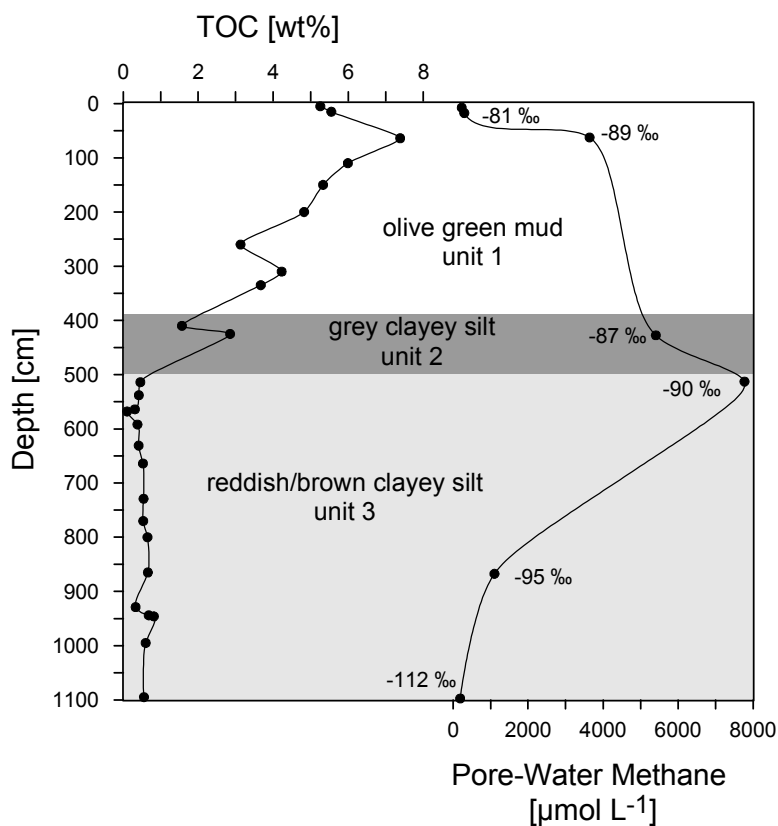


Fig. 4.4: TOC and pore-water methane profiles versus depth at core location SL07. Stable carbon isotope ratios of methane (‰; PDB) are given next to the correlating symbol for the measured concentration. The different macroscopic sedimentary units 1 to 3 are marked by different colours: white = unit 1 olive grey organic-rich mud; dark grey = unit 2 grey clayey silt; light grey = unit 3 reddish/brown clayey silt.

The quality (type) of organic matter does not vary significantly within unit 1, thus, we assume that the increasing steepness of the sulphate profiles and therefore shoaling of the sulphate-methane-transition (SMT) towards the seafloor from non turbid to turbid sediments is controlled by increased CH₄ accumulation related to higher production rather than to differences in the type of accumulated material.

Thießen et al. (sub.) estimate that a sediment thickness between 4 m and 6 m is necessary to generate methane concentrations exceeding the calculated solubility limit at shallow (40 m) marine Arkona Basin sediments. In addition even methane production itself seems to be coupled to the sediment thickness of unit 1 muddy deposits. As pointed out above the pore-water sulphate depth profile at core SL44 seems to be dominated by bacterial sulphate reduction, although low levels of methane are found. However, pore-water methane does not exceed about 5 µmol L⁻¹ in the whole core down to the reddish/brown clays at 6.5 m depth.

Detailed pore-water methane concentration profiles (Figs. 4.3 and 4.4) represent 3 types of methane-containing sediments in the sampling area (Tab. 4.3).

Type I: Represented by SL44, this type is defined by low-level (uniform) methane concentrations in unit 1 sediments (Fig. 4.3a) and by the acoustic transparency of the sediment (Fig. 4.2; Thießen et al., sub.). Organic carbon diagenesis in core SL44 is mainly controlled by sulphate reduction. Traces of methane in sulphate bearing sediments are also reported by Schmaljohann et al. (1998) who detected methane concentrations <50 µmol L⁻¹ in Arkona and Bornholm Basin near surface sediments (uppermost 22 cm) and Whiticar (2002) reported from low levels of methane (<200 µmol) in the sulphate zone.

Type II: SL07 and also SL35 represent the type II sediment (Tab. 4.3), when methane production exceeds methane degradation and thus methane is accumulated within the unit 1 muddy sediment layer (Fig. 4.3b and Fig. 4.4). However, methane formation does not exceed methane saturation levels, which would cause free gas formation and acoustic turbidity (e.g. Anderson and Hampton, 1980a; Abegg and Anderson, 1997).

Type III: Free gas was proposed by acoustic turbidity at stations SL17/41 and SL49 by Thießen et al. (sub.). These two stations represent type III sediment (Tab. 4.3), when methane is accumulated in the muddy sediment layer unit 1 and methane saturation exceeds the saturation limit determined by a minimum unit 1 thickness between 5 and 6.5 m (Thießen et al., sub.).

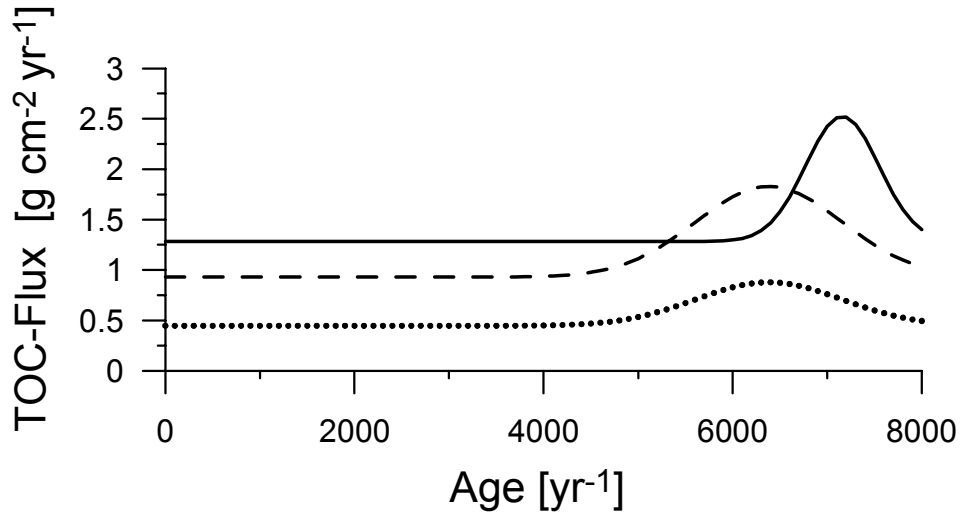


Fig. 4.5: Modelled TOC flux at the sediment surface of cores SL44 (dotted line), SL35 (dashed line) and SL17/41 (solid line) for the last 8000 yrs.

4.5.2 Hypothetic TOC accumulation and gas formation

We applied a numerical model (as described above) on geochemical data from cores SL44, SL 35 and SL17/41 in order to test the hypothesis, if sediment accumulation is the only or at least the dominant cause for determining the inset of acoustic turbidity. SL44 and SL35 are located in the zone with acoustic transparent sediments, whereas SL17/41 is located inside this zone (Figs. 4.1 and 4.2). However, sites SL35 and SL17/41 are located closely to each other, thus we can likely assume that the input of organic matter has been roughly the same over time. For modelling diagenetic processes of unit 1 muddy deposits we used the calculated average sedimentation rates of 0.040, 0.061 and 0.081 cm yr⁻¹ at stations SL44, SL35 and SL17/41, respectively (Tabs. 4.1, 4.5), causing higher TOC fluxes and accumulation rates over time. In order to adapt the model in this regard we simulated the variation of TOC at the sediment surface by:

$$[TOC](0, t) = [TOC_{t_0}] + [TOC_{max}] \cdot e^{-\left[\frac{(t - a_1 - (t_{max} + a_2) / a_3)}{a_4} \right]} \quad (15)$$

where $[TOC_{t_0}]$ is the TOC concentration at the start of the model run, $[TOC_{max}]$ is the maximum increase of TOC concentration as defined by the subsurface peak in both cores, t_{max} is the maximum simulation time, and $a_1 - a_4$ are constants defining the shape of the input curve of TOC over time. The parameterisation of equation (15) in the model has mainly been constrained to enable the simulation of the subsurface peak at about 100

cmbsf at all locations. However, in order to keep the results comparable the same $[\text{TOC}_{t_0}]$ and $[\text{TOC}_{\text{max}}]$ have been used for all model runs (Figs. 4.5, 4.5). Combining the results with average sedimentation rates for the past 8000 yrs., resulted in TOC-accumulation rates, defining the forcing functions for organic matter decomposition and methane production.

It is likely to assume that the highest TOC input at site SL17/41 has caused slightly elevated rates of organic matter decomposition as defined by Eq. 1-3. Hence, we aimed at reconstructing the present-day TOC profile by adjusting total rates of organic matter decomposition. In order to get reasonable approximations to the profiles only the k_2 -value (Eq. 2) has slightly been adjusted. A lower k_2 -value implies a smoother decrease of the total mineralisation rates with depth. This implies that a larger fraction of reactive TOC is mineralised at greater depth, which is in line with the rising sedimentation rates from site SL44, SL35 and SL17/41, respectively. Overall, all model runs only deviate in the k_2 -value, and the sedimentation and TOC accumulation rates, respectively. All model parameters and boundary conditions are given in Table 4.5.

The presented kinetic model for methane generation in organic-rich sediments fits well with the measured TOC, pore-water methane and sulphate depth profiles at sites SL44, SL35 and SL17/41, respectively (Fig. 4.6). As pointed out above methane accumulation does not exceed trace levels at SL44 (Fig. 4.6a). This is also shown by the model results, when sulphate reduction due to AOM is estimated to be 1% of the total reduced sulphate (Σ SRR; Tab. 4.3). Thus, consumption of SO_4 at site SL44 is solely driven by sulphate reduction due to organic matter decomposition. The minimum sediment thickness of unit 1 to initiate methane accumulation is therefore located between core SL44 and core SL07 (322 and 392 cm, respectively in Tab. 4.1). We estimated the required sediment thickness of muddy unit 1 deposits for methane production, using the model set-up of SL44 with a slightly higher sediment thickness (350 cm) and corresponding higher sedimentation rate (0.043 cm yr^{-1}).

Using the average sedimentation rate of 0.06 cm yr^{-1} at site SL35 our kinetic model proposed significant methane generation and accumulation in unit 1 deposits (Fig. 4.6b; Tab. 4.6) and hence increased sulphate reduction rates due to AOM (Tab. 4.3). However, the modelled methane concentration profile of SL35 is still below the methane saturation limit at all depths. Thus, no free methane gas bubbles should occur at SL35 (and SL07), which is determined by the absence of acoustic turbidity at these stations (Fig. 4.2).

Moreover, the model results show that methane concentrations at this site are closely below the solubility limit (Fig. 4.6b), hence we can assume that a sediment thickness of about 500 cm is required to exceed the solubility limit of methane. This is in accordance with SL35 being located closely to the zone of acoustic turbidity (Fig. 4.2).

Our diagenetic model fits also well to the geochemical profiles measured for core SL17/41 (type III), which is taken in the zone of acoustic turbidity. Free methane gas (e.g. gas bubble formation) is indicated below a sediment depth of about 2.5-2.8 m by the model using a mean sedimentation rate of 0.08 cm yr^{-1} (Fig. 4.6c, Tab. 4.5). This is accompanied by the highest modelled sulphate reduction rate due to anaerobic oxidation of methane (Tab. 4.3), but even at this site in the acoustic turbid zone sulphate reduction related to AOM is estimated to be just about 20% of the total sulphate reduction (ΣSRR). The measured methane concentrations, however, are below the calculated CH_4 -solubility line at all depth. This is most probably caused by gas loss due to decompression during core retrieval and sediment sampling.

Overall, it could be confirmed by the diagenetic model (Tab. 4.6) that methane formation and accumulation in the muddy unit 1 layer is controlled by the sedimentation rate (i.e. TOC input) and hence the sediment thickness as postulated before by Thießen et al. (sub.).

However, in contrast to the modelled sediment depth of 2.5-2.8 m for free gas accumulation, the onset depth of acoustic turbidity during the sampling campaign was about 160 cm below the sediment surface. The onset depth was estimated with a P-wave velocity of 1350 m s^{-1} for the non-gassy sediment surface from Boomer profile P21 (Fig. 4.2; Mathys, 2003). These findings indicate that already at that depth gas bubbles occur. Moreover, Abegg and Anderson (1997) showed in gas-rich muddy sediments of Eckernförde Bay, that the point of methane oversaturation (POO) is located already about 80-100 cm shallower than the onset depth of the related acoustic turbid layer. Estimating that this depth difference also occurs in Arkona Basin sediments the POO therefore has to be located at about 60-80 cm sediment depth, which is not in agreement with our model results. However, as pointed out above the SMT is at about 50 cm depth and moreover Thießen et al. (sub.) could show that high concentrations of methane are introduced to the sulphate reduction zone (possibly by bubble ebullition) due to a shift of the methane solubility limit to lower values which were caused by an atmospheric pressure drop and related wind driven shoaling of the water depth.

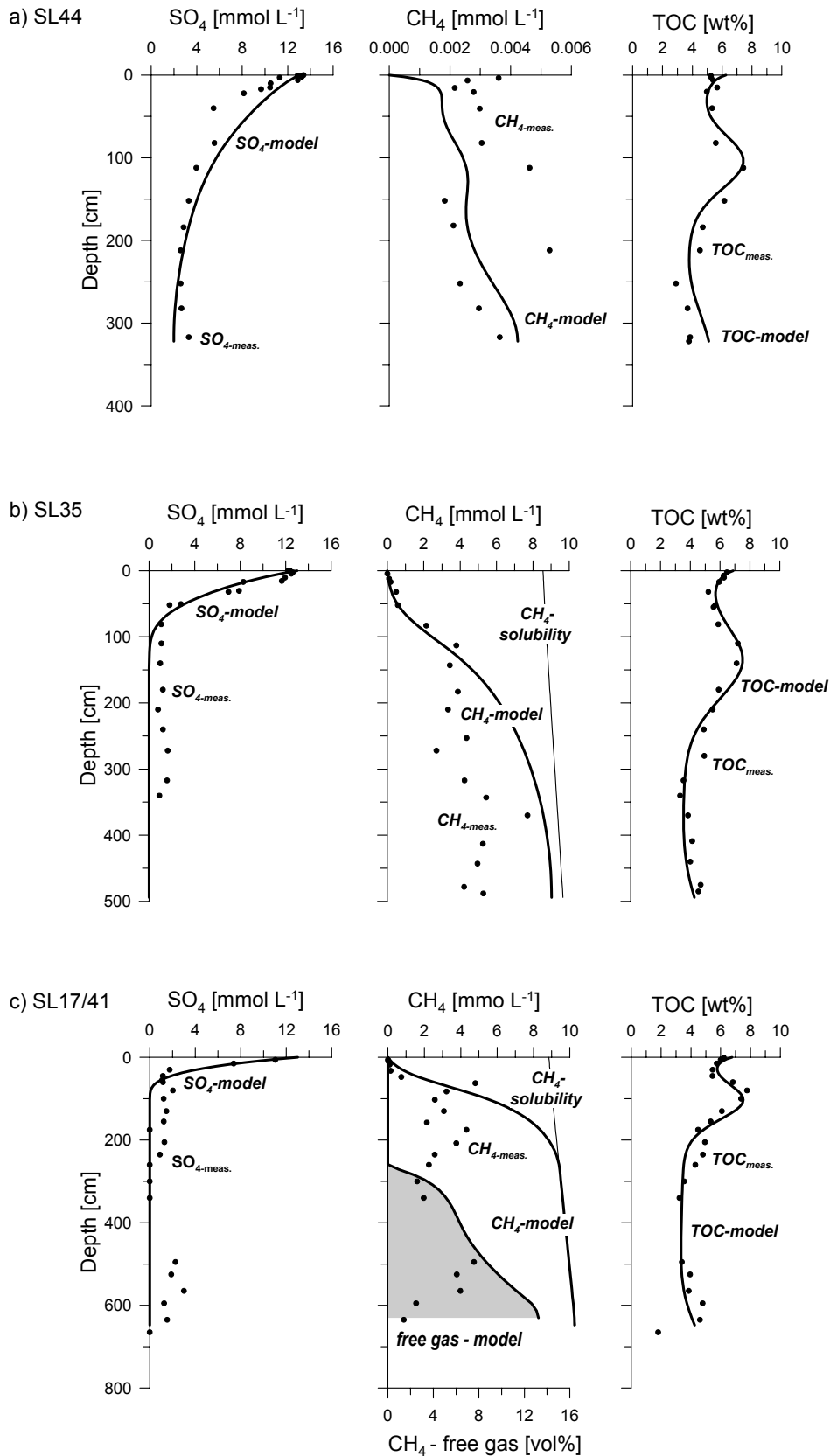


Fig. 4.6: Measured (filled dots) and modelled (bold line) pore-water concentration profiles of SO₄, CH₄ and TOC of cores SL44, SL35 and SL17/41. The thin black line marks the calculated methane solubility limit at the pressure, salinity and temperature conditions at sampling day. Model results show at core SL17/41 the occurrence of free gas (gas bubbles) in the sediment (grey shaded area).

Atmospheric pressure and wind driven water depth variations are common in the Baltic Sea region and in combination with seasonal temperature changes may cause variations in methane production and methane solubility, which may lead to depth variations of the acoustic turbid layer (Wever and Fiedler, 1995). Thus, we assume that the depth discrepancy between the modelled POO and the estimated/observed POO may be caused by intense methane upward flux by bubble ebullition or by migration of gas bubbles from the methane bearing sediments caused by non-stationary methane solubility limits and seasonal variability of methane production rates. Due to the lack of constraints it is impossible to properly parametrise a model for the simulation of such dynamic conditions. Nevertheless, assuming more stable conditions the model reveals that methane production and acoustic turbidity are ultimately controlled by small-scale differences in the accumulation of TOC.

4.5.3 Methane C-isotope fractionation

As shown above (Tab. 4.3) there is intense AOM beneath the sediment surface in unit 1 sediments of the Arkona Basin (see also Thießen et al., sub.). Hence, the stable carbon isotope shift of CH₄ from –89 to –81 ‰ in combination with decreasing CH₄ concentrations towards the sediment surface (SL07) is most likely also related to AOM (Fig. 4.4). In the core interval from 60-510 cm $\delta^{13}\text{C}_{\text{CH}_4}$ values are quite constant (about –90 ‰) and correlate with high pore-water methane concentrations ranging from about 3600 to 7700 $\mu\text{mol L}^{-1}$.

These values are typical for CH₄ generated by CO₂ reduction in anaerobic marine sediments (e.g. Claypool and Kaplan, 1974; Schoell, 1980; Whiticar et al., 1986). Interestingly, a pore-water $\delta^{13}\text{C}_{\text{CH}_4}$ shift from –90 ‰ at about 510 cm to –112 ‰ at 1100 cm (Fig. 4.4; Tab. 4.5) correlates with decreasing methane concentrations in the reddish/brown, suboxic to oxic sediments of unit 3.

Low-level methane concentrations detected in unit 2 and 3 sediments at type I sites and moderate CH₄ concentrations at type II sites (Tab. 4.3), allow the conclusion that the methane is diffusing down-ward from the overlying methane bearing deposits. Assuming that diffusion is the dominant transport process, the time required to reach the present-day penetration depth of CH₄ is about 1400 yrs.

Nevertheless, the reasons for the observed downward carbon isotope shift are questionable. One possibility to explain this observed shift might be diffusive isotope

Table 4.5: Model parameters and boundary conditions used for Holocene muddy sediments at Arkona Basin stations SL44, SL35 and SL17/41.

Parameter	Symbol	Core SL44	Core SL35	Core SL17/41	Reference
Thickness modeled muddy deposits		322 cm	494 cm	648 cm	this study
Sedimentation rate (base of muddy sediments)	ω_{bot}	0.04 cm yr ⁻¹	0.06 cm yr ⁻¹	0.08 cm yr ⁻¹	calc. after Emeis et al. (2002, etc.)
Porosity (sediment surface)	ϕ_{top}		0.9		this study
Porosity (base)	ϕ_{bot}		0.7		this study
Attenuation coefficient (porosity)	$const$		1/150 cm ⁻¹		this study
Grain density	d_s		2.65 g cm ⁻³		this study
Age of TOC at sediment surface	age_{t_0}		50 yr ⁻¹		
Coefficient 1 for TOC degradation	k_1	0.18	0.18	0.18	this study
Coefficient 2 for TOC degradation	k_2	1.05	1.0	0.95	this study
Reactive TOC at the sediment surface at t_0	$[TOC_{t_0}]$		6.2 wt%		this study
Max. TOC increase	$[TOC_{max}]$		6.0 wt%		this study
Maximum simulation time	t_{max}		8000		after Emeis et al. (2002, etc.)
Coefficient 1 for TOC input	a_1	2.6	2.6	2.65	this study
Coefficient 2 for TOC input	a_2	100	100	100	this study
Coefficient 3 for TOC input	a_3	3.3	3.3	3.0	this study
Coefficient 4 for TOC input	a_4	1.2·10 ⁵	1.2·10 ⁵	3.0·10 ⁶	this study
Monod constant for sulfate reduction	k_{SO_4}		0.1 mmol dm ⁻³		this study
Inhibition constant for inset methanogenesis	kI_{SO_4}		0.1 mmol dm ⁻³		this study
Inhibition constant for methane production	kI_{meth}		5		this study
Kinetic constant of AOM	k_{AOM}		0.1 dm ³ mmol ⁻¹ yr ⁻¹		Luff & Wallmann (2003)
Constant of free gas formation	K_{GF}		0.1 dm ³ dm ⁻³ yr ⁻¹		this study
Constant of free gas dissolution	k_{GD}		0.1 yr ⁻¹		this study

fractionation. However, there is no consensus on diffusive isotope fractionation estimated from laboratory experiments and field observations (e.g. Fuex, 1980; Reitsema et al., 1981; Clayton et al., 1997; Prinzenhofer and Pernaton, 1997; Zhang and Kroos, 2001). The isotope shift during downward diffusion may also be associated with a chromatographic effect in clay-silt sediments, or alternatively by preferred adsorption of ¹³C on clay minerals. As discussed above we predict, that the pore-water methane observed in unit 3 sediments is coupled to methane production in unit 1 organic-rich sediments. This means, that the methane found at the base of core SL07 is older than that one found in the unit 1 to unit 3 transition. Therefore, it is also likely that the measured

untypical stable carbon isotope values just reflect the depletion in ^{12}C of the precursor material during increasing methane production (Claypool and Kaplan, 1974) under non-steady-state conditions.

4.6 Conclusions

Muddy Holocene sediment of various thickness covers late glacial clayey sediment in the shallow Arkona Basin of the Baltic Sea. The anoxic conditions in the organic-rich (4-8% TOC) surface sediment coverage (unit 1) favours methane formation whereas only low methane concentrations could be measured in interstitial waters of the underlying reddish/brown clayey deposits (unit 3). Methane accumulation was found in the upper muddy segment, which starts at a minimum thickness of about 350 cm of unit 1. Methane accumulation is mainly controlled by pore-water sulphate concentrations and the sediment thickness of the muddy sediment segment. Application of a transport-reaction model considering sedimentation, organic matter diagenesis by microbial sulphate reduction and methane formation/oxidation shows that the onset of methane accumulation and the occurrence of free gas in interstitial waters is highly sensitive to the sedimentation rate ($0.6\text{-}0.8\text{ mm yr}^{-1}$) and to the deposition of organic matter. The model indicates methane oversaturation and hence gas bubble formation in sediments with a minimum sediment thickness of about 5 m. The results of geochemical modelling agree well with the distribution of acoustic turbidity in these sediments. We propose that the general outcome of the diagenetic model approach can be directly transferred to other Baltic Sea or similar shelf sea areas with fine grained sediments and high organic loading.

Acknowledgements

The authors thank the captains and crews of R.V. POSEIDON and R.V. ALKOR for their large efforts made during the sampling campaigns. We wish to thank Eckard Bedbur and Inge Dold at the Institute for Geosciences University Kiel, and Bettina Domeyer at the IFM-Geomar Institute, Kiel, who kindly provided us with pore-water sulphate and chloride and TOC measurements. The stable carbon isotope measurements were supported by Manfred Schmitt, Geochemische Analysen, Sehnde, Germany. Investigations were made in the NATLAB project (project leader F. Theilen) which was funded by the Federal Ministry for Education and Research (BMBF) and the German

Research Council (DFG; grant no. 03 G 0564 D to Kiel University) in the framework of the GEOTECHNOLOGIEN “gas hydrates in the geosystem” research program.

Chapter 5

Methane venting into the water column above the Pitcairn and the Society - Austral seamounts, South Pacific

Olaf Thießen^{a,b}, Mark Schmidt^a, Reiner Botz^a, Manfred Schmitt^b, Peter Stoffers^a

^a*Institut für Geowissenschaften der Universität Kiel, Abteilung Marine und Terrestrische Geochemie,
Ludewig-Meyn-Str. 10, D-24118 Kiel, Germany*

^b*Geochemische Analysen (GCA), Glückaufstr. 50, D-31319 Sehnde-Ilten, Germany*

Abstract

Three hotspot areas in the South Pacific at 17°S to 29°S Long and 150°W to 130°W Lat are characterised by volcanically active submarine seamounts (Pitcairn, Macdonald, Teahitia) that show T-, pH- and CH₄ anomalies in the bottom water which could be recorded by CTD systems or have been analysed onboard R.V. SONNE and R.V. L'ATALANTE, respectively. Spotted vent fields (bubble fields and shimmering waters) were directly sampled by an ocean floor observation system (OFOS) or the submersible *Nautilie*. The CH₄ concentration above the summits of the seamounts exceeds the surface water equilibrium value of 48 nl L⁻¹ by several orders of magnitude. The highest CH₄ concentration detected was 31,615 nl L⁻¹ in a bubble field at Macdonald.

The carbon isotopic composition of the CH₄ ranges between -22 and -56‰. The δD values of three hydrothermal CH₄ samples are between -103 and -117‰. According to the isotope values venting CH₄ from Bounty seamount consists of pure microbially produced (via CO₂ reduction at 88°C) CH₄, whereas hydrothermal gas at Macdonald contains some (up to 50%) isotopically "heavy" abiogenic CH₄ (produced via high-temperature CO₂ reduction) mixed with biogenic CH₄ formed at relatively low temperature within the shallow hydrothermal vent system. However, the relationship between CH₄ concentrations and isotope values also indicate that CH₄ oxidation has taken place. Thus, based on the (carbon) isotope values (δ¹³C = -22 and -29‰, resp.) of hydrothermal CH₄ from Teahitia seamount alone it cannot be decided whether this gas derived from abiogenic reactions in the deep subsurface or, alternatively, represents a residual fraction of CH₄ oxidation.

5.1 Introduction

In the past marine hydrothermal systems were studied by numerous work groups focusing on different research aspects. For instance mechanisms of fluid-associated particle transport and diverse hydrothermal mineralisations have been studied by von Damm and Bischoff (1987), Stüben et al. (1992), Halbach et al. (1993), Rona and Scott (1993), Butterfield et al. (1994), Hannington et al. (1995), Glasby et al. (1997) and others. Moreover, biologists found that hydrothermal vent systems can host chemosynthetic organisms (Tunnicliffe, 1991; Jannasch, 1995; Nelson and Fischer, 1995; Dando et al., 1995). Hydrocarbons observed in hydrothermal systems were ascribed to abiogenic and biogenic formation processes. In particular, numerous hydrothermal vents on deep seafloors show CH₄ of abiogenic origin (Welhan, 1988; Charlou et al., 1996; 2002). Hydrocarbon formation can occur via diverse processes like water-/ rock reactions (including serpentinisation processes) investigated by Seyfried and Dibble (1980), Seyfried and Janecky (1985), Alt (1995), and Charlou et al. (2002). Moreover, hydrothermal trace gases can also be introduced by mantle emanations (Craig and Lupton, 1981; Welhan, 1988) or formed in the earth's crust by thermocatalytic (Simoneit, 1983; Michaelis et al., 1990) or abiogenic reactions (Apps, 1985; Sherwood Lollar et al., 1993). On the other hand biogenic methane formation (and / or hydrocarbon oxidation) may be caused by microbial activities within the vents and at or near the sediment surface at temperatures below 113°C (Huber et al., 1990; Burggraf et al., 1990). These biogenic gases of relatively shallow origin may superimpose hydrothermal trace gas components formed by abiogenic reactions in the earth's crust.

More specifically, active hydrothermal systems in the Pacific Ocean are related to various tectonic settings such as the East Pacific Rise (Hekinian et al., 1984; Charlou et al., 1991; 1996; Urabe et al., 1995; Ishibashi et al., 1997), the Galapagos spreading center (Corliss et al., 1979), marginal basins (Lonsdale et al., 1980; Both et al., 1986; Fouquet et al., 1991; Ishibashi et al., 1994; 1995) and submarine intraplate hotspot related volcanoes as for instance Loihi (Malahoff et al., 1982; Gamo et al., 1987; Sakai et al., 1987; Karl et al., 1988; Sedwick et al., 1992), Teahitia (Hoffert et al., 1987; Stüben et al., 1992; Michard et al., 1993), Macdonald (Cheminée et al., 1991; Stüben et al., 1992) and Bounty seamounts (Stoffers and Hekinian, 1990) (Fig. 5.1).

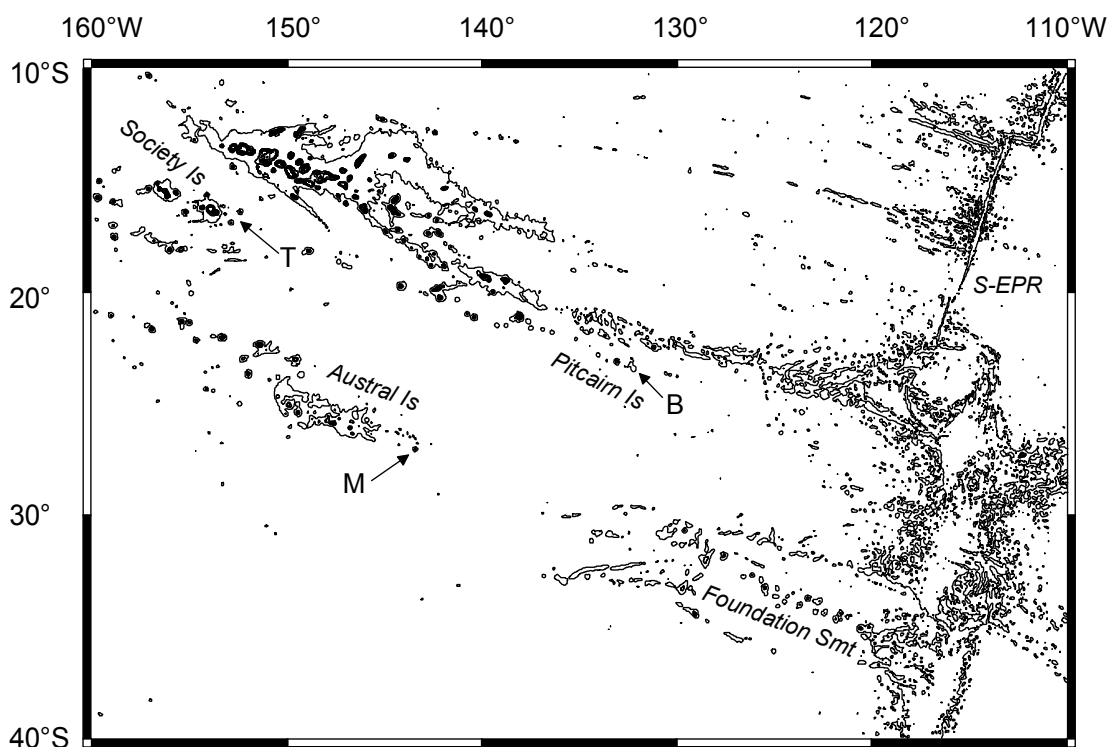


Fig. 5.1: Location map of the South Pacific Ocean showing the sampling areas at Bounty (B), Macdonald (M), and Teahitia (T) seamounts, bathymetry data, the southern East Pacific Rise (S-EPR) and the Pitcairn, Austral, and Society Island chains.

Two research cruises Midplate II (R.V. SONNE, in 1989) and Polynaut (R.V. L'ATALANTE with the submersible *Nautilie*, in 1999) focused on investigations of recent volcanic activity and associated hydrothermalism at submarine volcanic centers in the Societies, the Australs and near Pitcairn Island, respectively (10° to 40°S and 110° to 160°W; Fig. 5.1). It is well known that submarine hydrothermal activity is responsible for significant inputs of elements into the marine environment. In particular hydrothermal tracer substances such as Mn, CH₄ and ³He can be detected in the ocean water even far away from active hydrothermal vent sources (Ishibashi et al., 1994; 1997; Stüben et al., 1992; Charlou et al., 1991). On the occasions of the research cruises mentioned above we studied the distribution of methane in the water column which derived from hydrothermal vent systems of the Teahitia-, Bounty- and Macdonald seamounts (Tab. 5.1; Fig. 5.1). Moreover, we sampled the exsolved gases for later land-based stable isotope investigations of the gas compounds. This technique has proved to be of great value when studying the mode of formation of gaseous hydrocarbons on earth (Schoell, 1980; Welhan, 1988; Whiticar, 1990). Subsequent hydrocarbon oxidation can be recognised by significant kinetic enrichments of heavy isotopes in the residual

hydrocarbon fraction whereas the produced CO₂ becomes enriched in ¹²C (Whiticar and Faber, 1986).

Area	Seamount	CTD-Station	Dive station
			So65
<i>Australis</i>	<i>Macdonald Smt</i> 28°59'S/140°15'W Summit depth ~40m	So65 94MS	1070FOS
		So65 96MS	-
		So65 98MS	-
		So65 99MS	-
		So65 100MS	-
		So65 101MS	-
		So65 103MS	-
		So65 104MS	-
		So65 105MS	-
<i>Pitcairn</i>	<i>Adams Smt</i> 25°23'S/129°16'W Summit depth ~60m	So65 36MS	-
		So65 38MS	-
	<i>Bounty Smt</i> 25°11'S/129°24'W Summit depth ~430m	So65 32MS	-
		So65 41MS	-
		So 65 42MS	-
		So65 53MS	-
		So65 54MS	-
		So65 77MS	-
		Pol MS02	Nautile PN04
	Pol MS03	Nautile PN05	
	Pol MS04	Nautile PN06	
	Pol MS05	Nautile PN11	
	Pol MS09	Nautile PN12	
	<i>Christian Smt</i> 25°35'S/129°31'W Summit depth ~2000m	Pol MS06	-
		-	-
<i>Societies</i>	<i>Teahitia Smt</i> 17°34'S/148°49'W Summit depth ~1400m	So65 118MS	
		Pol MS13	Nautile PN18
		Pol MS14	Nautile PN19
		Pol MS15	-

Table 5.1: Sampling stations of various hotspot seamounts.

5.2 Geological setting

The Society-, Pitcairn (Pitcairn – The Gambiers – Mururoa – Duke of Gloucester) and Austral Island chains form broad NW-SE (roughly perpendicular to the EPR) striking lineaments (Fig. 5.1). These intraplate island chains are probably the result of a northwest directed movement of the Pacific plate across a mantle hotspot system (Morgan, 1971). The limits of hotspot activities in these regions are usually shallower than 3700m depth. Regional bulging (in the work area it is indicated by water depths

between 3500 and 3800 m) relative to the surrounding seafloor (>4000 m water depths) is characterised by numerous volcanic edifices (Crough, 1983; Hekinian et al., 1991; Binard et al., 2004).

More than 25 volcanoes are situated on the most westerly part of the bulge of the Societies. These 300 m to 3900 m high volcanoes are located approximately 30 nautical miles ESE from Tahiti. Three major volcanic centres are recognised in the area surrounding the larger edifices (Teahitia & Mehetia). Teahitia seamount (rising up to 1400 m below sea level), Mehetia Island (450 m above sea level), and the Mona Pihaa seamount (rising up to 160 m below sea level). The volcanic centres are generally NNW-SSE oriented similar to the fault scarps of the abyssal hill region (Hekinian et al., 1991; Binard et al., 2004). Formerly, hydrothermal activity was observed near the summit of Teahitia seamount (Cheminée et al., 1989; Stüben et al., 1992; Michard et al., 1993).

The Pitcairn hotspot area is characterised by many (> 90) small (< 500 m high) and two major submarine volcanoes (e.g. Adams- and Bounty seamounts). Adams seamount rises from 3500 m up to 59 m water depth. Its summit is covered with corals and coral sand. Underwater observations and methane concentration measurements in the water column did not reveal any indications of recent hydrothermal activity (Polynaut Cruise Report, 2000). Bounty seamount, however, which rises to approximately 430 m water depth appears to be younger than Adams seamount and its summit is covered with hydrothermal sediments (Stoffers and Hekinian, 1990; Polynaut Cruise Report, 2000). The sea floor between the seamounts and the 40 nautical miles distant Pitcairn Island is between 3500 m and 3700 m depth, and its surface consists of gently rolling hills with small seamounts and roughly N-S oriented horst and graben structures (100 to 200 m relief). It is believed that these N-S oriented horst and graben structures have been formed at or near to an ancient spreading ridge in the Farallon plate.

The Austral hotspot is characterised essentially by the presently active Macdonald seamount (Smt) and the more ancient Ra Smt (Fig. 1). The approximately 3000 m high Ra seamount, which rises up to 1040 m water depth, is located about 40 nautical miles NNW of Macdonald but did not show any indications of hydrothermal activity (Stoffers et al., 1987). However, seismic recordings revealed that Macdonald volcano, which rises from 4250 m to 40 m water depth, has been active in the late 1980ies (Talandier, 1989; 2004). A phreatomagmatic eruption occurred in January 1989 and hydrothermal activity

was observed (Stoffers et al., 1989; Stoffers and Hekinian, 1990; Cheminée et al., 1991; Stüben et al., 1992).

5.3 Methods

Water sampling was performed at individual water depths using a rosette water sampler CTD device (SeaSun Technology, Germany and Meerestechnik ME, Germany during Polynaut cruise and during research cruise with R.V. SONNE, respectively) equipped with 12 Niskin bottles of 5 and 10 L volume and, for comparison purpose, a gas-tight water sampler (Schmitt, 1989). Hydrographic parameters (temperature, pressure, conductivity, sound velocity, oxygen content, light transmission) were continuously recorded while lowering the CTD system (Stoffers and Hekinian, 1990; Polynaut Cruise Report, 2000). We decided to report the temperature and pH values together with the dissolved CH₄ concentrations as these parameters reliably indicate hydrothermal activity in the area, however, salinity/density/conductivity anomalies were not observed during Polynaut cruise.

During SONNE 65 cruise, emanating hydrothermal fluids (shimmering water) were directly sampled using an OFOS system, which was equipped with a Seabird CTD, in order to locate and directly sample seafloor sites where active venting occurred. Water sampling was done by controlled release of 5 L Niskin bottles which were connected to the OFOS system. At > 500 m water depths positioning of the OFOS was controlled with a AMF-sealink transponder system relative to the ship's position. At < 500 m water depths the ship's positioning system was used directly (since in this case the deviations of the OFOS system were smaller than the accuracy of the transponder system).

During the R.V. L'ATALANTE cruise ("Polynaut") in 1999 hydrothermal vent fluids were also directly sampled by the submersible *Nautile* using a 1.8 L Niskin bottle operated by the pilot. Temperature was measured "in situ", placing the *Nautile* temperature probe directly in the venting fluids near/in the sediment surface.

On board of the research vessels R.V. SONNE and R.V. L'ATALANTE, respectively, the water samples were immediately transferred into 1 L glass bottles (stored at 4°C for a maximum time of four hours) followed by subsequent degassing in an ultrasonic-vacuum system (Schmitt et al., 1991). Using this technique the detection limit of hydrocarbons in sea water is <5 nl L⁻¹ with a precision of ±13% in the range of 5-50 nl L⁻¹ CH₄).

Onboard analyses of hydrocarbons was performed using a DANI-Educational gas chromatograph equipped with a 30 m long, 0.32 mm diameter, $\text{Al}_2\text{O}_3/\text{KCl}$ column, a flame ionisation detector (FID) and a SHIMADZU C-R6A integrator; carrier gas nitrogen. Based on daily replicate standard analyses analytical precision was within $\pm 5\%$.

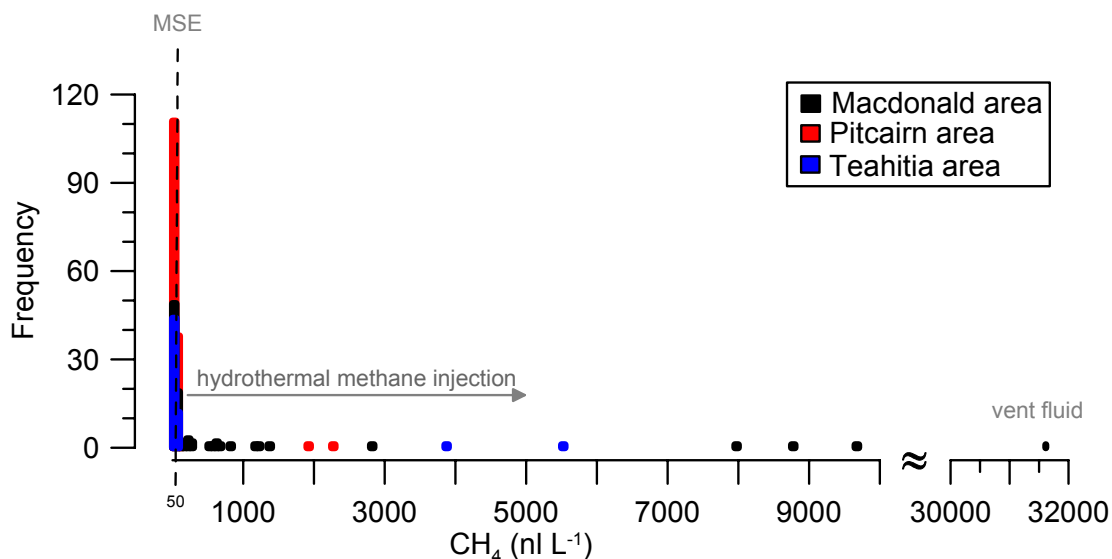


Fig. 5.2: Methane concentrations, detected on the Bounty, Macdonald, and Teahitia Seamounts are summarised by their frequency (50 nl L^{-1} interval).

Gas samples with relatively high hydrocarbon concentrations were stored in evacuated glass vessels for later stable isotope analyses. Preparation of gas samples for isotope measurements included gas chromatography (DANI-Educational GC, specifications see above), online transfer (He-carrier gas) of individual hydrocarbons into a combustion line (copper oxide, $T = 900^\circ\text{C}$), and stable isotope analyses of CO_2 using a Finnigan MAT 251 isotope ratio mass spectrometer (Faber et al., 1998). Three CH_4 samples with sufficient amounts ($8\text{-}31 \mu\text{l L}^{-1}$) were analysed for their hydrogen isotope composition according to the techniques described by Dumke et al. (1989). The analytical precision of analyses, including conversion of CH_4 , was $\pm 0.5\%$ ($\delta^{13}\text{C}$) and 4% (δD). Isotope values for international reference standards obtained in the GCA laboratory were -29.81% PDB (NBS-22) and -28.15% PDB (NBS-21). The isotope results are expressed in the common δ -notation relative to the PDB ($\delta^{13}\text{C}$) and SMOW (δD) standards.

5.4 Results and discussion

5.4.1 Water column characteristics and methane distribution

The methane content of ocean water is determined by diverse CH₄ sources such as biological activity in sediments and water column, thermal hydrocarbon production in organic-rich sediments, abiogenic reactions in the deep subsurface (e.g. in the deep crust or mantle) and subsequent exchange with the atmosphere. The major sink in the ocean water column is bacterial oxidation (Whiticar and Faber, 1986) but, depending on the location, the atmosphere may act as a source or sink for dissolved methane (e.g. Faber et al., 1994; Bange et al., 1996; Rehder et al., 1998). Methane concentration in sea surface water which is in equilibrium with atmospheric methane is controlled by temperature and salinity (Wiesenburg and Guinasso, 1979). The sea surface water in the area under investigation has temperatures between 20.7°C and 26.3°C at 36‰ salinity. Hence, the CH₄ concentrations in South Pacific ocean surface waters at equilibrium conditions with the atmosphere range between 43 nl L⁻¹ and 48 nl L⁻¹. In the following we refer to this equilibrium CH₄ concentrations in surface sea water as MSE = “Methane Sea Surface Equilibrium Concentration”. Methane concentrations measured on the Bounty, Macdonald, and Teahitia seamounts from the south Pacific are summarised in Table 5.2 (Appendix) and shown in histogram-Figure 5.2. The methane concentrations measured in the water columns and venting fluids exceed the MSE of about 50 nl L⁻¹ by several orders of magnitude at all three seamounts (Fig. 5.2). The various methane concentration profiles are discussed in detail for Pitcairn, Macdonald and Teahitia area.

5.4.1.1 CH₄ concentration profiles

In the Pitcairn area most of the water profiles (Figs. 5.3 – 5.5; Tab. 5.2) show methane concentrations in the range of about ±20-30 nl L⁻¹ off the background concentration of 48 nl L⁻¹. However, weak methane anomalies are recognised near to the summit of Bounty seamount at a water depth of 300 to 500m (MS02, MS05, MS09 in Figs. 5.3 and 5.4; 32MS, 42MS in Fig. 5.5) and near the summit of the SSW located Christian seamount (MS06 in Fig. 5.3). Methane anomalies near Bounty summit are associated with weak hydrothermal activity where yellow to reddish iron oxide sediments were discovered during sea floor observations made with Nautile (Polynaut Cruise

Report, 2000). Shimmering water also occurred at small holes, very small (< 10 cm high) and soft chimneys or veins. Temperatures of 14.4°C to 19.1°C measured directly in the venting fluids were high compared to ambient seawater with a temperature of about 10°C. However, corresponding temperature or pH anomalies were not detected in the hydrocast stations (Figs. 5.3-5.5) probably caused by efficient mixing of venting fluids with ambient seawater.

About six month after the eruptive phase of Macdonald seamount in 1989 (Stoffers et al., 1989; Cheminée et al., 1991) a number of CTD stations show large methane anomalies near Macdonald summit (99MS; 100MS; 101MS; 103MS; 104MS in Fig. 5.6). Strongest methane enrichments up to 9,691 nl L⁻¹ were measured at 191m depth at CTD station 104MS (Fig. 5.6; Tab. 5.2) and correspond to a pH 6.3 anomaly.

In some areas of the sea bottom (OFOS 107 and MS105 in Tab. 5.2, Fig. 5.6) near to the summit of Macdonald seamount we observed bubble fields and small (1°C to 2°C) temperature anomalies in bottom sea water. This indicates gas oversaturation and/or boiling conditions at the shallow water depth of some 200 m under the assumed high temperature of 200°C (Cheminée et al., 1991) within fracture systems of the submarine volcano. CO₂ is a major gas component (Cheminée et al., 1991) and thus, dissolution of CO₂ in sea water occurs when hydrothermal fluids are cooling down on their way to the sea surface due to mixing with ambient sea water ($T_{\text{bottom water}} \sim 16.5^\circ\text{C}$). Locally low pH values (up to 5.8) of bottom water (104 MS, OFOS 107 in Tab. 5.2) reflect these high CO₂ contents (Cheminée et al., 1991). The drop in pH is always associated with injections of hydrothermal methane (up to 31,615 nl L⁻¹; Fig. 5.6) clearly exceeding the local CH₄ background values at stations MS 100, 101, 103, 104, 105, OFOS 107 (Fig. 5.6).

At Teahitia seamount the most active area is located near the southernmost summit (Fig. 5.7). Almost the whole area is covered with Fe-oxide-rich sediments. Intensive venting and shimmering water occurred at numerous small ridges with cm to m large chimneys or at fissures in surface sediments. However, we did not detect comparable large CH₄ anomalies near to sea bottom above Teahitia seamount (Fig. 5.7) as we found at Macdonald. Moreover, at Teahitia gas oversaturation conditions did not prevail and visible gas bubble formation was not observed. This is probably due to a lower total gas content at Teahitia (but note that the pH values of 5.33 and 5.14 for the hydrothermal fluids of Teahitia are lower as the pH values from Macdonald indicating significantly

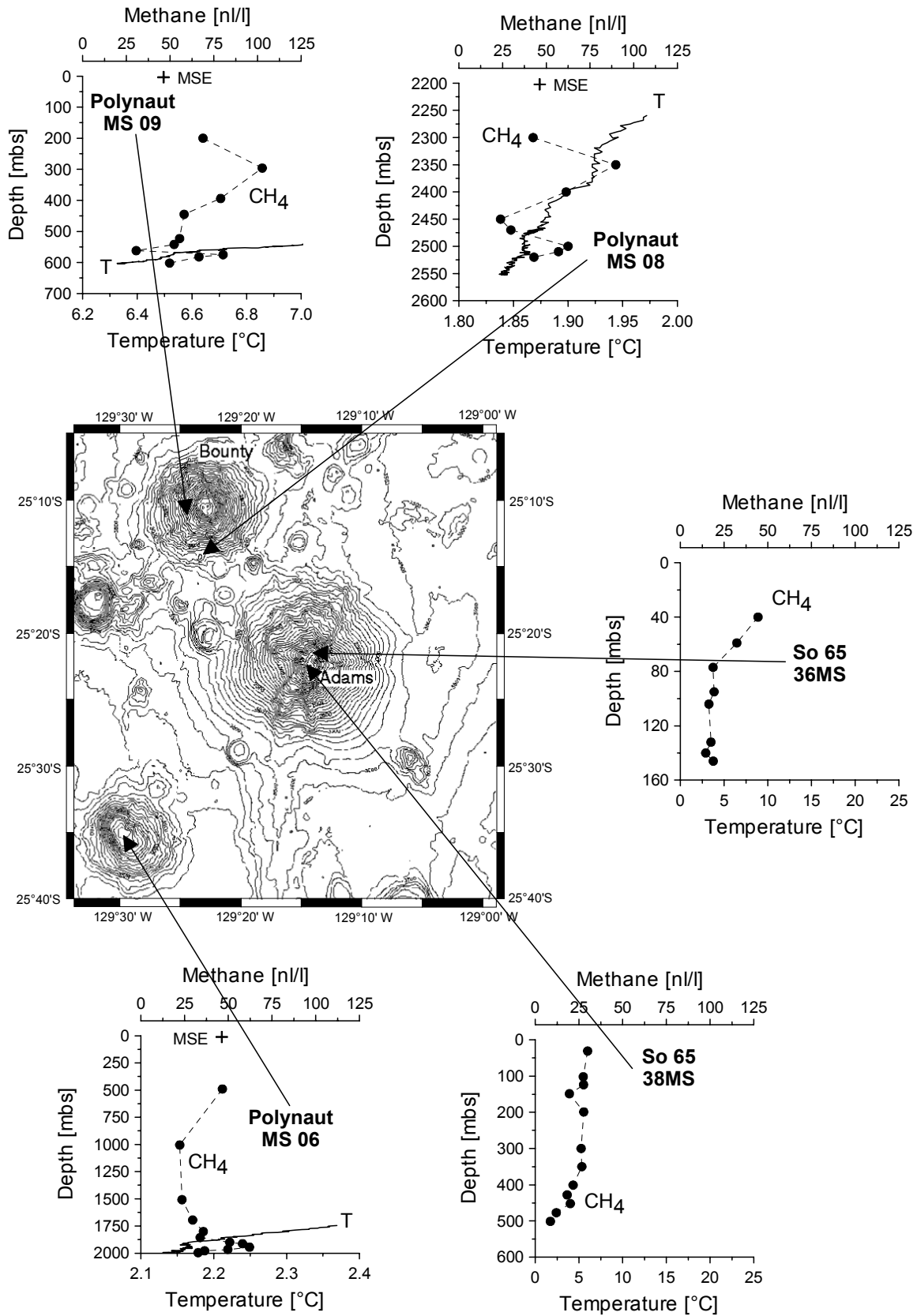


Fig. 5.3: Sampling stations and bathymetry map of the Pitcairn hotspot area showing the Bounty (summit depth ~430m), Adams (summit depth ~59m), and Christian (summit depth ~2000m) volcanoes. Methane concentration and temperature profiles are plotted vs. depth at; **a** Polynaut MS 09 station; **b** Polynaut MS 08 station; **c** SONNE 65 36MS station; **d** SONNE 65 38MS station; **e** Polynaut MS 06 station.

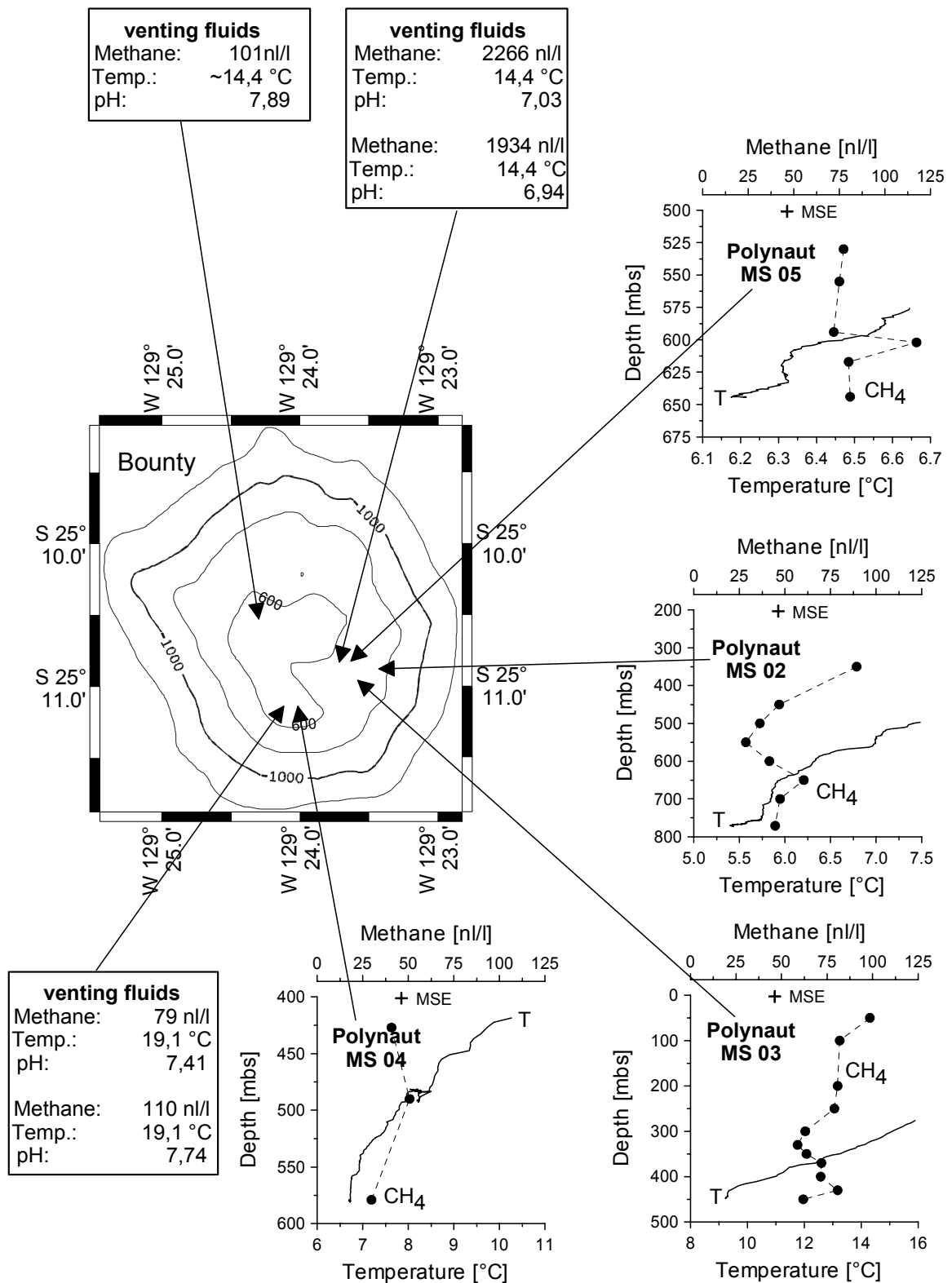


Fig. 5.4: Sampling stations and bathymetry map of the Bounty (summit depth ~430m) Seamount, Pitcairn hotspot area. Methane concentration and temperature profiles are plotted vs. depth at; **a** Polynaut MS 05 station; **b** Polynaut MS 02 station; **c** Polynaut MS 03 station; **d** Polynaut MS 04 station; methane concentrations, temperatures and pH of fluids from *Nautilie* dives during the 1999 Polynaut cruise.

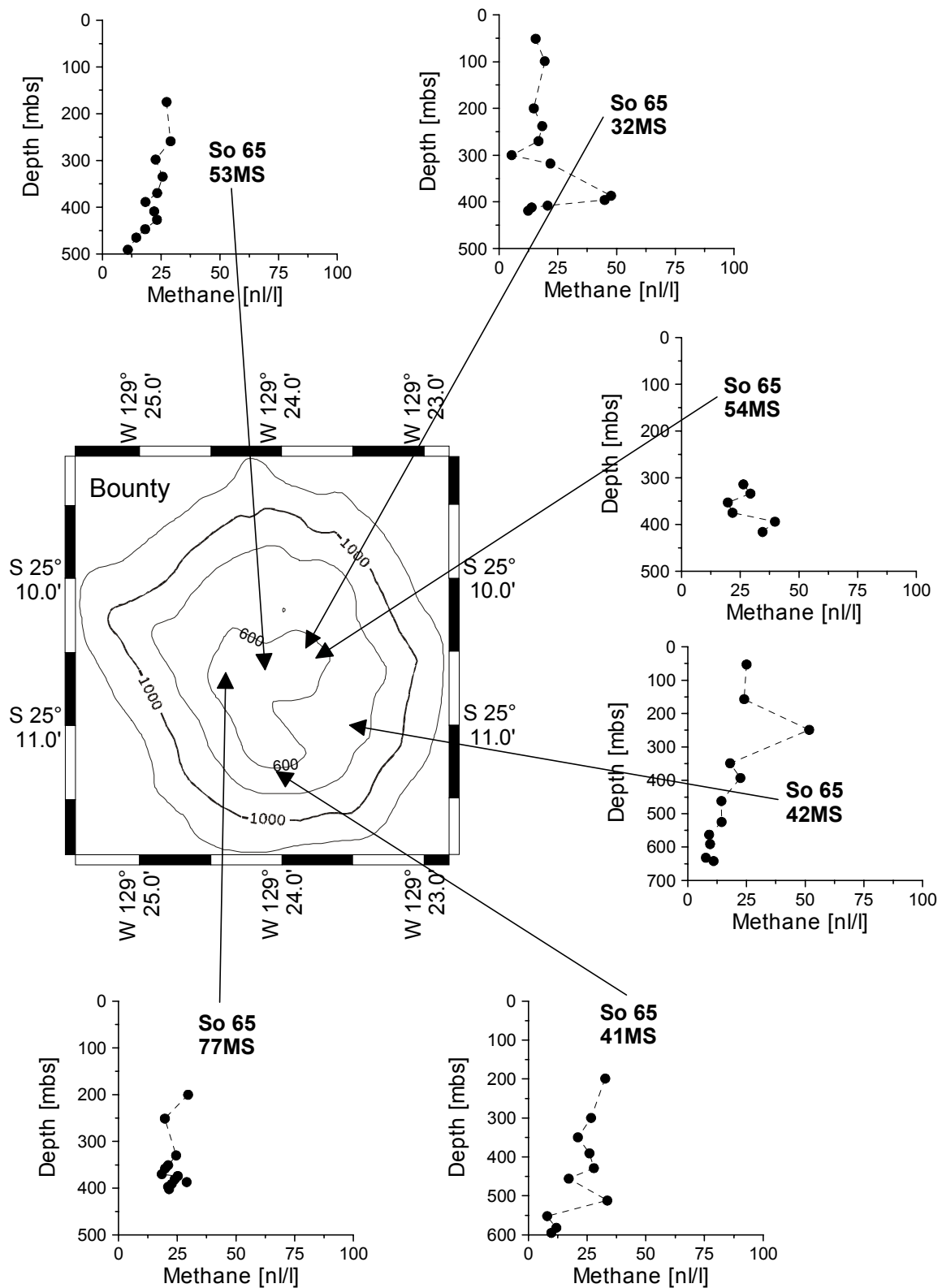


Fig. 5.5: Sampling stations and bathymetry map of the Bounty (summit depth ~430m) Seamount, Pitcairn hotspot area. Methane concentration profiles are plotted vs. depth at: **a** SONNE 65 53MS station; **b** SONNE 65 32MS station; **c** SONNE 65 54MS station; **d** SONNE 65 42MS station; **e** SONNE 65 41MS station; **f** SONNE 65 77MS station.

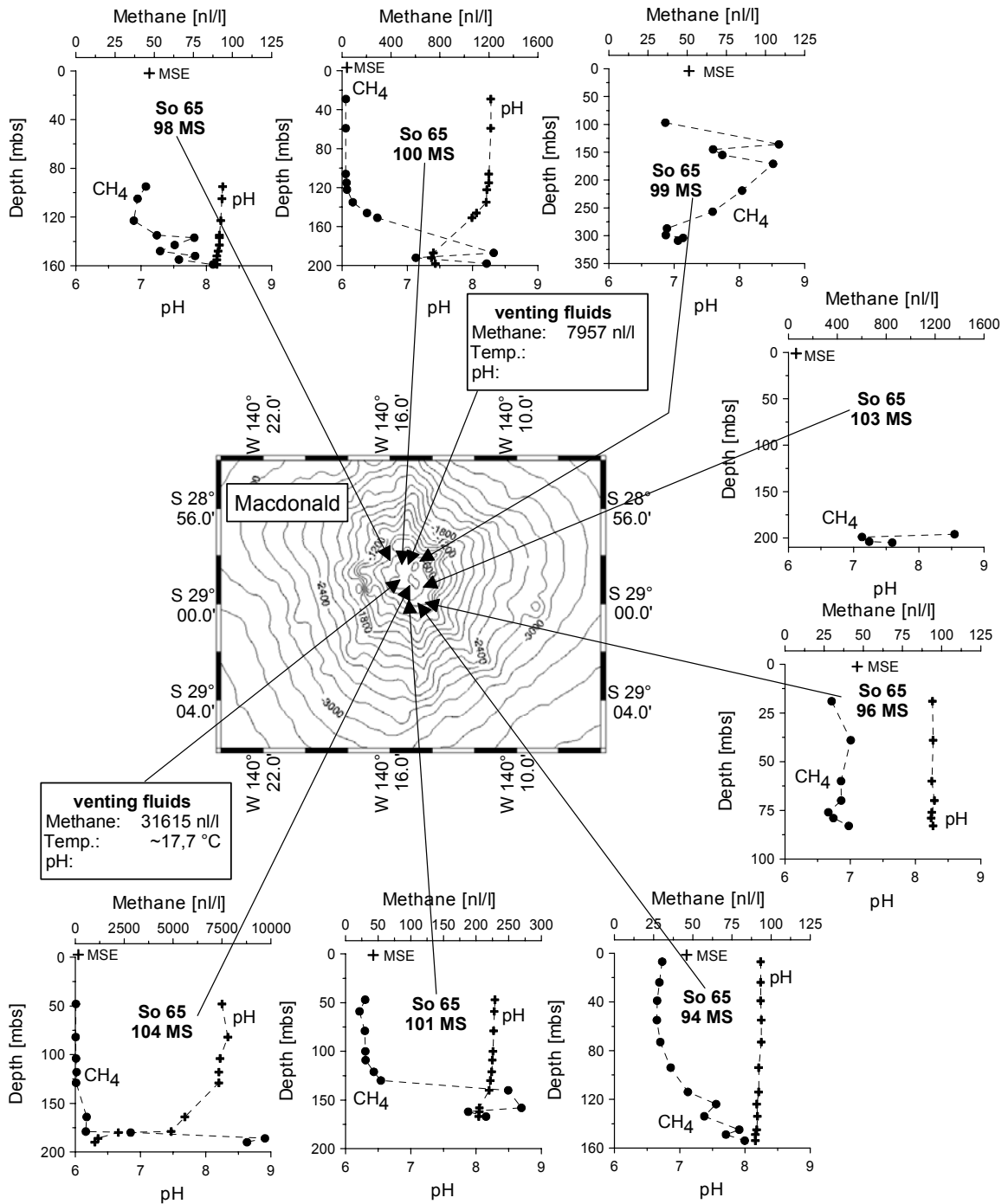


Fig. 5.6: Sampling stations and bathymetry map of the Macdonald (summit depth ~40m) Seamount, Austral hotspot area. Methane concentration profiles are plotted vs. depth at; **a** SONNE 65 98MS station; **b** SONNE 65 100MS station; **c** SONNE 65 99MS station; **d** SONNE 65 103MS station; **e** SONNE 65 96MS station; **f** SONNE 65 94MS station; **g** SONNE 65 101MS station; **h** SONNE 65 104MS station; methane concentrations and temperatures from deep-towed camera stations (OFOS) during the SONNE 65 cruise.

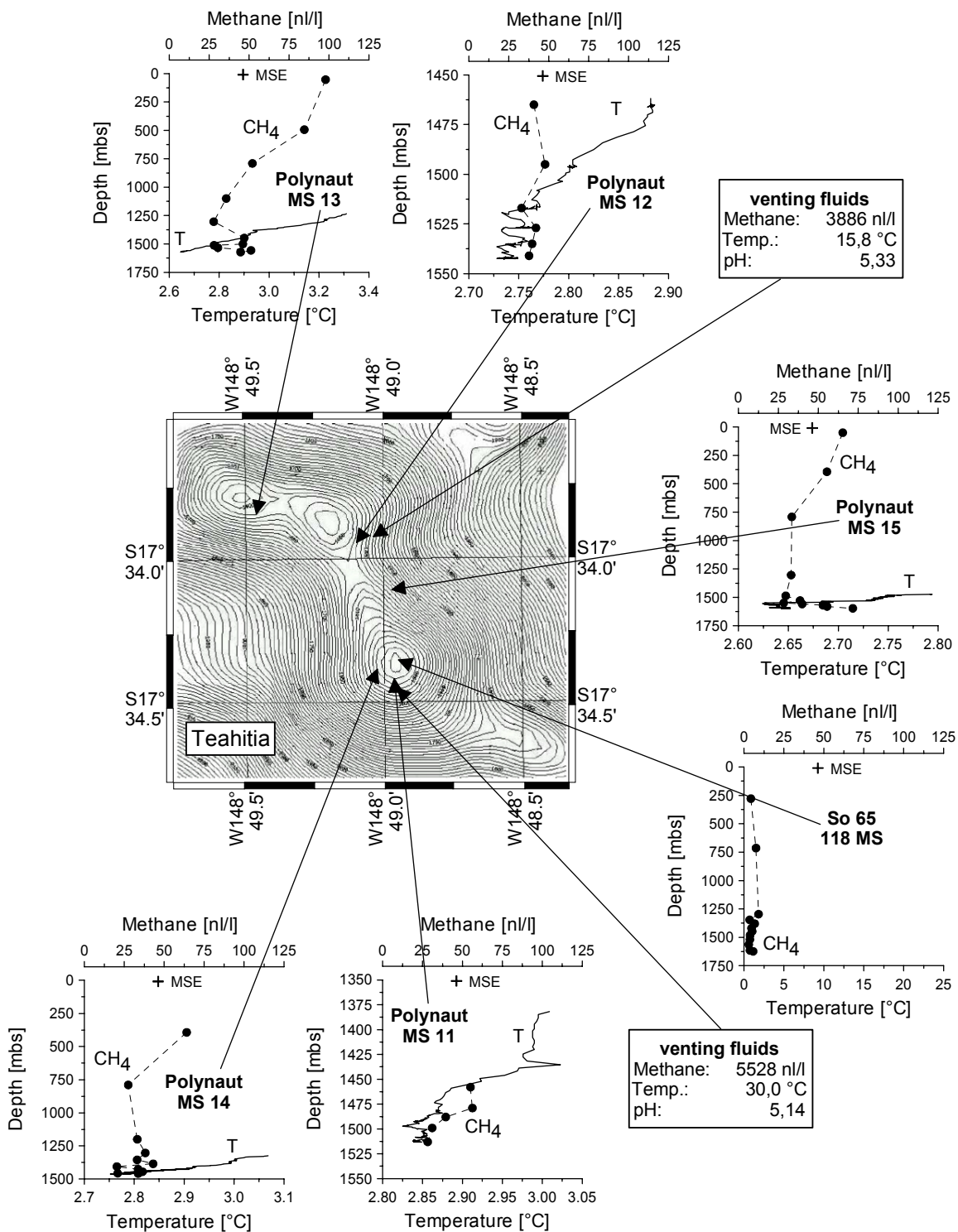


Fig. 5.7: Sampling stations and bathymetry map of the Teahitia (summit depth ~1400m) Seamount, Society hotspot area. Methane concentration and temperature profiles are plotted vs. depth at; **a** Polynaut MS 13 station; **b** Polynaut MS 12 station; **c** Polynaut MS 15 station; **d** SONNE 65 118MS station; **e** Polynaut MS 11 station; **f** Polynaut MS 14 station; methane concentrations, temperatures and pH of fluids from *Nautila* dives during Polynaut cruise.

higher CO₂ contents at Teahitia compared with Macdonald hydrothermal fluids) and/or the higher hydrostatic pressure (1455-1523 m water depths) at Teahitia seamount.

Direct sampling of vent fluids (shimmering water) by the submersible *Nautilie* indicated that Teahitia seamount is also hydrothermally active and the maximum CH₄ concentration measured in the vent fluids was 5,528 nl L⁻¹, significantly (about 100 times) enriched relative to the background value. Fluid temperatures up to 30°C were measured directly in the vent by *Nautilie* which is about 26°C higher than ambient sea water at the corresponding water depth. Strong currents occur at the summit of Teahitia and intensive mixing of ambient seawater with venting fluids is responsible that methane enrichments in the water column can only be found directly near the summit (Fig. 5.7).

A comparable mixing situation was found for the Pitcairn area, where we observed emanating hydrothermal fluids on Bounty seamount with CH₄ concentrations of up to 2,266 nl L⁻¹ near the vent (at water depth of 579 m), and with methane anomalies in the water column only directly at the summit (Fig. 5.4). It is noteworthy that the pH values of the vent fluids at the seafloor of Bounty seamount are only slightly lowered (pH = 6.94 – 7.74) relative to ambient seawater (pH = 7.9 of 580 m water depth) indicating small dissolved CO₂ contents only (~2,000 nl L⁻¹; calculated for pH 7).

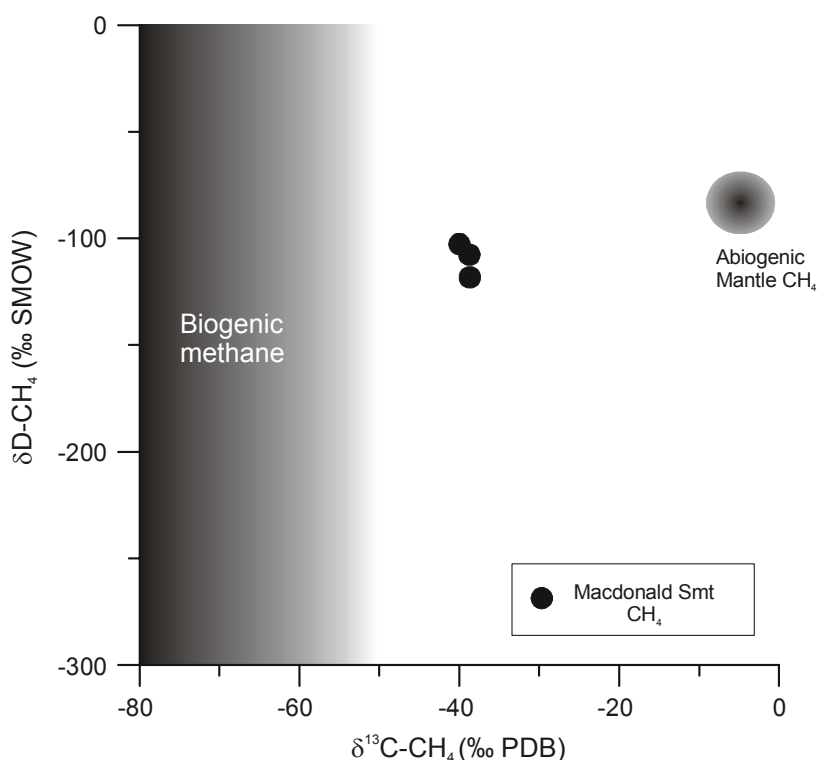


Fig. 5.8: δD and $\delta^{13}\text{C}$ values of methane (Tab. 3) of the Macdonald Seamount gas samples are plotted in a modified Welhan (1988) diagram. δD and $\delta^{13}\text{C}$ values of methane from biogenic and abiogenic origin are shaded in grey.

5.4.2 Origin of hydrothermal methane

The Macdonald, Teahitia and Bounty seamounts inject hydrothermal gas into the water column. The fluids released from Macdonald were found to be enriched in CO₂ and CH₄ compared to venting fluids at Galapagos and EPR vent sites (Cheminée et al., 1991) and the origin of gases was related to "shallow summit magma degassing". Higher hydrocarbons such as ethane and propane have not been detected in the gases from the seamounts indicating sediment-free subsurface conditions as thermal influences on organic matter not only produces methane but also the higher-ordered hydrocarbons (Simoneit et al., 1983). Theoretically, abiogenic reactions in the earth's crust such as hydrolysis of mafic rocks (Apps, 1985; Sherwood Lollar et al., 1993), Fischer Tropsch synthesis (Lancet and Anders, 1970) or mantle emanations (Craig et al., 1981) and/or biogenic gas formation could be responsible for the occurrence of hydrothermal CH₄ in the venting fluids of the three seamounts under consideration. In a $\delta^{13}\text{C}$ - δD diagram (Fig. 5.8) the stable isotope data of hydrothermal methane from Macdonald seamount (note that this is the only location where enough CH₄ for δD analyses was present) plot in between the two empirical fields "biogenic methane" and a field which is commonly referred to as "abiogenic/ mantle" methane (Whiticar, 1999). Based on the Richet et al. (1977) equation an isotopic equilibrium temperature near 200°C can be calculated from the carbon isotope values of CO₂ ($\delta^{13}\text{C} = -5.2\text{‰}$) and CH₄ ($\delta^{13}\text{C} = -38.6\text{‰}$). A similar temperature can be calculated based on the $\delta\text{D}_{\text{H}_2\text{O}-\text{CH}_4}$ equilibrium (Lyon and Hulston, 1984). This temperature shows that bacterial activity alone cannot account for the CH₄ formation since biological activity above 113°C is unlikely to occur (Blöchl et al., 1997). If a (bacterial) CH₄ formation temperature near 80°C is assumed within the vents (Huber et al., 1990) near to isotope equilibrium (Botz et al., 1996) with the CO₂ ($\delta^{13}\text{C}_{\text{CO}_2} = -5.2\text{‰}$) then the primary (un-oxidised) CH₄ should have an isotope value of -55‰ (Richet et al., 1977). Venting CH₄ with this isotope value was not found at Macdonald seamount. However, one CH₄ sample was taken directly by the submersible *Nautilie* from an active vent field at Bounty seamount. This CH₄ sample had an isotope value of -56‰ which is typical for bacterial CH₄ formation by CO₂ reduction at around 88°C.

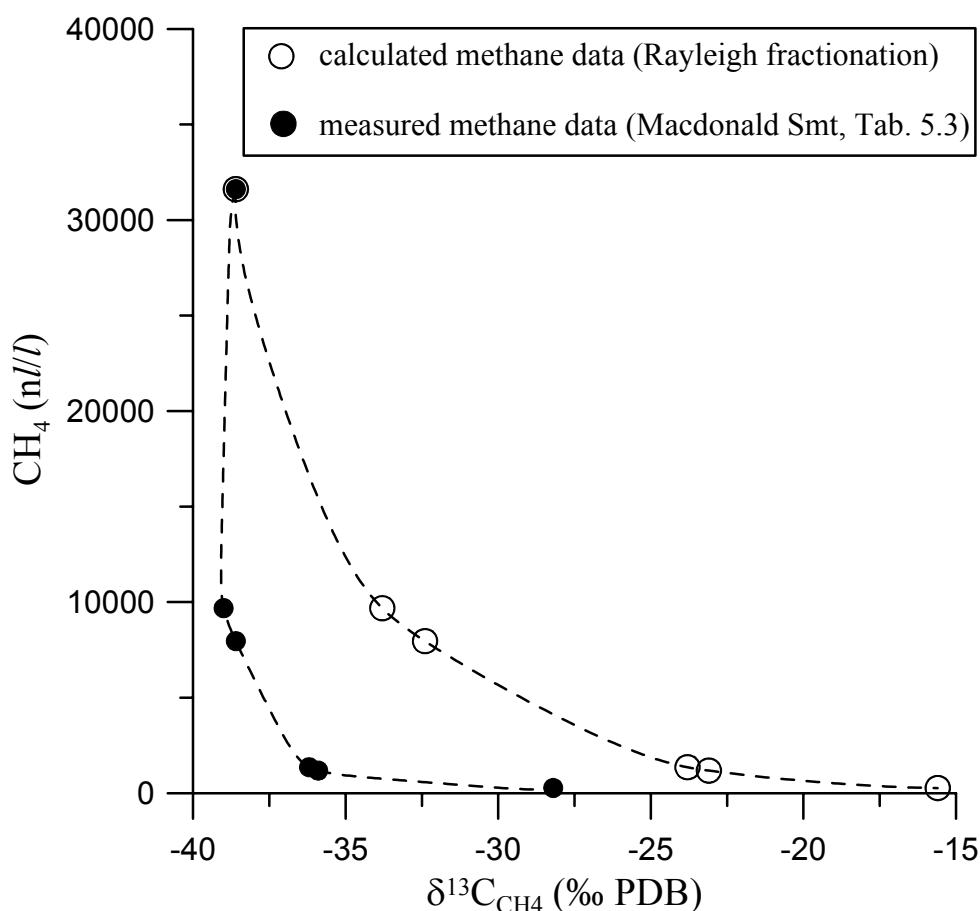


Fig. 5.9: Concentrations and $\delta^{13}\text{C}$ values of methane measured (*filled dots*) on the Macdonald Seamount. The calculated data (*dots*) shows the theoretical concentration decrease with increasing $\delta^{13}\text{C}_{\text{CH}_4}$ values assuming a Rayleigh type fractionation for the methane oxidation process ($\alpha = 1.005$; Tsunogai et al., 2000).

Bacterial CH_4 oxidation reduces the CH_4 content of the water and also leads to an increase in the heavy isotopes of the residual CH_4 which follows a Rayleigh-type equation (Fritz and Fontes, 1980). The theoretical change of both $\delta^{13}\text{C}$ and concentration of methane in course of oxidation (fractionation factor $\alpha = 1.005$; Tsunogai et al., 2000) is plotted in figure 5.9 and compared to the measured data at Macdonald seamount (Fig. 5.9; Tab. 5.3). It is shown by the calculated and measured data, that CH_4 quantities and isotope values are related to each other, and, furthermore, that early oxidation steps strongly affect the CH_4 concentration without changing significantly the isotope composition of the residual methane (Fig. 5.9; Tab. 5.3). Moreover, mixing processes of hydrothermal fluids with seawater with a low methane concentration also lowers the concentration values as indicated by the strong decrease in measured methane concentrations. This effect is not taken into account by the theoretical Rayleigh

fractionation (Fig. 5.9). However, calculated and measured methane data show that during late stage oxidation, when most (> 90%) of the CH₄ has already been oxidised to CO₂ (e.g. 101 MS with a low CH₄ concentration of 270 nl L⁻¹; Tab. 5.2), significant ¹³C isotope enrichment ($\delta^{13}\text{C} = -28.2\text{‰}$) of the residual methane occurs. It is concluded, therefore, that the isotope value of venting CH₄ ($\delta^{13}\text{C} = -38.6\text{‰}$) at Macdonald is probably not much affected by oxidation. Thus, we have to assume a carbon-13 rich CH₄ component admixed to the biogenic CH₄. This isotopically heavy CH₄ is known to be present in the tectonically active region at 17° – 19°S, East Pacific Rise (near -22 to -24‰; Charlou et al., 1996). Based on quantitative estimations Macdonald gas probably contains mixtures of two endmembers, e.g. 50% biogenic CH₄ ($\delta^{13}\text{C} = -55\text{‰}$ from bacterial CH₄ production at 80°C) and 50% of abiogenic CH₄ with an assumed mean $\delta^{13}\text{C}$ of -23‰ (Charlou et al., 1996).

Station	Methane nl L ⁻¹	$\delta^{13}\text{C}\text{-CH}_4$ ‰ PDB	$\delta\text{D}\text{-CH}_4$ ‰ SMOW	$\delta^{13}\text{C}\text{-CO}_2$ ‰ PDB
<i>Macdonald Smt</i>				
So65 100MS	1182	-35.9	-	-
So65 101MS	270	-28.2	-	-
So65 103MS	1358	-36.2	-	-
So65 104MS	9691	-39.0	-103	-
So65 105MS	7957	-38.6	-106	-
So65 107OFOS	31615	-38.6	-117	-5.2
<i>Bounty Smt</i>				
Nautile PN06	2266	-56.0	-	-
Nautile PN11	1934	-	-	-
<i>Teahitia Smt</i>				
Nautile PN18	3886	-22.0	-	-
Nautile PN19	5528	-29.0	-	-

Table 5.3: δD and $\delta^{13}\text{C}$ values of methane and $\delta^{13}\text{C}$ value of carbon dioxide detected in gas samples from the Macdonald, Bounty, and Teahitia Seamounts.

Warm vent fluids from Teahitia seamount contain CH₄ with significantly less negative $\delta^{13}\text{C}$ -values of -29 and -22‰ (Tab. 5.3). This range of values is similar to the values published for abiogenic CH₄ (see above). Thus, based on isotope evidence alone it cannot be decided whether Teahitia seamount injects hydrothermal CH₄ of abiogenic origin (EPR-type) into the water column or, alternatively, also represents an environment where biogenic CH₄ formation and oxidation processes are important. The CH₄ concentrations of Teahitia seamount are remarkably high for possible medium to late

stage (which is required for the strong isotope shift to -22‰ , see above) oxidation process. However, the geochemical similarity (Garbe-Schönberg, pers. comm.) of hydrothermal fluids from all three investigated seamounts (Macdonald, Bounty, Teahitia) does not indicate an extraordinary situation for Teahitia seamount.

5.5 Conclusions

Hydrothermal systems venting at submarine seamounts in hot spot areas in the South Pacific are recognised by temperature-, pH- and CH_4 anomalies in the bottom sea water. Bubbling vent fields were detected near to the summit of the active Macdonald seamount where sea water boiling occurs at shallow water depth (< 200 m) and high temperature ($>200^\circ\text{C}$). In contrast, the greater water depth prevents boiling at Teahitia and Bounty seamounts where shimmering water emerges the seafloor. The low pH values (to 5.8) associated with hydrothermal fluid injections are largely caused by magmatic CO_2 ($\delta^{13}\text{C} = -5.2\text{‰}$).

CH_4 is enriched in the hydrothermal fluids of Macdonald seamount up to $31,615 \text{ nl L}^{-1}$. Shimmering water emerging the seafloor of the two other seamounts (Bounty and Teahitia) contain lower CH_4 concentrations ($1,934$ to $5,528 \text{ nl L}^{-1}$). Carbon isotope values of CH_4 fall in the range between -22 and -56‰ PDB. The low carbon isotope value of -56‰ for hydrothermal CH_4 from Bounty seamount most likely reflects bacterial CH_4 formation by CO_2 reduction at a temperature near 90°C . The carbon isotope values of Macdonald seamount hydrothermal CH_4 are less negative between -28 and -39‰ and, together with the δD values of -103 to -117‰ SMOW, it reflects a mixture of abiogenic CH_4 originated in the deep subsurface mixed with biogenic CH_4 formed in the vent system at temperatures below 100°C . However, CH_4 oxidation causes secondary enrichment of the heavy isotopes in the residual CH_4 fraction. Hence, based on the CH_4 isotope values alone it cannot be decided whether hydrothermal CH_4 from Teahitia seamount derived from abiogenic subsurface reactions and/ or reflects an oxidised CH_4 of unknown origin. Nevertheless, significant amounts of hydrothermal CH_4 from active seamounts in the South Pacific are derived from biogenic processes. Our findings are substantiated by microbiologists who found hyperthermophilic archaeobacteria within the crater of erupting Macdonald seamount.

Acknowledgements

We are grateful to R Hekinian for valuable discussions regarding hotspot volcanism in the south Pacific. This manuscript was improved by comments and suggestions made by J.L. Charlou. We acknowledge the crews of R.V. SONNE, R.V. L'ATALANTE and submersible *Nautilie* (IFREMER, Brest) for their support during the sampling campaigns. This research project was funded by the Bundesministerium für Forschung und Technologie (BMFT) through grant no. 03G0543A to Kiel University.

References

- Abegg F. (1999) Gasuntersuchungen an schlickigen Sedimenten. *Berichte-Reports, Inst. Geowiss., Univ. Kiel* **4**, 120.
- Abegg F. and Anderson A. L. (1997) The acoustic turbid layer in muddy sediments of Eckernförde Bay, Western Baltic: methane concentration, saturation and bubble characteristics. *Marine Geology* **137**, 137-147.
- Albert D. B., Martens C. S., and Alperin M. J. (1998) Biogeochemical processes controlling methane in gassy coastal sediments-Part 2: groundwater flow control of acoustic turbidity in Eckernförde Bay sediments. *Continental Shelf Research* **18**, 1771-1793.
- Alt J. C. (1995) Subseafloor processes in Mid-Ocean Ridge hydrothermal Systems. *American Geophysical Union / Geophysical Monograph* **91**, 85-114.
- Anderson A. L. and Hampton L. D. (1980a) Acoustics of gas bearing sediments: I. Background. *Journal of the Acoustical Society of Amerika* **67**(6), 1865-1886.
- Anderson A. L. and Hampton L. D. (1980b) Acoustics of gas-bearing sediments. II. Measurements and models. *Journal of the Acoustical Society of Amerika* **67**(6), 1890-1903.
- Andrén E., Andrén T., and Sohlenius G. (2000) The Holocene history of the southwestern Baltic Sea as reflected in a sediment core from the Bornholm Basin. *Boreas* **29**, 233-250.
- Bange H. W., Rapsomanikis S., and Andreae M. O. (1996) The Aegean Sea as a source of atmospheric nitrous oxide and methane. *Marine Chemistry* **53**, 41-49.
- Barrer R. M. (1986) Expanded clay minerals: a major class of molecular sieves. *Journal of inclusion Phenomena* **4**, 109-119.
- Bernard B. B., Brooks J. M., and Sackett W. M. (1976) Natural gas seepage in the Gulf of Mexico. *Earth and Planetary Science Letters* **31**, 48-54.
- Bernard B. B., Brooks J. M., and Sackett W. M. (1978) Light hydrocarbons in recent Texas continental shelf and slope sediments. *Journal of Geophysical Research* **83**, 4053-4061.
- Binard N., Stoffers P., Hekinian R., and Cheminée J. L. (2004) South Pacific intraplate volcanism: Structure, morphology and style of eruption. In *Oceanic Hotspots* (ed. R. Hekinian, P. Stoffers, and J. L. Cheminée), pp. 157-207. Springer.
- Björck S. (1995) A review of the history of the Baltic Sea, 13.0-8.0 ka BP. *Quaternary International* **27**, 19-40.

- Blöchl E., Rachel R., Burggraf S., Hafenbradl D., Jannasch H. W., and Stetter K. O. (1997) *Pyrolobus fumarii*, gen and sp nov, represents a novel group of *archaea*, extending the upper temperature limit for life to 113°C. *Extremophiles* **1**, 14-21.
- Boetius A., Ravensschlag K., Schubert C. J., Rickert D., Widdel F., Gieseke A., Amann R., Jørgensen B. B., Witte U., and Pfannkuche O. (2000) A marine microbial consortium apparently mediating anaerobic oxidation of methane. *Nature* **407**, 623-626.
- Borg G. C. (1985) *Paleo-ecology reflected in physical and chemical properties of three Baltic cores*. Department of Quaternary Geology.
- Both R., Crook K., Taylor B., Brogan S., Chappell B., Frankel E., Liu L., Sinton J., and Tiffin D. (1986) Hydrothermal chimneys and associated fauna in the Manus Back-Arc Basin, Papua New Guinea. *Trans American Geophysical Union* **67**, 489-490.
- Botz R., Winckler G., Bayer R., Schmitt M., Schmidt M., Garbe-Schönberg D., Stoffers P., and Kristjansson J. K. (1999) Origin of trace gases in submarine hydrothermal vents of the Kolbeinsey Ridge, north Iceland. *Earth and Planetary Science Letters* **171**, 83-93.
- Boudreau B. P. (1997) *Diagenetic models and their implementation: modelling transport and reactions in aquatic sediments*. Springer.
- Brandes H. G., Silva A. J., Ag A., and Veyera G. E. (1996) Consolidation and permeability characteristics of high-porosity surficial sediments in Eckernförde Bay. *Geo-Marine Letters* **16**, 175-181.
- Burggraf S., Fricke H., Neuner A., Kristjansson J., Rouvier P., Mandelco L., Woese C. R., and Stetter K. O. (1990) *Methanococcus igneus* sp nov, a novel hyperthermophilic methanogen from shallow submarine hydrothermal system. *System Applied Microbiology* **13**, 263-269.
- Butterfield D. A. and Massoth G. J. (1994) Geochemistry of north Cleft segment vent fluids: Temporal changes in chlorinity and their possible relation to recent volcanism. *Journal of Geophysical Research* **99**, 4951-4969.
- Charlou J. L., Bougault H., P. A., Jean-Baptiste P., Etoubleau J., and Biroleau A. (1991) Water column anomalies associated with hydrothermal activity between 11°40' and 13°N on the east Pacific Rise: Discrepancies between tracers. *Deep Sea Research* **38**, 569-596.
- Charlou J. L., Donval J. P., Fouquet Y., Jean-Baptiste P., and Holm N. (2002) Geochemistry of high H₂ and CH₄ vent fluids issuing from ultramafic rocks at the Rainbow hydrothermal field (36°14'N, MAR). *Chemical Geology* **191**, 345-359.

- Charlou J. L., Fouquet Y., Donval J. P., Auzende J. M., Jean-Baptiste P., Stievenard M., and Michel S. (1996) Mineral and gas chemistry of hydrothermal fluids on an ultrafast spreading ridge: East Pacific Rise: 17° to 19°S (Naudur cruise, 1993) phase separation processes controlled by volcanic and tectonic activity. *Journal of Geophysical Research* **101**, 15899-15919.
- Cheminée J. L., Stoffers P., McMurtry G. M., Richnow H., Puteanus D., and Sedwick P. (1991) Gas-rich submarine exhalations during the 1989 eruption of Macdonald Seamount. *Earth and Planetary Science Letters* **107**, 318-327.
- Claypool G. E. and Kaplan I. R. (1974) The origin and distribution of methane in marine sediments. In *Natural Gases in Marine Sediments* (ed. I. R. Kaplan), pp. 99-139. Plenum Press.
- Clayton C. J., Hay S. J., Baylis S. A., and Dipper B. (1997) Alteration of natural gas during leakage from a North Sea salt diapir field. *Marine Geology* **137**, 69 - 80.
- Corliss J. B., Dymond J., Gordon L. I., Edmond J. M., Von Herzen R. P., Ballard R. D., Green K., Williams D., Brainbridge A., Crane K., and Van Adel T. H. (1979) Submarine thermal springs on the Galapagos Rift. *Science* **203**, 1073-1083.
- Craig H. and Lupton J. E. (1981) Helium-3 and mantle volatiles in the ocean and oceanic crust. In *The Sea* (ed. C. Emiliani), pp. 391-428. Wiley.
- Crough S. T. (1983) Hotspot swells. *Annual Review Earth Planet Science* **11**, 165-193.
- Dando P. R., Hughes J. A., and Thiermann F. (1995) Preliminary observations on biological communities at shallow hydrothermal vent in the Aegean Sea. In *Hydrothermal vents and processes*, Vol. 87 (ed. L. M. Parson, C. L. Walker, and D. R. Dixon), pp. 301-317.
- Davis A. M. (1992) Shallow gas: an overview. *Continental Shelf Research* **12**(10), 1077-1079.
- Dippner J. W. and Voss M. (2004) Climate reconstruction of the MWP in the Baltic Sea area based on biogeochemical proxies from a sediment record. *Baltica* **17**(1), 5-16.
- Dumke I., Faber E., and Poggenburg J. (1989) Determination of stable carbon and hydrogen isotopes of light hydrocarbons. *Analytical Chemistry* **61**, 2149-2154.
- Duphorn K., Kliewe H., Niedermeyer R.-O., Janke W., and Werner F. (1995) *Die deutsche Ostseeküste*. Gebrüder Bornträger.
- Emeis K.-C., Endler R., Struck U., and Kohly A. (2002) The post-glacial evolution of the Baltic Sea. In *Climate development and history of the North Atlantic realm* (ed. G. Wefer, W. Berger, K. H. Behre, and E. Jansen), pp. 205-221. Springer-Verlag.

References

- Emeis K.-C., Struck U., Blanz T., Kohly A., and Voß M. (2003) Salinity changes in the central Baltic Sea (NW Europe) over the last 10 000 years. *The Holocene* **13**(3), 411-421.
- Emelyanov E. M., Christiansen C., and Michelsen O.(eds.). (1995) Geology of the Bornholm Basin. *Aarhus Geoscience* **5**, pp. 236.
- Endler R. (1990) Akustische Eigenschaften des seebodennahen Schlicks im Arkonabecken, Akademie der Wissenschaften.
- Endler R. (1998) Acoustic studies. In *Gotland Basin Experiment (GOBEX) Status Report on Investigations concerning Benthic Processes, Sediment Formation and Accumulation*, Vol. Marine Science Reports No. 34 (ed. K.-C. Emeis and U. Struck), pp. 21-34. Institut für Ostseeforschung - Baltic Sea Research Institute.
- Faber E., Botz R., Poggenburg J., Schmidt M., Stoffers P., and Hartmann M. (1998) Methane in Red Sea brines. *Organic Geochemistry* **29**(1-3), 363-379.
- Faber E., Gerling P., Berner U., and Sohns E. (1994) Methane in ocean waters; concentration and carbon isotope variability at East Pacific Rise and in the Arabian Sea. *Environmental Monitoring and Assessment* **31**, 139-144.
- Faber E. and Stahl J. W. (1983) Analytical procedure and results of an isotope geochemical survey in an area of the British North Sea. In *Petroleum Geochemistry and Exploration in Europe* (ed. J. Brooks), pp. 51-63. Blackwell Scientific Publication.
- Fleischer P., Orsi T. H., Richardson M. D., and Anderson A. L. (2001) Distribution of free gas in marine sediments: a global overview. *Geo-Marine Letters* **21**, 103-122.
- Fouquet Y., Von Stackelberg U., Charlou J. L., Donval J. P., Erzinger J., Foucher J. P., Herzig P., Mühe R., Soakai S., Wiedicke M., and Whitechurch H. (1991) Hydrothermal activity and metallogenesis in the Lau back-arc basin. *Nature* **349**, 778-781.
- Fritz P. and Fontes J. C. (1980) *Handbook of Environmental Isotope Geochemistry, Volume 1*. Elsevier Scientific Publishing Company.
- Gamo T., Ishibashi J. J., and Sakai H. (1987) Methane anomalies in seawater above the Loihi submarine summit area, Hawaii. *Geochimica et Cosmochimica Acta* **51**, 2857-2864.
- Geodekyan A. A., Berlin Y. M., Bol'Shakov A. M., and Trotsyuk V. Y. (1991) Distribution of methane in sediments and bottom water of the southern Baltic Sea. *Oceanology* **31**(1), 54-59.
- Glasby G. P., Stüben D., Jeschke G., Stoffers P., and Garbe-Schönberg D. (1997) A model for information of the hydrothermal manganese crusts from the Pitcairn Island hot spot. *Geochimica et Cosmochimica Acta* **61**, 4583-4597.

- Halbach P., Pracejus B., and Märten A. (1993) Geology and mineralogy of massive sulfide ores from the Central Okinawa Trough, Japan. *Economy Geology* **88**, 2206-2221.
- Hannington M. D., Jonasson I. R., Herzig P., and Petersen S. (1995) Physical and chemical processes of seafloor mineralization at Mid-Ocean Ridges. *American Geophysical Union / Geophysical Monograph* **91**, 115-157.
- Hansen L. B., Finster K., Fossing H., and Iversen N. (1998) Anaerobic methane oxidation in sulfate depleted sediments: effects of sulfate and molybdate additions. *Aquatic Microbial Ecology* **14**, 195-204.
- Hekinian R., Bideau D., Stoffers P., Cheminée J. L., Mühe R., Puteanus D., and Binard N. (1991) Submarine Intraplate Volcanism in the South Pacific: Geological Setting and Petrology of the Society and Austral Regions. *Journal of Geophysical Research* **96**, 2109-2138.
- Hekinian R., Renard V., and Cheminée J. L. (1984) Hydrothermal Deposits on the East Pacific Rise near 13°N: Geological Setting and Distribution of active Sulfide Chimneys. In *Hydrothermal Processes at Seafloor Spreading Centers* (ed. P. A. Rona, K. Bostrom, L. Laubier, and K. L. Smith), pp. 571-602. Plenum Publishing Corporation.
- Hensen C. and Wallmann K. (2005) Methane formation at Costa Rica continental margin - constraints for gas hydrate inventories and cross-décollement fluid flow. *Earth and Planetary Science Letters* **236**, 41-60.
- Hensen C., Zabel M., Pfeifer K., Schwenk T., Kasten S., Riedinger N., Schulz H. D., and Boetius A. (2003) Control of sulfate pore-water profiles by sedimentary events and the significance of anaerobic oxidation of methane for the burial of sulfur in marine sediments. *Geochimica et Cosmochimica Acta* **67**(14), 2631-2647.
- Hoehler T. M., Alperin M. J., Albert D. B., and Martens C. S. (1994) Field and laboratory studies of methane oxidation in an anoxic marine sediment: Evidence for a methanogen-sulfate reducer consortium. *Global Biogeochemical Cycles* **8**(4), 451-463.
- Hoffert M., Cheminée J. L., Person A., and Larque P. (1987) Dépot hydrothermal associé au volcanisme sous-marin intraplaque: prélèvements effectués avec la Cyana sur le volcan actif de Teahitia (Polynésie Française). *C R Acad Sci, Paris* **304**, 829-832.
- Huber R., Stoffers P., Cheminée J. L., Richnow H. H., and Stetter K. O. (1990) Hyperthermophilic archaeobacteria within the crater and open-sea plume of erupting Macdonald Seamount. *Nature* **345**, 179-182.
- Huckriede H., Clasen S., and Meischner D. (1996) Hydrographic and climatic changes recorded in Holocene sediments of the central Baltic Sea. *Baltica* **9**, 76-91.

- Hunt J. M. (1996) *Petroleum Geochemistry and Geology*. W.H. Freeman & Company.
- Ishibashi J., Sano Y., Wakita H., Gamo T., Tsutsumi M., and Sakai H. (1995) Helium and carbon geochemistry of hydrothermal fluids from the Mid-Okinawa Trough Back Arc Basin, southwest of Japan. *Chemical Geology* **123**, 1-15.
- Ishibashi J., Wakita H., Nojiri Y., Grimaud D., Jean-Baptiste P., Gamo T., Auzende J. M., and Urabe T. (1994) Helium and carbon geochemistry of hydrothermal fluids from the North Fiji Basin spreading ridge (southwest Pacific). *Earth and Planetary Science Letters* **128**, 183-197.
- Ishibashi J., Wakita H., Okamura K., Nakayamy E., Feely R. A., Lebon G. T., Baker E. T., and Marumo K. (1997) Hydrothermal methane and manganese variation in the plume over the superfast spreading southern East Pacific Rise. *Geochimica et Cosmochimica Acta* **61**, 485-500.
- Jackson D. R., Williams K. L., Wever T. F., Friedrichs C. T., and Donelson Wright L. (1998) Sonar evidence for methane ebullition in Eckernförde Bay. *Continental Shelf Research* **18**, 1893-1915.
- Jannasch H. W. (1995) Microbial interactions with hydrothermal fluids. In *Physical, Chemical, Biological and Geological Interactions within seafloor Hydrothermal Systems*, Vol. 91 (ed. S. Humphris, R. Zierenberg, L. Mullineaux, and R. Thomson), pp. 273-296.
- Jensen J. B. (1992) Late Pleistocene and Holocene depositional evolution in the shallow waters near the island of Møn, SE Denmark. Ph.D., Geological Survey of Denmark.
- Jensen J. B., Bennike O., Witkowski A., Lemke W., and Kuijpers A. (1997) The Baltic Ice Lake in the southwestern Baltic: sequence-, chrono- and biostratigraphy. *Boreas* **26**, 217-236.
- Jensen J. B., Bennike O., Witkowski A., Lemke W., and Kuijpers A. (1999) Early Holocene history of the southwestern Baltic Sea: the Ancylus Lake stage. *Boreas* **28**, 437-453.
- Judd A. G. and Hovland M. (1992) The evidence of shallow gas in marine sediments. *Continental Shelf Research* **12**(10), 1081-1095.
- Karl D. M., McMurtry G. M., Malahoff A., and Garcia M. O. (1988) Loihi seamount, Hawaii: A mid-plate volcano with a distinctive hydrothermal system. *Nature* **335**, 532-535.
- Keller G.H. (1982) Organic matter and the geotechnical properties of submarine sediments. *Geo-Marine Letters* **2**, 191-198.
- Krauss W. and Brüggel B. (1991) Wind-produced water exchange between the deep basins of the Baltic. *Journal of Physical Oceanography* **21**, 373-384.

- Lammers S. (1994) Methane cycling in the Marine Environment. unpubl. PhD, Christian-Albrechts-Universität zu Kiel.
- Lancet H. S. and Anders E. (1970) Carbon isotope fractionation in the Fischer-Tropsch synthesis of methane. *Science* **170**, 980-982.
- Lass H. U. and Mohrholz V. (2003) On dynamics and mixing of inflowing saltwater in the Arkona Sea. *Journal of Geophysical Research* **108**(C2), 1 - 15.
- Lehmann A., Lorenz P., and Jacob D. (2004) Modelling the exceptional Baltic Sea inflow events in 2002-2003. *Geophysical Research Letters* **31**, L21308, doi:10.1029/2004GL0208830.
- Lein A. Y. (1983) Biogeochemistry of the anaerobic diagenesis of recent Baltic Sea sediments. In *Environmental Biogeochemistry, Proc. 5th Int. Symp. Env. Biogeochemistry (ISEB)*, Vol. 35 (ed. R. Hallberg), pp. 441-461. Ecological Bulletin.
- Lemke W. (1998) Sedimentation und paläogeographische Entwicklung im westlichen Ostseeraum (Mecklenburger Bucht bis Arkona Becken) vom Ende der Weichselvereisung bis zur Litorinatransgression, pp. 155. Institut für Ostseeforschung - Baltic Sea Research Institute.
- Lemke W., Endler R., Tauber F., Jensen J. B., and Bennike O. (1998) Late- and postglacial sedimentation in the Tromper Wiek northeast of Rügen (western Baltic). *Meyniana* **50**, 155-173.
- Liljebladh B. and Stigebrandt A. (1996) Observations of the deepwater flow into the Baltic Sea. *Journal of Geophysical Research* **101**(C4), 8895-8911.
- Lonsdale P. F., Bischoff J. L., Burns V. M., Kastner M., and Sweeny R. E. (1980) A high temperature hydrothermal deposit on the seabed at the Gulf of California spreading center. *Earth and Planetary Science Letters* **49**, 8-20.
- Luff R. and Wallmann K. (2003) Fluid flow, methane fluxes, carbonate precipitation and biogeochemical turnover in gas hydrate-bearing sediments at Hydrate Ridge, Cascadia Margin: Numerical modeling and mass balances. *Geochimica et Cosmochimica Acta* **67**(18), 3403-3421.
- Lyon G. L. and Hulston J. R. (1984) Carbon and hydrogen isotopic compositions of New Zealand geothermal gases. *Geochimica et Cosmochimica Acta* **48**, 1161-1171.
- Malahoff A., McMurtry G., Wishire J. C., and Yehy H. W. (1982) Geology and chemistry of hydrothermal deposits from active submarine volcano Loihi, Hawaii. *Nature* **298**, 234-239.

References

- Martens C. S., Albert D. B., and Alperin M. J. (1998) Biogeochemical processes controlling methane in gassy coastal sediments-Part 1. A model coupling organic matter flux to gas production, oxidation and transport. *Continental Shelf Research* **18**, 1741-1770.
- Martens C. S., Albert D. B., and Alperin M. J. (1999) Stable isotope tracing of anaerobic methane oxidation in the gassy sediments of Eckernförde Bay, German Baltic Sea. *American Journal of Science* **299**, 589 - 610.
- Martens C. S. and Berner R. A. (1974) Methane production in the interstitial waters of sulphate-depleted marine sediments. *Science* **185**, 1167-1169.
- Mathys M. (2003) Seismic characterisation and sedimentological investigation of gas-rich near surface sediments in Arkona Basin (Baltic Sea). unpubl. Msc.-Thesis, Christian-Albrechts-University.
- Mathys M., Thießen O., Theilen F., and Schmidt M. (2005) Seismic characterisation of gas-rich near surface sediments in the Arkona Basin, Baltic Sea. *Marine Geophysical Researches*, 1-18.
- Mattson M. D. and Likens G. E. (1990) Air pressure and methane fluxes. *Nature* **347**, 717-718.
- Michaelis W., Jenisch A., and Richnow H. H. (1990) Hydrothermal petroleum generation in Red Sea sediments from the Kebrit and Shaban Deeps. *Applied Geochemistry* **5**, 103-114.
- Michard A., Michard G., Stüben D., Stoffers P., Cheminée J. L., and Binard N. (1993) Submarine thermal springs associated with young volcanoes: The Teahitia vents, Society Island, Pacific Ocean. *Geochimica et Cosmochimica Acta* **57**, 4977-4986.
- Middelburg J. J. (1989) A simple rate model for organic matter decomposition in marine sediments. *Geochimica et Cosmochimica Acta* **53**, 1577-1581.
- Milkert D. (1994) Auswirkungen von Stürmen auf die Schlicksedimente der westlichen Ostsee, pp. 153. Institut für Geowissenschaften.
- Miltner A. and Emeis K.-C. (2000) Origin and transport of terrestrial organic matter from the Oder lagoon to the Arkona Basin, Southern Baltic Sea. *Organic Chemistry* **31**, 57-66.
- Miltner A., Emeis K.-C., Struck U., Leipe T., and Voss M. (2005) Terrigenous organic matter in Holocene sediments from the central Baltic Sea, NW Europe. *Chemical Geology* **216**, 313-328.
- Morgan W. J. (1971) Convection plumes in the Lower Mantle. *Nature* **230**, 42-43.
- Mörner N.-A. (1995) The Baltic Ice Lake – Yoldia Sea Transition. *Quaternary International* **27**, 95-98.

- Moros M. (1999) Spätquartäre Sedimentation am Reykjanes Rücken und in der Westlichen Ostsee - Rekonstruktion anhand hochauflösender sedimentphysikalischer Eigenschaften, Ernst-Moritz-Arndt-Universität.
- Moros M., Lemke W., Kuijpers A., Endler R., Jensen J. B., Bennike O., and Gingele F. (2002) Regressions and transgressions of the Baltic basin reflected by a new high-resolution deglacial and postglacial lithostratigraphy for Arkona Basin sediments (western Baltic Sea). *Boreas* **31**, 151-162.
- Nelson D. C. and Fisher C. R. (1995) Chemoautotrophic and methanotrophic endosymbiotic bacteria at vents and seeps. In *Microbiology of Deep Sea Hydrothermal Vent Habitats*. (ed. D. M. Karl). CRC Press.
- Neumann G. (1981) Lagerungsverhältnisse spät- und postglazialer Sedimente im Arkona-Becken. *Unveröffentlichte Dissertation, Institut für Meereskunde, Warnemünde*.
- Nytoft H. P. and Larsen B. (2001) Triterpenoids and other organic compounds as markers of depositional conditions in the Baltic Sea deep basins during the Holocene. *Baltica* **14**, 95-107.
- Oremland R. S., Whiticar M. J., Strohmaier F. E., and Kiene R. P. (1988) Bacterial ethane formation from reduced, ethylated sulfur compounds in anoxic sediments. *Geochimica et Cosmochimica Acta* **52**, 1895-1904.
- Orsi T. H., Werner F., Milkert D., Anderson A. L., and Bryant W. R. (1996) Environmental overview of Eckernförde Bay, northern Germany. *Geo-Marine Letters* **16**, 140-147.
- Piker L., Schmaljohann R., and Imhoff J. F. (1998) Dissimilary sulfate reduction and methane production in Gotland Deep sediments (Baltic Sea) during a transition period from oxic to anoxic bottom water (1993-1996). *Aquatic Microbial Ecology* **14**, 183-193.
- Prinzhofer A. and Pernaton É. (1997) Isotopically light methane in natural gas: Bacterial imprint or diffusive fractionation? *Chemical Geology* **142**, 193-200.
- Rehder G., Keir R. S., Suess E., and Pohlmann T. (1998) The multiple sources and patterns of methane in North Sea waters. *Aquatic Geochemistry* **4**, 403-427.
- Reitsemá R. H., Kaltenback A. J., and Lindberg F. A. (1981) Source and migration of light hydrocarbons indicated by carbon isotopic ratios. *AAPG Bulletin* **65**, 1536-1542.
- Rempel H. (1992) Erdölgeologische Bewertung der Arbeiten der Gemeinsamen Organisation "Petrobaltic" im deutschen Schelfbereich. *Geologisches Jahrbuch* **D 99**, 3-32.

- Rempel H. and Schmidt-Thomé M. (2004) Hydrocarbon Potential of the Baltic Sea Region. In *Mineral Resources of the Baltic Sea*, Vol. 2 (ed. J. Harff, E. M. Emelyanov, M. Schmidt-Thomé, and M. Spiridonov). Zeitschrift für Angewandte Geologie - Special Issue 2.
- Repecka M. (2001) Physical properties of bottom sediments from three Baltic Sea basins. *Baltica* **14**, 24-33.
- Rheinheimer G. E. (1995) *Meereskunde der Ostsee*. Springer.
- Richardson M. D. (1998) Coastal Benthic Boundary Layer (CBBL) Research Programm: Final Reports, pp. 386.
- Richet P., Bottinga Y., and Javoy M. (1977) A review of hydrogen, carbon, nitrogen, oxygen, sulphur and chlorine stable isotope fractionation among gaseous molecules. *Annual Review Earth Planet Science* **5**, 65-110.
- Rona P. A. and Scott S. D. (1993) A special issue on sea-floor hydrothermal mineralization; new perspectives; preface. *Economic Geology and the Bulletin of the Society of Economic Geologists* **88**, 1933-1974.
- Sakai H., Tsubota H., Nakai T., Ishibashi J., Akagi T., Gamo T., Tilbrock B., Igarashi G., Kodera M., Shitashima K., Nalamura S., Fujioka K., Watanabe M., McMurtry G. M., Malahoff A., and Oruma M. (1987) Hydrothermal activity on the summit of Loihi Seamount, Hawaii. *Geochemical Journal* **21**, 11-21.
- Schlüter H. U., Best G., Jürgens U., and Binot F. (1997) Interpretation reflexionsseismischer Profile zwischen baltischer Kontinentalplatte und Kaledonischem Becken in der südlichen Ostsee - erste Ergebnisse. *Zeitschrift der deutschen Geologischen Gesellschaft* **148**(1), 1 - 32.
- Schlüter M., Sauter E., Hansen H. P., and Suess E. (2000) Seasonal variations of bioirrigation in coastal sediments: Modelling of field data. *Geochimica et Cosmochimica Acta* **64**(5), 821-834.
- Schlüter M., Sauter E. J., Andersen C. E., Dahlgaard H., and Dando P. R. (2004) Spatial distribution and budget for submarine ground water discharge in Eckernförde Bay (Western Baltic Sea). *Limnological Oceanography* **49**(1), 157-167.
- Schmaljohann R., Piker L., and Imhoff J. F. (1998) The distribution of methane and hydrogen sulfid in basin sediments of the central and southern Baltic Sea. *Meyniana* **50**, 191-211.
- Schmitt M., Faber E., Botz R., and Stoffers P. (1991) Extraction of methane from seawater using ultrasonic vacuum degassing. *Analytical Chemistry* **63**, 529-532.

- Schmitt M. and Thießen O. (2003) A new designed sediment degassing system for small sample sizes to analyse free-, total-, and adsorbed-gases. *7th International Conference on Gas Geochemistry (ICGG 7) - Poster Abstracts*.
- Schoell M. (1980) The hydrogen and carbon isotopic composition of methane from natural gases of various origins. *Geochimica et Cosmochimica Acta* **44**, 649-661.
- Schoell M. (1988) Multiple origins of methane in the earth. *Chemical Geology* **71**, 1-10.
- Sedwick P. N., McMurtry G. M., and Macdougall J. D. (1992) Chemistry of hydrothermal solutions from Pele's Vents, Loihi Seamount, Hawaii. *Geochimica et Cosmochimica Acta* **57**, 5087-5097.
- Seyfried W. E. and Dibble W. E. (1980) Seawater-peridotite interaction at 300°C and 500 bars; implications for the origin of oceanic serpentinites. *Geochimica et Cosmochimica Acta* **44**, 309-322.
- Seyfried W. E. and Janecky D. R. (1985) Sr and Ca exchange during hydrothermal alteration of basalt/diabase. *Eos, Transaction, American Geophysical Union* **66**, 921.
- Shepard F. P. (1954) Nomenclature based on sand-silt-clay ratios. *Journal of Sedimental Petrology* **24**(3), 151-158.
- Sherwood-Lollar B., Frapé S. K., Weise S. M., Fritz P., Macko S. A., and Welhan J. A. (1993) Abiogenic methanogenesis in crystalline rocks. *Geochimica et Cosmochimica Acta* **57**, 5087-5097.
- Silva A. J., Brandes H. G., and Veyera G. E. (1996) Geotechnical characterization of surficial high-porosity sediments in Eckernförde Bay. *Geo-Marine Letters* **16**, 167-174.
- Simoneit B. R. T. (1983) Effects of hydrothermal activity on sedimentary organic matter: Guaymas Basin, Gulf of California - Petroleum genesis and protokerogen degradation. In *Hydrothermal processes at Seafloor Spreading Centers* (ed. P. A. Rona, K. Bostöm, and L. Laubier), pp. 451-471. Plenum Press.
- Stoffers P. (1987) Cruise Report SO-47: Midplate Volcanism, Central South Pacific, French Polynesia. *Berichte-Reports, Inst. Geowiss., Univ. Kiel* **19**.
- Stoffers P., Botz R., Cheminée J. L., Devey C. W., Froger V., Glasby G. P., Hartmann M., Hekinian R., Kögler F., Laschek D., Larque P., Michaelis W., Mühe R., Puteanus D., and Richnow H. H. (1989) Geology of MacDonald Seamount Region, Austral Islands: Recent Hotspot Volcanism in the South Pacific. *Marine Geophysical Researches* **11**, 101-112.
- Stoffers P. and Hekinian R. (1990) Cruise Report Sonne 65 - Midplate II, Hot Spot Vulkanismus im zentralen Südpazifik. *Berichte-Reports, Inst. Geowiss., Univ. Kiel* **40**.

- Stüben D., Stoffers P., Cheminée J. L., Hartmann M., McMurtry G., Richnow H. H., Jenisch A., and Michaelis W. (1992) Manganese, methane, iron, zinc, and nickel anomalies in hydrothermal plumes from Teahitia and Macdonald volcanoes. *Geochimica et Cosmochimica Acta* **56**, 3693-3704.
- Talandier J. (1989) Submarine volcanic activity; detection, monitoring, and interpretation. *Eos, Transaction, American Geophysical Union* **70**, 568-569.
- Talandier J. (2004) Seismicity of the Society and Austral hotspots in the South Pacific: Seismic detection, monitoring and interpretation of underwater volcanism. In *Oceanic Hotspots* (ed. R. Hekinian, P. Stoffers, and J. L. Cheminée), pp. 29-71. Springer.
- Thießen O., Schmidt M., Theilen F., Schmitt M. and Klein G. (sub.) Methane formation and distribution of acoustic turbidity in organic-rich surface sediments in the Arkona Basin, Baltic Sea. *Continental Shelf Research*.
- Tishchenko P., Hensen C., Wallmann K., and Wong C. S. (2005) Calculation of the stability and solubility of methane hydrate in seawater. *Chemical Geology* **219**, 37-52.
- Tissot B. P. and Welte D. H. (1984) *Petroleum Formation and Occurrence*. Springer Verlag.
- Torres M. E., Wallmann K., Tréhu A. M., Bohrmann G., Borowski W. S., and Tomaru H. (2004) Gas hydrate growth, methane transport, and chloride enrichment at the southern summit of Hydrate Ridge, Cascadia margin off Oregon. *Earth and Planetary Science Letters* **226**, 225-241.
- Trask P. D. (1932) Origin and environment of source sediments of petroleum. Gulf Publishing Company.
- Tunnicliffe V. (1991) The biology of hydrothermal vents: ecology and evolution. *Oceanography and Marine Biology Annual Review* **29**, 319-407.
- Urabe T., Baker E. T., Ishibashi J., Feely R. A., Marumo K., Massoth G. J., Maruyama A., Shitashima K., Okamura K., Lupton J. E., Sonoda A., Yamazaki T., Aoki M., Gendron J., Kaiho Y., Kisimoto K., Lebon G., Matsumoto T., Nakamura K., Nishizawa A., Okano O., Paradis G., Roe K., Shibata T., Dennant D., Vance T., Walker S. L., Yabuki T., and Ytow N. (1995) The effect of magmatic activity on hydrothermal venting along the superfast-spreading East Pacific Rise. *Science* **269**, 1092-1095.
- Von Damm K. L. and Bischoff J. L. (1987) Chemistry of hydrothermal solutions from the southern Juan de Fuca Ridge. *Journal of Geophysical Research* **92**, 11334-11346.

- Voss M., Kowalewska G., and Brenner W. W. (2001) Microfossil and biogeochemical indicators of environmental changes in the Gotland Deep during the last 10,000 years. *Baltica* **14**, 131-143.
- Wallmann K., Pavlova G., Tishchenko P., Aloisi G., Haeckel M., Obzhirov A., and Suess E. (submitted) Kinetics of sulphate reduction, methane generation and gas hydrate formation in anoxic marine sediments.
- Welhan J. A. (1988) Origins of methane in hydrothermal systems. *Chemical Geology* **71**, 183-198.
- Wever T. F., Abegg F., Fiedler H. M., Fechner G., and Stender I. H. (1998) Shallow gas in the muddy sediments of Eckernförde Bay, Germany. *Continental Shelf Research* **18**, 1715-1739.
- Wever T. F. and Fiedler H. M. (1995) Variability of acoustic turbidity in Eckernförde Bay (southwestern Baltic Sea) related to the annual temperature cycle. *Marine Geology* **125**, 21-27.
- Whiticar M. J. (1990) A geochemical perspective of natural gas and atmospheric methane. *Organic Geochemistry* **16**(1-3), 531-547.
- Whiticar M. J. (1999) Carbon and hydrogen isotope systematics of bacterial formation and oxidation of methane. *Chemical Geology* **161**, 291-314.
- Whiticar M. J. (2002) Diagenetic relationships of methanogenesis, nutrients, acoustic turbidity, pockmarks and freshwater seepages in Eckernförde Bay. *Marine Geology* **182**, 29 - 53.
- Whiticar M. J. and Faber E. (1986) Methane oxidation in sediment and water column environments - isotope evidence. *Organic Geochemistry* **10**, 759-768.
- Whiticar M. J., Faber E., and Schoell M. (1986) Biogenic methane formation in marine and freshwater environments: CO₂ reduction vs. acetate fermentation-Isotope evidence. *Geochimica et Cosmochimica Acta* **50**, 693-709.
- Whiticar M. J. and Werner F. (1981) Pockmarks: Submarine vents of natural gas or freshwater seeps? *Geo-Marine Letters* **1**, 193-199.
- Wiesenburg D. A. and Guinasso N. L. (1979) Equilibrium solubilities of methane, carbon monoxide, and hydrogen in water and sea water. *Journal of Chemical and Engineering Data* **24**(4), 356-360.
- Wilkens R. H. and Richardson M. D. (1998) The influence of gas bubbles on sediment acoustic properties: *in situ*, laboratory, and theoretical results from Eckernförde Bay, Baltic Sea. *Continental Shelf Research* **18**, 1859-1892.

References

- Yamamoto S., Alcauskas J. B., and Crozier T. E. (1976) Solubility of methane in distilled water and seawater. *Journal of Chemical and Engineering Data* **21**(1), 78-80.
- Yeh H.-W. (1980) D/H Ratios and late-stage dehydration of shales during burial. *Geochimica et Cosmochimica Acta* **44**(1), 341-352.
- Zhang T. and Krooss B. M. (2001) Experimental investigation on the carbon isotope fractionation of methane during gas migration by diffusion through sedimentary rocks at elevated temperature and pressure. *Geochimica et Cosmochimica Acta* **65**(16), 2723-2742.

List of Figures

1.1	Generalised diagenetic scheme for anaerobe marine environments after Whiticar and Faber (1986).	9
1.2	Generalised scheme of diagenetic and thermogenic hydrocarbon gas generation.	11
2.1	Map of the study area Arkona Basin with locations of coring sites and of seismo-acoustic profile P21.	18
2.2	N-S Boomer profile P21 with interpretative sketch (below) and with core locations SL02, SL44, SL07, SL35, SL17/41 and SL49 (SL14).	20
2.3	Ternary diagrams (Shepard, 1954) showing the grain-size distribution in the sand-silt-clay and the coarse silt - medium silt - fine silt systems for sediment samples of cores SL44, SL07, and SL49.	24
2.4	Lithostratigraphy and proportions of coarse silt, medium silt, fine silt and clay for sites SL44, SL07, and SL49.	26
2.5	Depth profiles of bulk density, water content, porosity and undrained shear strength of all cores taken at the northern rim of the Arkona Basin.	28
3.1	Overview of the western Baltic region with location of the study area Arkona Basin.	35
3.2	Typical redox voltage (mV) profiles versus depth at core locations SL02 and SL44.	40
3.3	SE-NW Boomer profile P14 with interpretative sketch.	43
3.4	N-S Boomer profile P21 with interpretative sketch and with core locations SL02, SL44, SL35, SL17/41 and SL49 (SL14).	44
3.5	Estimated acoustic turbidity zone (ATZ) as interpreted from seismic profiles.	45
3.6	Methane concentrations versus depth at core locations SL02, SL14, SL17/41, SL35, SL44, and SL49.	46
3.7	Molecular $C_1/(C_2+C_3)$ gas ratios and $\delta^{13}C-CH_4$ values versus depth of stations SL17/41 and SL35.	46
3.8	Comparison of the acoustic turbidity area with the sediment thickness of unit 1.	49
3.9	Detailed 160 cm depth section of muddy surface sediments showing methane concentrations (filled symbols) and redox voltage (E_H) values (open symbols) versus depth in Arkona Basin.	52

List of Figures

3.10	Modified 'Bernard diagram', after Bernard et al. (1976), for classification of bacterial and thermogenic natural gas.	55
3.11	Diagram for classification of bacterial and thermogenic natural gas by the combination of $\delta^{13}\text{C}_{\text{CH}_4}$ and $\delta\text{D}_{\text{CH}_4}$ values.	56
4.1	Map of the Arkona Basin situated in the western Baltic proper with locations of the cores investigated.	60
4.2	Modified North-South shallow seismic Boomer profile P21.	62
4.3	Pore-water concentration profiles of SO_4 and CH_4 and profiles of TOC of gravity cores SL44, SL35, SL17/41 and SL49.	74
4.4	TOC and pore-water methane profiles versus depth at core location SL07.	75
4.5	Modelled TOC flux at the sediment surface of cores SL44, SL35 and SL17/41 for the last 8000 yrs.	77
4.6	Measured (filled dots) and modelled (bold line) pore-water concentration profiles of SO_4 , CH_4 and TOC of cores SL44, SL35 and SL17/41.	80
5.1	Location map of the South Pacific Ocean showing the sampling areas at Bounty (B), Macdonald (M), and Teahitia (T) seamounts.	87
5.2	Methane concentrations, detected on the Bounty, Macdonald, and Teahitia Seamounts are summarised by their frequency.	91
5.3	Sampling stations and bathymetry map of the Pitcairn hotspot area showing the Bounty, Adams, and Christian volcanoes.	94
5.4	Sampling stations and bathymetry map of the Bounty Seamount, Pitcairn hotspot area.	95
5.5	Sampling stations and bathymetry map of the Bounty Seamount, Pitcairn hotspot area.	96
5.6	Sampling stations and bathymetry map of the Macdonald Seamount, Austral hotspot area.	97
5.7	Sampling stations and bathymetry map of the Teahitia Seamount, Society hotspot area.	98
5.8	δD and $\delta^{13}\text{C}$ values of methane (Tab. 3) of the Macdonald Seamount gas samples.	99
5.9	Concentrations and $\delta^{13}\text{C}$ values of methane measured on the Macdonald seamount.	101

List of Tables

1.1	Pathways of organic matter oxidation and hydrogen transformation in the seafloor and their standard energy yields, ΔG^0 , per mol of organic carbon.	7
2.1	Stations, sampling locations, water depths and recoveries from sediment cores taken in the Arkona Basin, Baltic Sea.	19
2.2	Summarised data of grain size analyses.	27
2.3	Grain size data from Arkona Basin sediments.	123
2.4	Summarised and averaged amounts of physical properties as water content, wet bulk density, porosity and shear strength from Arkona Basin sediments.	29
2.5	Physical properties as water content, wet bulk density, porosity, and shear strength from Arkona basin sediments.	126
3.1	Stations, sampling locations, water depth and recoveries from sediment cores taken during Alkor 201 and Alkor 214 cruises in the Arkona Basin.	37
3.2	Redox voltage (E_H) values and calculated redox gradients in Arkona Basin surface sediments.	41
3.3	Methane concentrations and “Bernard” ratios at stations SL02, SL44, SL35, SL17/41, SL49 and SL14 from Arkona Basin sediments.	47
3.4	Isotopic composition of free gases extracted from Arkona Basin sediments.	53
4.1	Data from coring stations, positions, water depths, recoveries, unit 1 sediment thickness and calculated average sedimentation rates for unit 1 deposits.	64
4.3	Summary of sediment features which describe the distinguished zones in the transition from acoustic transparent to acoustic turbid sediments.	69
4.2	Pore-water chloride (Cl) and sulphate (SO ₄) concentrations and total organic carbon (TOC) of Arkona Basin cores SL44, SL07, SL35, SL17/41 and SL49.	70
4.4	Pore-water methane and stable carbon isotope composition of methane.	73
4.5	Model parameters and boundary conditions used for Holocene muddy sediments at Arkona Basin stations SL44, SL35 and SL17/41.	82
4.6	Not presented geochemical data determined from Arkona Basin sediments.	131
5.1	Sampling stations of various hotspot seamounts.	88
5.2	Measured methane concentrations. pH and temperature of seawater and hydrothermal fluid at the Macdonald, Teahitia, Adams, Bounty, and Christian Seamounts.	137
5.3	δD and $\delta^{13}C$ values of methane and $\delta^{13}C$ value of carbon dioxide detected in gas samples from the Macdonald, Bounty, and Teahitia Seamounts.	102

List of Figures

Appendix

Table 2.3: Grain size data from Arkona Basin sediments determined from cores SL44, SL07, and SL49 (from North to South). The different macroscopic sedimentary units 1 to 3 are marked by different colours: white = unit 1 olive grey organic-rich mud; dark grey = unit 2 grey clayey silt; light grey = unit 3 reddish/brown clayey silt.

Sample Interval	Fractions %							MD (Trask, 1932)	SO (Trask, 1932)
	Fine Sand 0.2 - 0.06 mm	Coarse Silt 0.06 - 0.02 mm	Medium Silt 0.02 - 0.006 mm	Fine Silt 0.006 - 0.002 mm	Clay < 0.002 mm	<0.06 mm	<0.01 mm		
<i>Alk 201 SL-44</i>									
<i>54°58.48' N 013°30.07' E Depth 46.0 m</i>									
1-2	0	0	27.78	47.59	24.63	100.00	89.48	0.004	1.74
2-3	0.18	0.42	31.32	46.30	21.78	99.82	86.59	0.004	1.71
6-7	0.14	0.40	29.36	45.41	24.68	99.86	88.05	0.004	1.79
15-16	0	2.29	23.23	47.24	27.25	100.00	93.40	0.004	1.80
20-21	0.21	0.74	32.57	43.55	22.92	99.79	84.17	0.004	1.82
40-41	0	5.95	26.81	43.95	23.29	100.00	83.11	0.004	1.81
82-83	0	4.79	24.50	44.82	25.90	100.00	86.56	0.004	1.84
112-113	0	4.28	26.44	45.73	23.56	100.00	86.59	0.004	1.76
152-153	0.04	0.35	23.95	49.96	25.70	99.97	92.70	0.004	1.71
182-183	0	4.24	26.54	44.20	25.02	100.00	84.73	0.004	1.85
212-213	0.18	13.70	30.60	35.30	20.25	100.00	71.11	0.005	2.14
252-253	0.72	31.74	27.66	27.69	12.19	99.28	52.13	0.009	2.60
282-283	0	2.50	28.46	44.46	24.58	100.00	86.72	0.004	1.81
317-318	0.02	0.46	23.37	50.80	25.35	100.00	93.10	0.004	1.71
322-323	0.07	5.00	24.20	48.60	22.09	97.40	85.26	0.004	1.72
352-353	0	2.06	23.37	44.96	29.61	100.00	89.71	0.004	1.88
383-384	0	0	24.27	47.21	28.52	100.00	92.14	0.004	1.83
384-385	0.34	53.91	22.30	14.90	8.60	99.96	32.09	0.022	2.25
385-386	1.57	33.95	36.75	22.01	5.72	98.43	41.66	0.013	2.25
387-388	0	5.03	44.55	39.41	11.01	100.00	73.03	0.006	1.75
412-413	2.23	22.89	18.64	32.35	23.89	97.77	66.40	0.005	3.06
452-453	0	0	10.49	46.27	43.24	100.00	97.78	0.003	1.86
482-483	0	0	12.96	56.27	30.77	100.00	99.51	0.003	1.67
512-513	0	0	8.75	46.15	45.11	100.00	100.00	0.002	1.87
552-553	0	0.44	10.61	50.62	38.34	100.00	98.80	0.003	1.79
582-583	0	2.06	24.05	49.64	24.24	100.00	91.75	0.004	1.68
612-613	0	0	10.08	55.14	34.78	100.00	98.24	0.003	1.68
652-653	3.27	10.66	10.46	45.17	30.44	96.73	84.57	0.003	1.87

Table 2.3: continued

Sample Interval	Fractions %							MD (Trask, 1932)	SO (Trask, 1932)
	Fine Sand 0.2 - 0.06 cm	Coarse Silt 0.06 - 0.02 mm	Medium Silt 0.02 - 0.006 mm	Fine Silt 0.006 - 0.002 mm	Clay < 0.002 mm	<0.06 mm	<0.01 mm		
<i>Po 266 SL-07</i>									
<i>54°57.00' N 013°30.17'E Depth 48.0 m</i>									
5-6	0	13.35	32.02	37.35	17.28	100.00	71.87	0.005	1.99
15-16	4.01	29.65	28.08	26.73	11.54	95.99	49.97	0.010	2.69
64-65	3.39	43.81	21.21	21.50	10.08	96.61	41.01	0.018	2.78
110-111	10.16	45.52	17.02	19.17	8.13	89.84	35.13	0.026	3.03
260-261	1.13	31.30	25.51	28.71	13.35	98.87	54.13	0.008	2.68
310-311	6.80	52.21	17.89	16.39	6.72	93.20	30.75	0.026	2.54
335-336	0.74	12.40	30.42	38.26	18.17	99.26	71.45	0.005	2.04
384-385	0.04	0.77	27.05	51.13	21.01	99.96	90.45	0.004	1.60
410-411	6.00	23.45	27.41	27.69	15.45	94.00	55.47	0.008	3.01
425-426	3.70	10.53	26.89	36.27	22.63	96.31	74.26	0.005	2.10
514-515	0	1.39	21.00	58.21	19.41	100.00	96.02	0.004	1.48
538-539	0	12.02	33.42	36.94	17.63	100.00	72.45	0.005	1.94
564-565	0	0.21	18.93	47.34	33.52	100.00	95.99	0.003	1.89
568-569	3.07	36.41	33.00	21.35	6.18	96.93	41.22	0.014	2.39
592-593	0	0	15.47	52.02	32.51	100.00	95.87	0.003	1.77
631-632	0	0	10.18	46.01	43.81	100.00	99.46	0.003	1.92
664-665	0	0	31.82	44.75	23.43	100.00	88.02	0.004	1.75
710-711	0	3.73	16.00	38.49	41.78	100.00	90.41	0.003	2.06
770-771	0	0	7.88	44.57	47.56	100.00	99.88	0.002	1.87
865-866	0	0	7.48	51.31	41.20	100.00	98.89	0.003	1.77
929-930	0	0	14.04	56.94	29.03	100.00	98.31	0.003	1.61
944-945	0	0.23	12.86	57.66	29.26	100.00	99.49	0.003	1.62
946-947	0	0	1.24	30.36	68.40	100.00	100.00	0.001	1.76
1095-1096	65.60	2.54	1.38	15.64	14.84	30.89	33.36	0.089	5.73

Table 2.3: continued

Sample Interval	Fractions %							MD (Trask, 1932)	SO (Trask, 1932)
	Fine Sand	Coarse Silt	Medium Silt	Fine Silt	Clay	<0.06	<0.01		
	0.2 - 0.06 mm	0.06 - 0.02 mm	0.02 - 0.006 mm	0.006 - 0.002 mm	< 0.002 mm	mm	mm		
<i>Alk 201 SL-49</i>									
<i>54°54.80' N 013°30.00' E Depth 48.0 m</i>									
1-2	0.12	0.92	31.87	44.87	22.22	99.88	86.37	0.004	1.74
2-3	0	5.82	31.13	41.49	21.55	100.00	80.10	0.004	1.83
6-7	0	4.86	31.38	42.99	20.78	100.00	80.37	0.004	1.80
15-16	0	0	28.70	49.89	21.41	100.00	90.71	0.004	1.62
20-21	0	5.05	23.66	46.07	25.23	100.00	91.20	0.004	1.77
40-41	0	9.87	33.02	38.53	18.58	100.00	76.44	0.005	1.84
45-46	0.08	0.78	29.78	46.45	22.91	99.92	88.21	0.004	1.73
53-54	0	0	17.73	55.37	26.90	100.00	97.12	0.003	1.64
88-89	3.06	31.03	27.98	26.33	11.59	96.94	50.19	0.010	2.71
118-119	0.22	0.01	31.39	45.81	22.59	99.78	86.91	0.004	1.73
148-149	0	4.75	30.86	43.44	20.95	100.00	83.04	0.004	1.76
188-189	0	3.50	29.05	45.14	22.31	100.00	83.60	0.004	1.75
218-219	0	1.34	25.16	48.04	25.46	100.00	95.32	0.004	1.74
288-289	0	4.26	30.94	42.88	21.92	100.00	82.39	0.004	1.79

Table 2.5: Physical properties as water content, wet bulk density, porosity and shear strength from Arkona Basin sediments determined from cores SL02, SL44, SL22, SL07, SL35, SL15, SL17/41, SL14, SL49, and SL29 (from North to South). The different macroscopic sedimentary units 1 to 3 are marked by different colours: white = unit 1 olive grey organic-rich mud; dark grey = unit 2 grey clayey silt; light grey = unit 3 reddish/brown clayey silt.

Sample Interval	Water Content	Wet Bulk Density	Porosity	Shear Strength	Sample Interval	Water Content	Wet Bulk Density	Porosity	Shear Strength
cm	wt%	g cm ⁻³	%	kg cm ⁻²	cm	wt%	g cm ⁻³	%	kg cm ⁻²
<i>Alk 201 SL-44</i>					<i>Po 266 SL-07</i>				
<i>54°58.48' N 013°30.07' E Depth 46.0 m</i>					<i>54°57.00' N 013°30.17' E Depth 48.0 m</i>				
1-2	521.1	1.09	91.5	0.06	5-6	270.5	1.09	84.8	---
2-3	421.4	1.09	89.7	0.10	15-16	257.1	1.13	84.1	---
6-7	337.7	1.13	87.4	0.31	64-65	257.1	1.13	84.1	---
15-16	307.6	1.19	86.4	0.42	110-111	264.2	1.14	84.5	0.44
20-21	281.2	1.17	85.3	0.42	260-261	99.4	1.41	67.2	0.99
40-41	241.9	1.25	83.3	0.59	310-311	139.8	1.25	74.2	0.55
82-83	241.9	1.24	83.3	0.67	335-336	121.1	1.35	71.4	0.99
112-113	256.2	1.19	84.1	1.01	384-385	141.4	1.29	74.5	0.88
152-153	212.2	1.27	81.4	1.18	410-411	121.9	1.32	71.5	1.11
182-183	147.8	1.27	75.3	1.37	425-426	130.8	1.36	72.9	---
212-213	145.8	1.27	75.0	1.37	514-515	74.3	1.15	60.5	---
252-253	95.1	1.41	66.2	1.23	538-539	74.9	1.54	60.7	0.44
282-283	124.7	1.21	72.0	1.18	564-565	88.7	1.43	64.6	0.66
317-318	138.7	1.31	74.1	0.95	568-569	24.1	2.01	33.2	1.54
322-323	145.2	1.35	75.0	---	592-593	82.9	1.52	63.1	0.88
352-353	127.7	1.41	72.5	0.95	631-632	88.9	1.47	64.7	0.77
383-384	96.4	1.44	66.5	1.57	664-665	71.4	1.51	59.5	0.88
384-385	27.4	1.89	36.1	1.12	710-711	87.9	1.44	64.4	0.99
385-386	30.9	1.80	38.9	1.15	770-771	86.3	1.54	64.0	1.10
387-388	38.6	1.65	44.3	1.68	865-866	82.2	1.10	62.9	1.32
412-413	76.4	1.54	61.2	1.68	929-930	45.7	1.71	48.5	1.54
452-453	73.6	1.65	60.3	1.79	944-945	60.9	1.64	55.6	1.65
482-483	73.6	1.55	60.3	1.74	946-947	97.9	1.45	66.9	---
512-513	82.4	1.55	62.9	1.60	1095-1096	73.8	1.22	60.3	---
552-553	66.9	1.63	58.0	1.20					
582-583	63.7	1.63	56.8	---					
612-613	69.1	1.56	58.8	---					
652-653	66.5	1.56	57.8	---					

Table 2.5: continued

Sample Interval	Water Content	Wet Bulk Density	Porosity	Shear Strength	Sample Interval	Water Content	Wet Bulk Density	Porosity	Shear Strength
cm	wt%	g cm ⁻³	%	kg cm ⁻²	cm	wt%	g cm ⁻³	%	kg cm ⁻²
<i>Po 266 SL-15</i>					<i>Po 266 SL-22</i>				
<i>54°55.50' N 013°27.10' E Depth 45.0 m</i>					<i>54°57.01' N 013°38.38' E Depth 48.0 m</i>				
19-20	250.4	1.13	83.8	0.28	210-211	162.3	1.23	77.0	0.77
35-36	249.6	1.21	83.7	0.28	240-241	151.8	1.30	75.8	0.99
45-46	257.1	1.19	84.1	0.31	290-291	149.3	1.24	75.5	1.10
80-81	240.3	1.17	83.2	0.34	330-331	126.5	1.25	72.3	1.32
90-91	239.4	1.21	83.2	---	360-361	126.0	1.37	72.2	0.99
180-181	185.8	1.23	79.3	---	410-411	128.1	1.40	72.5	1.21
220-221	170.8	1.24	77.9	0.88	455-456	118.9	1.39	71.0	1.43
240-241	158.3	1.26	76.5	1.10	462-463	137.1	1.33	73.9	1.10
275-276	152.0	1.28	75.8	1.10	484-485	122.4	1.42	71.6	0.88
320-321	138.8	1.29	74.1	---	505-506	114.2	1.37	70.2	0.77
340-341	113.4	1.06	70.0	---	519-520	108.5	1.42	69.1	1.10
420-421	107.0	1.10	68.8	1.54	543-544	130.7	1.35	72.9	1.10
450-451	114.4	1.39	70.2	1.54	573-574	104.2	1.42	68.2	1.10
500-501	114.1	1.35	70.2	---	584-585	102.9	1.53	68.0	0.55
540-541	116.7	1.37	70.6	---	620-621	104.4	1.40	68.3	0.55
609-610	119.6	1.38	71.1	1.32	644-645	84.2	1.43	63.5	0.66
660-661	116.7	1.40	70.6	1.54	684-685	70.0	1.58	59.1	0.77
685-686	133.3	1.32	73.3	---	730-731	69.9	1.55	59.0	0.99
					762-763	48.6	1.60	50.1	0.66
					764-765	22.1	1.92	31.3	2.64
					806-807	47.7	1.70	49.6	1.43
					823-824	32.6	1.90	40.2	1.54
					870-871	80.1	1.43	62.3	0.99
					899-900	87.5	1.20	64.3	---

Table 2.5: continued

Sample Interval	Water Content	Wet Bulk Density	Porosity	Shear Strength	Sample Interval	Water Content	Wet Bulk Density	Porosity	Shear Strength
cm	wt%	g cm ⁻³	%	kg cm ⁻²	cm	wt%	g cm ⁻³	%	kg cm ⁻²
<i>Po 266 SL-29</i>					<i>Alk 201 SL-49</i>				
<i>54°52.25' N 013°34.41' E Depth 44.0 m</i>					<i>54°54.80' N 013°30.00' E Depth 48.0 m</i>				
10-11	206.5	1.18	81.0	0.25	1-2	409.2	1.09	89.4	---
50-51	218.0	1.15	81.8	0.39	2-3	356.2	1.19	88.0	---
100-101	219.8	1.03	81.9	0.59	6-7	320.9	1.20	86.9	---
140-141	205.6	1.11	80.9	0.78	15-16	308.7	1.18	86.4	0.11
180-181	183.9	1.11	79.1	0.66	20-21	265.9	1.13	84.6	0.28
250-251	159.5	1.22	76.7	0.99	40-41	266.8	1.14	84.6	0.28
300-301	159.6	1.19	76.7	1.21	45-46	287.3	1.24	85.6	0.45
359-360	157.5	1.19	76.5	---	53-54	245.5	1.20	83.5	0.53
350-351	147.8	1.19	75.3	1.21	88-89	253.6	1.19	83.9	0.56
400-401	134.6	1.24	73.5	1.21	118-119	233.0	1.18	82.8	0.67
450-451	128.7	1.24	72.6	1.58	148-149	207.5	1.19	81.1	0.78
484-485	136.1	1.03	73.7	---	188-189	187.5	1.18	79.4	0.84
540-541	136.1	1.05	73.7	---	218-219	164.6	1.25	77.2	0.95
580-581	119.0	1.30	71.0	1.76	248-249	145.5	1.25	75.0	1.12
635-636	114.5	1.31	70.2	---	288-289	127.9	1.27	72.5	1.32
675-676	117.1	1.32	70.7	---					
734-735	109.1	1.32	69.2	---					
770-771	128.0	1.33	72.5	---					
810-811	114.2	1.34	70.2	---					
825-826	114.5	1.35	70.3	1.76					
845-846	126.1	1.35	72.2	2.09					
900-901	126.1	1.35	72.2	1.65					

Table 2.5: continued

Sample Interval	Water Content	Wet Bulk Density	Porosity	Shear Strength	Sample Interval	Water Content	Wet Bulk Density	Porosity	Shear Strength
cm	wt%	g cm ⁻³	%	kg cm ⁻²	cm	wt%	g cm ⁻³	%	kg cm ⁻²
<i>Alk 201 SL-17/41</i>					<i>Alk 201 SL-35</i>				
<i>54°55.50' N 013°27.70' E Depth 47.8 m</i>					<i>54°56.29' N 013°26.96' E Depth 46.0 m</i>				
1-2	493.2	1.09	91.0	---	2-3	478.9	1.13	90.8	---
6-7	396.7	1.10	89.1	---	7-8	456.5	1.14	90.4	---
15-19	310.1	1.15	86.5	---	10-11	387.6	1.15	88.9	---
30-35	259.6	1.14	84.3	---	16-17	311.7	1.16	86.5	---
45-47	253.9	1.09	84.0	0.59	30-31	---	---	---	0.08
60-61	184.6	1.24	83.3	0.59	32-33	252.4	1.17	83.9	---
80-81	158.2	1.09	83.5	---	50-51	---	---	---	0.20
100-101	101.4	1.13	82.3	0.67	51-52	242.0	1.18	83.3	---
119-120	---	---	---	0.70	55-56	252.1	1.32	83.9	0.22
130-131	112.1	1.15	80.1	0.78	60-61	---	---	---	0.31
155-156	117.6	1.29	78.8	0.84	81-82	235.1	1.24	82.9	0.42
175-176	123.8	1.34	76.1	0.95	110-111	243.8	1.29	83.4	0.56
205-206	128.8	1.31	76.0	1.06	140-141	235.9	1.16	82.9	0.56
235-236	117.1	1.28	75.0	1.06	180-181	197.3	1.17	80.3	0.71
260-261	132.2	1.27	74.8	1.18	210-211	179.4	1.18	78.7	0.78
300-301	104.3	1.31	69.4	1.18	240-241	156.1	1.19	76.3	0.90
340-341	80.1	1.38	67.7	1.34	280-281	142.4	1.26	74.6	1.01
495-496	101.4	1.28	67.6	1.51	317-318	105.4	1.38	68.5	1.04
525-526	112.1	1.23	69.8	1.57	340-341	92.4	1.36	65.6	1.34
565-566	117.6	1.22	70.8	1.57	370-371	110.2	1.32	69.4	1.29
595-596	123.8	1.21	71.9	1.58	409-410	113.0	1.28	70.0	1.58
635-636	128.8	1.11	72.6	1.49	440-441	108.8	1.37	69.2	1.49
665-666	117.1	1.45	70.7	0.95	475-476	123.4	1.25	71.8	1.58
695-696	132.2	1.32	73.2	1.19	480-481	---	---	---	1.58
725-726	104.3	1.49	68.3	0.90	485-486	128.2	1.17	72.5	
760-761	80.1	1.36	62.3	---	490-491	---	---	---	1.39
774-775	---	---	---	0.20	500-501	---	---	---	1.29
					510-511	---	---	---	1.10
					515-516	114.9	1.26	70.3	

Table 2.5: continued

Sample Interval	Water Content [wt/wt]	Wet Bulk Density g cm ⁻³	Porosity %	Shear Strength kg cm ⁻²	Sample Interval	Water Content [wt/wt]	Wet Bulk Density g cm ⁻³	Porosity %	Shear Strength kg cm ⁻²
cm	wt%	g cm ⁻³	%	kg cm ⁻²	cm	wt%	g cm ⁻³	%	kg cm ⁻²
<i>Alk 214 SL-02</i>					<i>Alk 214 SL-14</i>				
<i>54°59.29' N 013°30.14' E Depth 48.0 m</i>					<i>54°54.81' N 013°30.01' E Depth 48.0 m</i>				
0-1	617.9	1.01	92.7	---	10-11	265.5	1.18	84.6	
1-2	451.7	1.10	90.3	---	56-57	---	---	---	0.39
4-5	348.5	1.14	87.8	---	66-67	228.8	1.12	82.5	
6-7	347.1	1.09	87.7	---	88-89	---	---	---	0.45
9-10	277.8	1.18	85.1	---	135-136	227.4	1.18	82.4	
19-20	---	---	---	0.17	150-151	---	---	---	0.67
26-27	257.2	1.17	84.1	0.17	177-178	---	---	---	0.73
50-51	---	---	---	0.28	193-194	---	---	---	0.64
82-83	133.2	1.17	73.3		231-232	163.7	1.24	77.1	1.15
86-87	---	---	---	0.95	265-266	---	---	---	1.23
128-129	---	---	---	1.01	292-293	---	---	---	1.26
159-160	---	---	---	0.73	320-321	139.1	1.24	74.1	
168-169	142.3	1.33	74.6	---	368-369	---	---	---	1.57
196-197	103.4	1.64	68.1	---	397-398	---	---	---	1.54
200-201	---	---	---	1.29	429-430	118.3	1.38	70.9	---
207-208	67.5	1.58	58.2		435-436	116.2	1.40	70.6	---
236-237	---	---	---	1.54	464-467	---	---	---	1.79
266-267	---	---	---	1.57	512-513	---	---	---	1.93
296-297	---	---	---	1.65	547-548	---	---	---	1.93
306-307	91.1	1.43	65.2	---					
346-347	---	---	---	1.57					
360-361	---	---	---	1.37					
374-375	65.5	1.64	57.5	---					
446-447	---	---	---	1.62					
466-467	77.5	1.44	61.5	1.62					
526-527	83.1	1.50	63.2	1.79					

Table 4.6: Additional data determined from Arkona Basin sediments. The different macroscopic sedimentary units 1 to 3 are marked by different colours: white = unit 1 olive grey organic-rich mud; dark grey = unit 2 grey clayey silt; light grey = unit 3 reddish/brown clayey silt.

Sample Interval cm	N wt%	C _{org} wt%	C _{anorg} wt%	CaCO ₃ wt%	C/N	Redox Voltage mV	Sediment Temperature °C
<i>Alk 201 SL-44 54°48.48' N 013°30.07' E Depth 46.0 m</i>							
1-2	0.68	5.25	0.57	4.75	7.71	208	5.5
2-3	0.68	5.23	0.59	4.91	7.71	---	---
6-7	0.70	5.39	0.54	4.50	7.74	-277	---
15-16	0.72	5.67	0.40	3.33	7.93	---	---
20-21	0.61	4.97	0.32	2.67	8.11	-498	---
40-44	0.66	5.33	0.33	2.75	8.12	-510	---
82-83	0.63	5.58	<0.01	<0.01	8.83	---	---
104-105	---	---	---	---	---	-322	5.5
112-113	0.84	7.43	<0.01	<0.01	8.88	---	---
134-135	---	---	---	---	---	-338	---
152-153	0.66	6.15	<0.01	<0.01	9.27	---	6.4
174-175	---	---	---	---	---	-279	---
182-183	0.50	4.70	<0.01	<0.01	9.47	---	---
204-205	---	---	---	---	---	-325	6.4
212-213	0.46	4.51	<0.01	<0.01	9.71	---	---
234-235	---	---	---	---	---	-332	---
252-253	0.29	2.90	0.01	0.10	10.01	---	---
274-275	---	---	---	---	---	-263	7.1
282-283	0.35	3.68	0.19	1.61	10.65	---	---
304-305	---	---	---	---	---	-242	---
317-318	0.30	3.85	0.02	0.19	12.75	---	---
322-323	0.30	3.77	<0.01	<0.01	12.49	---	---
334-335	---	---	---	---	---	-202	---
339-340	---	---	---	---	---	-316	---
352-353	0.17	1.55	<0.01	<0.01	9.16	---	---
374-375	---	---	---	---	---	-147	7.4
383-384	0.10	1.26	<0.01	<0.01	12.17	---	---
384-385	<0.01	0.20	0.55	4.57	---	---	---
385-386	<0.01	0.23	1.82	15.19	---	---	---
387-388	<0.01	0.27	1.51	12.56	---	---	---
402-403	---	---	---	---	---	-245	7.5
409-410	---	---	---	---	---	-285	---
412-413	0.04	0.41	0.98	8.17	10.87	---	---
442-443	---	---	---	---	---	45	---
452-453	0.06	0.65	1.22	10.15	10.69	---	---
482-483	0.06	0.66	1.55	12.91	10.44	---	---
504-505	---	---	---	---	---	42	7.5
512-513	0.06	0.60	1.13	9.41	9.53	---	---
534-535	---	---	---	---	---	-49	---
552-553	0.06	0.75	1.60	13.33	11.58	---	---
574-575	---	---	---	---	---	152	---
582-583	0.07	0.71	1.65	13.74	10.67	---	---
604-605	---	---	---	---	---	-52	7.5
612-613	0.06	0.73	1.65	13.74	11.56	---	---
634-635	---	---	---	---	---	-40	---
652-653	0.06	0.67	1.52	12.66	10.38	---	---
674-675	---	---	---	---	---	60	7.5

Table 4.6: continued

Sample Interval cm	N wt%	C _{org} wt%	C _{anorg} wt%	CaCO ₃ wt%	C/N	Redox Voltage mV	Sediment Temperature °C
<i>Po 266 SL-07 54°57.00' N 013°30.17' E Depth 48.0 m</i>							
5-6	0.57	5.26	0.29	2.38	9.26	-287	---
10-11	---	---	---	---	---	-213	9.0
15-16	0.60	5.55	0.29	2.39	9.30	-289	---
29-30	---	---	---	---	---	-261	---
64-65	0.77	7.39	0.30	2.47	9.60	-220	5.6
110-111	0.64	5.99	0.24	1.97	9.37	-309	---
150-151	0.53	5.33	0.24	1.98	9.98	---	---
200-201	0.46	4.82	0.26	2.18	10.55	---	---
260-261	0.28	3.13	0.24	1.99	11.14	---	---
310-311	0.40	4.23	0.28	2.30	10.66	---	---
335-336	0.31	3.67	0.59	4.91	11.76	---	---
410-411	0.18	1.57	0.02	0.16	8.71	---	---
425-426	0.21	2.85	<0.01	<0.01	13.65	-188	---
514-515	<0.01	0.46	1.66	13.85	---	51	---
538-539	<0.01	0.42	0.01	0.11	---	---	---
564-565	<0.01	0.31	<0.01	<0.01	---	---	---
568-569	<0.01	0.11	0.07	0.59	---	---	---
592-593	<0.01	0.38	1.22	10.13	---	---	---
631-632	<0.01	0.41	0.66	5.50	---	---	---
664-665	<0.01	0.53	0.93	7.74	---	---	---
729-730	<0.01	0.54	0.85	7.11	---	---	---
770-771	<0.01	0.53	0.98	8.16	---	---	---
800-801	<0.01	0.65	1.69	14.05	---	---	---
865-866	<0.01	0.66	1.54	12.84	---	97	5.9
929-930	<0.01	0.33	1.59	13.24	---	100	---
944-945	<0.01	0.68	2.15	17.93	---	---	---
946-947	<0.01	0.82	0.73	6.11	---	---	---
995-996	<0.01	0.60	1.33	11.05	---	---	---
1095-1096	<0.01	0.55	1.54	12.80	---	109	6.5
<i>Alk 201 SL-49 54°54.80' N 013°30.00' E Depth 48.0 m</i>							
1-2	0.70	5.90	0.02	0.15	8.40	---	5.5
2-3	0.70	5.84	0.15	1.22	8.36	-229	---
6-7	0.69	5.93	0.13	1.05	8.59	---	---
15-16	0.68	5.79	0.19	1.59	8.57	---	---
17-18	---	---	---	---	---	-301	---
20-21	0.62	5.62	0.00	0.00	9.03	-270	---
40-41	0.66	5.68	0.11	0.88	8.60	-247	---
45-46	0.70	6.09	0.04	0.29	8.74	---	---
47-48	---	---	---	---	---	-283	---
53-54	0.69	6.02	0.05	0.41	8.76	---	---
88-89	0.88	7.48	0.07	0.55	8.50	-209	---
118-119	0.82	7.02	0.27	2.27	8.53	-210	5.7
148-149	0.70	6.38	0.04	0.32	9.12	-247	---
188-189	0.65	5.83	0.07	0.55	8.96	---	---
218-219	0.61	5.69	0.03	0.24	9.29	-124	7.1
248-249	0.57	5.32	0.04	0.30	9.41	-142	---
288-289	0.52	4.82	0.13	1.06	9.33	---	7.4

Table 4.6: continued

Sample Interval cm	N wt%	C _{org} wt%	C _{anorg} wt%	CaCO ₃ wt%	C/N	Redox Voltage mV	Sediment Temperature °C
<i>Po 266 SL-15 54°55.50' N 013°27.10' E Depth 45.0 m</i>							
19-20	---	4.14	0.34	2.84	---	-305	7.8
28-29	---	---	---	---	---	-272	7.8
35-36	---	5.40	0.00	0.25	---	---	---
45-46	---	6.26	0.02	0.20	---	---	---
80-81	---	5.34	0.04	0.31	---	---	---
90-91	---	6.19	0.03	0.23	---	---	---
137-138	---	---	---	---	---	-294	6.8
180-181	---	5.56	0.04	0.33	---	-200	---
220-221	---	5.22	0.01	0.06	---	-214	6.5
240-241	---	4.21	0.03	0.25	---	---	---
275-276	---	4.67	0.04	0.37	---	---	---
320-321	---	4.05	0.18	1.54	---	---	---
340-341	---	3.28	0.04	0.34	---	-191	5.9
380-381	---	---	---	---	---	-116	---
420-421	---	3.35	0.07	0.59	---	-173	---
450-451	---	3.76	0.15	1.21	---	---	---
500-501	---	3.90	0.36	3.00	---	---	---
540-541	---	3.77	0.32	2.65	---	-119	5.5
609-610	---	4.30	0.17	1.44	---	-99	---
660-661	---	1.40	0.21	1.73	---	---	---
685-686	---	3.34	0.01	0.07	---	---	---
<i>Po 266 SL-22 54°57.01' N 013°38.38' E Depth 48.0 m</i>							
210-211	0.52	5.06	0.16	1.30	9.74	---	---
240-241	0.48	4.64	0.24	1.98	9.72	---	---
290-291	0.50	4.82	0.22	1.87	9.58	---	---
330-331	0.40	3.89	0.30	2.50	9.69	---	---
360-361	0.40	3.29	0.98	8.14	8.20	---	---
410-411	0.41	4.06	0.64	5.34	9.88	---	---
455-456	0.35	3.72	0.54	4.52	10.62	---	---
462-463	0.26	2.46	0.08	0.63	9.52	---	---
484-485	0.20	1.62	0.08	0.71	8.11	---	---
505-506	0.17	1.56	0.00	0.00	9.01	---	---
519-520	0.16	1.52	0.00	0.00	9.62	---	---
543-544	0.27	3.72	0.00	0.00	13.73	---	---
573-574	0.00	0.79	0.03	0.23	---	---	---
584-585	0.00	0.66	0.10	0.83	---	---	---
620-621	0.00	0.57	0.01	0.06	---	---	---
644-645	0.00	0.54	0.34	2.87	---	---	---
684-685	0.00	0.46	1.76	14.66	---	---	---
730-731	0.00	0.32	0.00	0.00	---	---	---
762-763	0.00	0.21	0.00	0.00	---	---	---
764-765	0.00	0.09	0.02	0.19	---	---	---
806-807	0.00	0.39	1.82	15.12	---	---	---
823-824	0.00	0.46	2.22	18.52	---	---	---
870-871	0.00	0.38	1.02	8.47	---	---	---
899-900	0.00	0.39	0.73	6.12	---	---	---

Table 4.6: continued

Sample Interval cm	N wt%	C _{org} wt%	C _{anorg} wt%	CaCO ₃ wt%	C/N	Redox Voltage mV	Sediment Temperature °C
<i>Po 266 SL-29 54°52.25' N 013°34.41' E Depth 44.0 m</i>							
10-11	0.54	4.49	0.36	3.03	8.34	---	---
50-51	0.61	5.18	0.38	3.16	8.54	-237	4.6
100-101	0.76	6.31	0.44	3.64	8.34	---	---
115-116	---	---	---	---	---	-251	4.5
140-141	0.69	5.84	0.44	3.68	8.47	---	---
155-156	---	---	---	---	---	-174	---
180-181	0.67	6.24	0.00	0.00	9.37	---	---
190-191	---	---	---	---	---	-236	---
215-216	---	---	---	---	---	-174	---
250-251	0.55	4.79	0.46	3.82	8.67	-111	4.8
290-292	---	---	---	---	---	-157	---
300-301	0.60	5.36	0.38	3.15	8.98	---	---
315-316	---	---	---	---	---	-145	4.9
359-360	0.56	5.31	0.27	2.21	9.48	---	---
350-351	0.27	5.07	0.37	3.08	18.46	-130	---
385-386	---	---	---	---	---	-181	---
400-401	0.51	4.80	0.36	3.03	9.33	---	---
450-451	0.50	4.58	0.44	3.64	9.12	---	---
461-462	---	---	---	---	---	-108	---
484-485	0.50	4.68	0.30	2.50	9.37	-110	5.6
540-541	0.51	4.86	0.32	2.70	9.47	-201	---
580-581	0.45	4.31	0.40	3.31	9.55	---	---
635-636	0.40	3.97	0.39	3.26	9.92	41	---
675-676	0.39	4.05	0.65	5.38	10.39	113	---
710-711	---	---	---	---	---	37	---
734-735	0.30	3.78	0.25	2.07	12.61	90	3.9
770-771	0.30	2.62	0.39	3.29	8.67	136	---
810-811	0.22	1.81	0.04	0.32	8.18	---	---
825-826	0.23	1.76	0.04	0.30	7.77	---	---
845-846	0.20	1.68	0.00	0.00	8.40	---	---
900-901	0.31	4.17	0.00	0.00	13.60	---	---

Table 4.6: continued

Sample Interval cm	N wt%	C _{org} wt%	C _{anorg} wt%	CaCO ₃ wt%	C/N	Redox Voltage mV	Sediment Temperature °C
<i>Alk 201 SL-17/41 54°55.50' N 013°27.70' E Depth 47.8 m</i>							
1.0-2.0	0.77	6.21	0.26	2.17	8.09	126	6.2
6.0-7.0	0.72	6.00	0.19	1.58	8.28	-422	---
15-19	0.69	5.74	0.20	1.67	8.29	-500	---
30-35	0.65	5.46	0.22	1.83	8.40	---	---
45-47	0.64	5.45	0.17	1.42	8.51	-622	---
60-61	0.75	6.82	0.00	0.00	9.14	-610	7.0
80-81	0.85	7.77	0.00	0.00	9.11	---	---
100-101	0.81	7.37	0.00	0.00	9.14	---	---
130-131	0.62	6.08	0.00	0.00	9.73	-547	7.5
155-156	0.60	5.33	0.40	3.33	8.95	-563	---
175-176	0.49	4.48	0.34	2.83	9.10	-546	---
205-206	0.53	4.94	0.38	3.17	9.23	---	---
235-236	0.60	4.80	0.46	3.83	7.99	-520	7.5
260-261	0.49	4.29	0.50	4.17	8.72	-533	---
300-301	0.40	3.55	0.50	4.17	8.82	-485	---
340-341	0.35	3.23	0.61	5.08	9.32	-368	7.5
495-496	0.33	3.39	0.38	3.17	10.35	-348	---
525-526	0.39	3.94	0.38	3.17	10.11	-419	---
565-566	0.41	3.85	0.52	4.33	9.48	-136	---
595-596	0.37	4.78	0.08	0.64	13.09	-164	---
635-636	0.34	4.60	0.13	1.10	13.59	-248	---
665-666	0.21	1.80	0.00	0.00	8.63	---	---
695-696	0.43	4.31	0.22	1.83	9.98	-390	---
725-726	0.12	0.58	0.13	1.08	4.73	-767	---
760-761	0.06	0.49	0.96	8.00	8.00	---	---
774-775						-164	9.0

Table 4.6: continued

Sample Interval cm	N wt%	C _{org} wt%	C _{anorg} wt%	CaCO ₃ wt%	C/N	Redox Voltage mV	Sediment Temperature °C
<i>Alk 201 SL-35 54°56.29' N 013°26.96' E Depth 46.0 m</i>							
0	---	---	---	---	---	---	5.5
0-1	---	---	---	---	---	146	---
1-2	---	---	---	---	---	---	---
2-3	0.80	6.26	0.20	1.67	7.79	---	---
7-8	0.74	6.04	0.20	1.67	8.20	-482	---
10-11	0.72	6.09	0.17	1.42	8.46	---	---
17-18	0.66	5.88	0.06	0.50	8.97	---	---
30-31	---	---	---	---	---	-454	---
30-34	0.61	5.01	0.20	1.67	8.28	---	---
50-51	---	---	---	---	---	-476	5.6
52-53	0.62	5.60	0.08	0.67	9.02	---	---
55-56	0.64	5.23	0.33	2.75	8.23	-533	---
81-82	0.64	5.93	0.00	-0.42	9.22	-560	---
110-111	0.81	7.18	0.01	0.08	8.90	-490	---
140-141	0.79	6.91	0.20	1.67	8.76	-557	6.2
180-181	0.63	5.84	0.07	0.58	9.20	-526	---
210-211	0.58	5.56	0.00	-0.50	9.59	-480	---
240-241	0.52	4.66	0.24	2.00	8.91	-476	7.1
280-281	0.50	4.68	0.25	2.08	9.27	-544	---
317-318	0.38	3.27	0.27	2.25	8.60	-451	---
340-341	0.42	2.99	0.32	2.67	7.19	-418	7.3
370-371	0.38	3.48	0.36	3.00	9.22	-483	---
409-410	0.36	3.62	0.50	4.17	10.13	-401	---
440-441	0.33	3.51	0.48	4.00	10.53	-396	7.9
475-476	0.41	4.25	0.44	3.67	10.26	-418	---
485-486	0.50	4.04	0.50	4.17	8.15	---	---
510-511	---	---	---	---	---	-343	---
515-516	0.28	1.44	0.11	0.92	5.17	---	7.2

Table 5.2: Measured methane concentrations, pH and temperature of seawater and hydrothermal fluid at the Macdonald, Teahitia, Adams, Bounty, and Christian Seamounts.

Station	Depth	Methane concentration	pH	Temperature
Latitude/Longitude	m	nL L ⁻¹		°C
<i>Macdonald Smt</i>				
So65 94MS	7	31	8.24	-
28°58.90'S/140°14.96'W	24	39	8.24	-
	39	27	8.24	-
	55	27	8.25	-
	73	29	8.25	-
	94	36	8.21	-
	114	47	8.21	-
	124	65	8.18	-
	134	57	8.19	-
	145	80	8.18	-
	149	71	8.16	-
	154	83	8.16	-
	So65 96MS	19	30	8.26
28°58.97'S/140°14.87'W	39	42	8.27	-
	60	36	8.25	-
	70	36	8.29	-
	76	28	8.25	-
	79	31	8.24	-
	83	41	8.27	-
So65 98MS	95	45	8.25	-
28°58.66'S/140°14.68'W	105	39	8.24	-
	123	37	8.22	-
	135	52	8.20	-
	137	76	8.20	-
	143	63	8.20	-
	148	54	8.18	-
	152	76	8.16	-
155	66	8.16	-	
159	88	8.16	-	

Table 5.2. continued

Station Latitude/Longitude	Depth m	Methane concentration nL L ⁻¹	pH	Temperature °C
So65 99MS	97	36	-	20.41
28°58.71'S/140°14.71'W	136	109	-	19.00
	145	67	-	18.44
	155	72	-	17.82
	171	105	-	17.59
	219	85	-	16.63
	257	66	-	16.23
	287	37	-	14.19
	299	36	-	14.14
	304	47	-	14.12
	309	44	-	14.08
So65 100MS	29	31	8.28	-
28°58.76'S/140°15.73'W	59	31	8.28	-
	106	30	8.25	-
	115	37	8.25	-
	122	41	8.22	-
	135	88	8.21	-
	146	204	8.06	-
	151	389	7.99	-
	187	1240	7.40	-
	192	603	7.37	-
	198	1182	7.43	-
So65 101MS	47	30	8.29	20.98
28°58.76'S/140°15.39'W	59	21	8.28	20.98
	79	30	8.27	20.95
	100	30	8.26	20.07
	109	31	8.25	19.72
	121	43	8.24	19.44
	130	54	8.22	19.44
	140	249	8.20	19.02
	158	270	8.05	18.63
	162	188	8.05	18.56
	167	215	8.04	18.52
So65 103MS	188	1358	7.30	-
28°58.92'S/140°15.39'W				

Table 5.2. continued

Station Latitude/Longitude	Depth m	Methane concentration nL L ⁻¹	pH	Temperature °C
So65 104MS	48	35	8.25	21.00
28°58.85'S/140°15.09'W	82	24	8.34	20.97
	104	40	8.22	19.80
	118	69	8.20	19.41
	129	44	8.20	19.16
	164	584	7.68	18.42
	179	541	7.47	18.11
	180	2831	6.66	18.07
	186	9691	6.35	17.94
	190	8774	6.30	17.79
	So65 105MS	187	7957	6.80
28°58.83'S/140°15.12'W				
So65 107OFOS	226	31615	5.80	17.70
28°58.82'S/140°15.24'W				
<i>Teahitia Smt</i>				
So65 118MS	279	4	-	-
17°34.50'S/148°49.30'W	714	8	-	-
	1296	9	-	-
	1346	4	-	-
	1380	7	-	-
	1420	5	-	-
	1448	5	-	-
	1482	3	-	-
	1520	4	-	-
	1564	3	-	-
	1615	4	-	-
1624	6	-	-	
Polynaut MS13	53	98	-	26.22
17°33.79'S/148°49.40'W	494	85	-	8.73
	791	52	-	5.29
	1100	36	7.81	3.78
	1304	28	7.80	3.21
	1448	47	7.79	2.87
	1501	46	7.77	2.78
	1512	28	7.78	2.76
	1534	31	7.80	2.72
	1557	51	7.81	2.67
	1572	45	7.83	2.63

Table 5.2. continued

Station	Depth	Methane concentration	pH	Temperature
Latitude/Longitude	m	nL L ⁻¹		°C
Polynaut MS14	393	64	-	12.20
17°34.36'S/148°48.95'W	790	28	-	5.17
	1200	33	7.80	3.34
	1303	38	-	3.08
	1355	33	7.79	3.02
	1385	43	-	2.99
	1406	20	7.80	2.96
	1426	34	-	2.92
	1445	36	7.73	2.79
	1457	21	7.72	2.77
	1459	34	-	2.77
Polynaut MS15	50	65	8.27	26.28
17°34.17'S/148°48.97'W	394	55	7.95	13.04
	792	33	7.76	5.23
	1304	33	7.74	3.06
	1487	30	7.73	2.76
	1528	39	7.73	2.74
	1549	28	7.73	2.68
	1559	40	7.71	2.63
	1569	53	7.70	2.64
	1580	56	7.70	2.65
	1597	72	7.65	2.65
Nautile PN18	1523	3886	5.33	15.80
17°33.92'S/148°49.17'W				
Nautile PN19	1455	5528	5.14	30.00
17°34.40'S/148°48.95'W				
<i>Adams Smt</i>				
So 65 36MS	40	44	-	-
25°22.90'S/129°15.80'W	59	32	-	-
	77	19	-	-
	95	19	-	-
	104	16	-	-
	132	18	-	-
	140	15	-	-
	146	19	-	-

Table 5.2. continued

Station	Depth	Methane concentration	pH	Temperature
Latitude/Longitude	m	nL L ⁻¹		°C
So 65 38MS	31	30	-	22.66
25°23.64'S/129°15.57'W	102	28	-	21.65
	124	28	-	20.58
	149	20	-	19.78
	199	28	-	18.00
	300	26	-	15.54
	350	27	-	13.06
	401	22	-	10.87
	428	18	-	10.01
	452	20	-	8.87
	477	12	-	8.35
	501	9	-	7.87
<i>Bounty Smt</i>				
So 65 32MS	51	16	-	22.85
25°10.51'S/129°23.87'W	99	19	-	22.32
	200	15	-	18.60
	238	18	-	17.42
	270	17	-	16.14
	300	5	-	15.22
	318	22	-	14.76
	387	48	-	12.04
	396	45	-	11.78
	408	21	-	10.87
	412	14	-	10.58
	419	12	-	10.17
So 65 41MS	199	33	-	18.55
25°11.32'S/129°23.57'W	300	27	-	15.52
	350	21	-	13.72
	391	26	-	11.55
	429	28	-	9.50
	456	17	-	8.94
	512	34	-	7.64
	552	8	-	7.11
	582	12	-	6.47
	595	10	-	6.38

Table 5.2. continued

Station	Depth	Methane concentration	pH	Temperature
Latitude/Longitude	m	nL L ⁻¹		°C
So 65 42MS	53	25	-	22.62
25°10.80'S/129°23.66'W	157	24	-	19.76
	249	52	-	16.98
	349	18	-	12.91
	393	22	-	11.16
	462	14	-	9.00
	525	14	-	7.58
	563	9	-	7.08
	591	10	-	6.47
	632	8	-	6.29
	642	11	-	6.15
So 65 53MS	175	27	-	19.24
25°10.80'S/129°24.03'W	259	29	-	16.33
	298	23	-	15.49
	335	26	-	13.64
	370	23	-	12.56
	389	18	-	11.81
	409	22	-	11.20
	427	23	-	10.93
	447	18	-	9.94
	465	14	-	9.20
	491	11	-	8.28
So 65 54MS	314	26	-	15.01
25°10.52'S/129°23.68'W	334	29	-	13.92
	353	20	-	13.08
	375	22	-	12.03
	394	40	-	11.50
	416	35	-	11.17

Table 5.2. continued

Station	Depth	Methane concentration	pH	Temperature
Latitude/Longitude	m	nL L ⁻¹		°C
So 65 77MS	200	30	8.19	18.32
25°10.70'S/129°24.38'W	251	20	8.17	17.12
	330	25	8.10	14.52
	351	21	8.08	12.84
	358	20	8.07	12.46
	370	18	8.05	11.17
	374	25	8.04	10.05
	381	24	8.04	11.02
	387	29	8.03	-
	391	23	8.02	-
	397	21	8.02	-
	402	22	8.01	-
	Polynaut MS02	350	89	-
25°11.07S/129°23.49'W	400	-	-	10.98
	450	47	7.93	9.26
	500	36	-	7.61
	550	29	-	7.01
	600	41	7.89	6.34
	650	60	7.89	5.91
	700	47	7.87	5.81
	771	45	7.87	5.42
Polynaut MS03	50	99	8.24	21.31
25°11.06S/129°23.45'W	100	82	-	21.10
	200	801	8.23	18.41
	250	79	8.13	17.43
	300	63	8.08	15.18
	330	59	8.04	14.13
	350	64	8.01	13.21
	370	72	7.99	12.51
	400	72	-	11.11
	430	81	7.90	9.54
	450	62	-	9.22
Polynaut MS04	427	41	-	9.86
25°11.04S/129°24.00'W	490	51	7.87	8.21
	579	30	7.88	6.72

Table 5.2. continued

Station	Depth	Methane concentration	pH	Temperature
Latitude/Longitude	m	nL L ⁻¹		°C
Polynaut MS05	530	77	7.91	7.22
25°10.97S/129°23.50'W	555	75	7.92	6.75
	594	72	7.90	6.55
	602	117	7.91	6.40
	617	80	7.90	6.31
	644	81	7.90	6.21
Polynaut MS09	200	69	-	17.96
25°11.94S/129°24.31'W	296	103	-	15.05
	394	79	-	11.25
	445	58	-	8.92
	523	55	-	7.15
	542	52	-	6.93
	562	31	-	6.65
	575	80	-	6.53
	582	67	-	6.43
	602	50	-	6.35
Nautile PN04	430	101	7.89	-
25°10.63S/129°24.30'W				
Nautile PN05	444	79	7.41	19.10
25°11.08S/129°24.10'W				
Nautile PN06	579	2266	7.03	14.50
25°10.88S/129°23.62'W				
Nautile PN11	585	1934	6.94	14.50
25°10.86S/129°23.60'W				
Nautile PN12	445	110	7.74	19.10
25°11.08S/129°24.10'W				

Table 5.2. continued

Station	Depth	Methane concentration	pH	Temperature
Latitude/Longitude	m	nL L ⁻¹		°C
<i>Christian Smt</i>				
Polynaut MS06	490	47	-	8.66
25°34.93S/129°31.03'W	1005	22	-	4.27
	1508	24	-	2.75
	1695	30	-	2.42
	1801	36	-	2.31
	1856	34	-	2.21
	1900	51	-	2.16
	1913	58	-	2.17
	1945	62	-	2.16
	1966	50	-	2.17
	1978	36	-	2.17
	1996	33	-	2.14
<i>Pitcairn Area</i>				
Polynaut MS08	2300	43	-	1.93
25°14.30S/129°24.58'W	2350	90	-	1.92
	2400	61	-	1.88
	2450	24	-	1.86
	2470	30	-	1.86
	2500	63	-	1.85
	2510	57	-	1.84
	2520	43	-	1.84

Ich versichere an Eides statt, dass die vorliegende Abhandlung ausschließlich unter Verwendung der angegebenen Hilfsmittel entstanden ist und, abgesehen von der Beratung durch meine akademischen Lehrer, nach Inhalt und Form meine eigene Arbeit darstellt.

Kiel, den

.....
Olaf Thießen

Lebenslauf

Olaf Thießen

geboren am 05.04.1966

in Celle

Staatsangehörigkeit: deutsch

- | | |
|---------------------|--|
| 1987 | Allgemeine Hochschulreife; Berufsbildende Schulen I in Celle; Fachgymnasium Wirtschaft |
| Jul. '87 – Jun. '91 | Wehrdienst |
| Okt. '91 – Mrz. '98 | Christian-Albrechts-Universität zu Kiel
Studium Geologie und Paläontologie
Diplom im März 1998 |
| seit April 1999 | Geochemische Analysen, Glückaufstr. 50, 31319 Sehnde |
| Jul. '99 – Dez. '02 | Christian-Albrechts-Universität zu Kiel
Institut für Geowissenschaften |
| seit Januar 2001 | Promotion an der Christian-Albrechts-Universität zu Kiel,
Institut für Geowissenschaften |
| seit September '05 | Christian-Albrechts-Universität zu Kiel
Institut für Geowissenschaften |